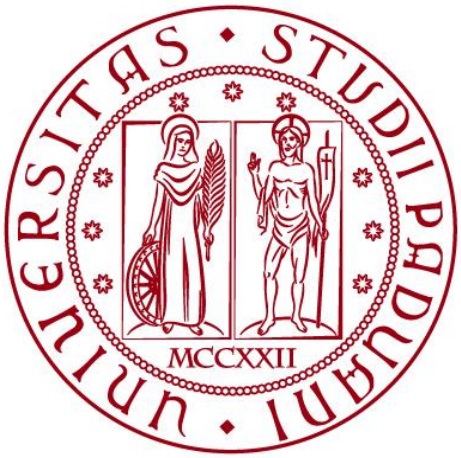

UNIVERSITÀ DEGLI STUDI DI PADOVA

DIPARTIMENTO DI INGEGNERIA INDUSTRIALE

CORSO DI LAUREA MAGISTRALE IN INGEGNERIA DEI MATERIALI

Effects of nitrogen and heat treatments on the thermoelectric power , magnetic and hardness properties of C75 high carbon steel

Relatori: Prof.ssa Irene Calliari

Prof. István Mészáros

Laureando: Alessandro Del Grosso

Matricola: 1163251

ANNO ACCADEMICO 2019-2020

INTRODUCTION

In this thesis a C75 will be analysed which is one type of non-alloy steel with a high carbon content will be analysed; the steel used will be described in more detail in its features in chapter 1.
The main purpose of this thesis can be divided into two different main objectives.

The first objective concerns the evaluation of the effect of nitrogen as an interstitial alloy element on some magnetic properties (measured with an alternating current device), on the TEP values (Thermoelectric power), and on the Vickers hardness; the quantities involved and the procedures used to carry out these tests, which will be the same also in the subsequent part of the thesis, will be discussed in more detail in chapter 1.
In this case it should be noted that the initial hypothesis is that nitrogen, present as an interstitial alloy element, strongly influences many properties previously mentioned in steel. The samples taken into consideration for this analysis were taken from the same production coil in order to have samples with similar characteristics between each other; 12 samples were then chosen with a respective copy (24 initial total samples) and then the copies were sent to an external company to verify the exact nitrogen content present. Once the nitrogen content was known for each of the 12 samples, the tests were performed; we then reported, in chapter 2, the results in graphs, also comparing the various quantities between them to verify any correlations, and finally the conclusions were written.

The second objective of the thesis concerned the effect of some heat treatments on C75 steel with reference to some magnetic properties, TEP and Vickers hardness.
For this second objective 4 boxes of samples from different reels with different starting conditions were used; the production details and the characteristics of the various boxes are described in chapter 3.
The objective was therefore to see how the changes in the microstructure due to the various thermal treatments influenced the properties listed above; the tests were then conducted before and after the heat treatments.
Also in this case the results obtained have been studied not only between quantities and samples but comparisons have been made between the various quantities to verify any correlations between them.
Comparisons have also been made between all 4 boxes to verify any correlations or particular trends of the quantities.
Finally, the final evaluations and conclusions in the final paragraph were reported.

The experimental part of this work was carried out in Budapest, at the BME - Budapesti Műszaki és Gazdaságtudományi Egyetem - University of Budapest, Department of Materials Science & Engineering under the supervision of Professor Mészáros István.

INTRODUZIONE

Nella tesi verrà analizzato un acciaio non legato con alto contenuto di carbonio, per la precisione un C75; l'acciaio utilizzato verrà descritto più approfonditamente nelle sue caratteristiche nel capitolo 1.

Lo scopo principale di questa tesi può essere diviso in due differenti obiettivi principali.

Il primo obiettivo riguarda la valutazione dell'effetto dell'azoto come elemento di lega interstiziale su alcune proprietà magnetiche (misurate con un dispositivo in corrente alternata), sui valori di TEP (Thermoelectric power), e sulla durezza Vickers; le grandezze interessate e le procedure utilizzate per svolgere tali prove, che saranno le stesse anche nella parte successiva della tesi, saranno approfondite nel capitolo 1.

In tal caso si noti che l'ipotesi iniziale è che l'azoto, presente come elemento di lega interstiziale, influenzi fortemente molte proprietà prima citate dell'acciaio. I campioni presi in considerazione per questa analisi sono stati presi dalla stessa bobina di produzione in modo tale da avere campioni con caratteristiche simili tra loro; sono stati scelti quindi 12 campioni con una rispettiva copia (24 campioni totali iniziali) e successivamente le copie sono state mandate in un'azienda esterna per verificare l'esatto contenuto di azoto presente. Una volta venuti a conoscenza del contenuto di azoto per ognuno dei 12 campioni si è passati all'esecuzione delle prove; si sono successivamente riportati, nel capitolo 2, i risultati in dei grafici, mettendo a confronto anche le varie grandezze tra di loro per verificare eventuali correlazioni, e se ne sono scritte infine le conclusioni.

Il secondo obiettivo della tesi ha riguardato l'effetto di alcuni trattamenti termici sull'acciaio C75 in riferimento ad alcune proprietà magnetiche, la TEP e la durezza Vickers.

Per questo secondo obiettivo sono stati utilizzati 4 box di campioni provenienti da bobine differenti con condizioni di partenza diverse; i dettagli produttivi e le caratteristiche dei vari box sono descritti nel capitolo 3.

L'obiettivo era quindi quello di vedere come i cambiamenti della microstruttura dovuti ai vari trattamenti termici influenzassero le proprietà sopra elencate; i test sono quindi stati condotti prima e dopo i trattamenti termici.

Anche in questo caso i risultati ottenuti sono stati oggetto di studio non solo tra grandezze e campioni ma sono stati fatti confronti tra le varie grandezze per verificare eventuali correlazioni tra le stesse.

Sono inoltre stati fatti confronti tra tutti e 4 i box per verificare eventuali correlazioni o andamenti particolari delle grandezze.

Si sono infine riportate le valutazioni finali e le conclusioni nel paragrafo finale.

La parte sperimentale di questo lavoro è stata svolta a Budapest, presso la BME - Budapesti Műszaki és Gazdaságtudományi Egyetem – University of Budapest, Department of Materials Science & Engineering sotto la supervisione del Professor Mészáros István.

INDEX

CHAPTER 1
THEORETICAL REFERENCES AND TYPE OF TEST

1.1 Defects and effects of interstitial elements on properties

Point defects are an atomic discontinuity and are normally associated with one or two atomic positions. All point defects are thermodynamic equilibrium defects. The main types of point defects are [1]:

- *Vacancies* = A first kind of point defect is the vacancy, that is, a lack of an iron atom within the regular crystal lattice. The consequence of a vacancy is the movement of the surrounding atoms from their original position to compensate the electromagnetic vacuum, locally generating a distortion of the lattice; vacancies are point defects that originate mainly during solidification, plastic deformation, or heat treatment of steel.

  The presence of vacancies, along with lattice interstitial sites, explains the movement of the atoms within the metal lattices; this phenomenon is called diffusion.
- *Substitutional atoms* = This defect is present when one or more atoms of the iron lattice are replaced with atoms of other chemical elements having an atomic radius comparable to the atomic radius of iron
- *Interstitial atoms* = This defect is present when an atom outside the iron lattice slides into the lattice interstitial sites, that is, into the spaces left between the iron atoms.

  Only small atoms have the potential to occupy the interstitial spaces of FCC or BCC cells, i.e. the tetrahedral and octahedral interstitial sites in the iron lattice

An interstitial element is an impurity found in "pure" metals or crystals. The quantity of these elements affects the physical properties of the host material. They can be introduced during the manufacturing process.

The most common interstitial elements in metals are hydrogen, carbon, nitrogen, and oxygen; these elements are small enough to fit between normal crystalline lattice locations. In contrast, those elements that replace locations in the crystalline structure are called substitutional elements.

The combination of several characteristics, such as magnetism, allotropic phase changes and the different solubility and diffusion behaviour of interstitial and substitutional elements, makes iron-based alloys unique and is responsible for a diversity of phase transformations. [2]

In addition to iron carbide, Fe3C , that is the most important one, many other chemical compounds can also be present in steel.

The compounds are divided into two categories: interstitial compounds when formed between a metal and a non-metal, and intermetallic compounds when formed between two metals.

Rather common in steel are interstitial compounds, such as carbides, nitrides, sulphides, and oxides. The case of intermetallic compounds is less common. Iron can form all four types of interstitial compounds mentioned above: carbides, (Fe_3C, Fe_2,4C), nitrides (Fe_4N, $Fe_{2-3}N$), sulphides (FeS), oxides (FeO, Fe_2O_3, Fe_3O_4).

In addition, many alloying elements may also form interstitial compounds, such as:

- Ti, V, Mo, W, and Cr for the formation of carbides
- Ti, Al, V, Mo , and Cr for the formation of nitrides
- Cr, Al, Si, and Mn for the formation of oxides
- Mo, Cr, and Mn for the formation of sulphides

So carbon, nitrogen and hydrogen play a significant and often different role on the structure and properties of the iron-based alloys. Carbon and nitrogen are the main elements in two classes of steels based on the Fe-C and Fe-N systems, whereas hydrogen is known as a harmful element causing the embrittlement of engineering materials. [1]

Three main features differentiate the nitrogen steels from the carbon ones.

First, it is a higher stability of nitrogen austenitic and martensitic steels in relation to phase transformations and precipitation reactions. Second, the alloying of austenitic steels with nitrogen maintains the high fracture toughness in spite of the increase in the yield and ultimate strength and also provides a better combination of strength and plasticity of tempered martensitic steels. Third, nitrogen improves corrosive properties of steels, mainly the resistance to pitting and crevice corrosion, whereas carbon accelerates degradation of steel in aggressive environments.

About phase transformations the nitrogen-induced tendency to short-range atomic ordering is responsible for higher thermodynamic stability of nitrogen austenitic steels in relation to the martensitic transformation as compared to that of carbon steels. The fraction of the retained austenite after martensitic transformation is significantly increased if, at the same basic composition, nitrogen substitutes carbon.

In the tempered nitrogen matensite, the precipitation reactions are shifted to higher temperatures and extended over the large temperature range. As a result, the nitride precipitates have a smaller size, which is in particular pronounced in the effect of secondary hardness.

They also induce large lattice stresses therefore normally they increase the hardness.

Another effect reported in literature is that nitrogen and hydrogen increase the concentration of vacancies in the γ-iron solid solution and assist migration of substitutional solutes; no carbon effect on the vacancy formation occurs because of the low carbon solubility in austenitic steels.

Concerning Interactions between dislocations and interstitial atoms we have to distinguish two different cases while analysing the effect of interstitials on mobility of dislocations:

1) *Interstitial atoms are immobile within the studied range of temperatures and strain rates*:

   The pinning of moving dislocations occurs if they cross immobile interstitial atoms. The binding enthalpy of interstitial atoms with dislocations was measured using the strain-dependent internal friction. The test results show that the pinning of dislocations by nitrogen atoms is stronger than that by carbon atoms. This explains why the strain aging is so effective for the strengthening of nitrogen austenitic steels.

   A reason for stronger affinity of nitrogen atoms to dislocations lies in the different electron exchange in the nitrogen and carbon austenite. In spite of a smaller size of the free nitrogen atom, the cloud of the conduction electrons around the nitrogen atom leads to higher contribution of nitrogen to the dilatation of the FCC austenitic lattice and, correspondingly, assists the formation of the Cottrell atmospheres at dislocations.

   An additional electrostatic contribution comes from the different electric charge of the interstitial atoms and dislocations. The attraction has to exist between the negatively charged nitrogen atoms and the positively charged dislocation core, whereas the electrostatic repulsion from the dislocation is expected for the positively charged carbon atoms in austenite.

2) *Interstitials can follow the dislocations during their movement:*

   The situation is expected to be strikingly changed in the range of temperatures and strain rates where the mobility of interstitial atoms is comparable with that of the dislocations during their slip. In this case the velocity of dislocations has to depend on the local electron structure within the volume of the accompanying interstitial atmospheres and can be increased or decreased. In these terms, the nitrogen and hydrogen clouds moving together with dislocations are expected to enhance the metallic character of interatomic bonds and thereby locally decrease the shear modulus.

In relation to mechanical properties the nitrogen-increased toughness of austenitic steels is obviously due to the enhanced metallic character of interatomic bonds, which compensates the embrittling effect of interstitial atoms. Based on the similar effect of nitrogen and hydrogen on the electron structure, one could expect a similarity in mechanical properties of nitrogen- and hydrogen-containing austenitic steels in contrast to the carbon ones.

Another effect, reported in literature, is the strengthening at low temperatures of the nitrogen in austenitic steels compared to the classic carbon steel; this unusual effect was reported to the

nitrogen-caused splitting of the dislocation core in the several planes like it occurs in the BCC lattice and a theory of such a BCC behaviour was proposed.

An interpretation of this nitrogen effect was proposed based on the measurements of the temperature dependence of stacking fault energy in the carbon and nitrogen austenitic steels. It was shown that, in contrast to carbon, nitrogen strikingly decreases the SFE (stacking fault energy) at low temperatures, which results in a larger applied stress for the formation of constriction in the gliding split dislocations while intersecting dislocations threading the slip plane. The low temperature increase of the yield strength in the carbon austenitic steels is rather small because of the weak temperature dependence of the SFE resulted from prevailing covalent bonds. [3]

Among magnetic properties, the maximum permeability and coercive force are known to be susceptible to grain size and impurities (especially interstitial elements such as C, O, P and N); in the literature it is reported that the increasing of the interstitial element can also increase the value of coercivity. [4]

In general it is also important to remember that the nitrogen doesn't necessarily exist in interstitial positions of the crystal but It can form different metallic-nitrides; so the effect of nitride grains differs from the interstitial elements.

1.2 Thermoelectric power investigation

It is useful to give some definition in order to define the thermoelectric power test.

A temperature difference between two points in a conductor or semiconductor results in a voltage difference between these two points; In other words, is it possible to say that a temperature gradient in a conductor or a semiconductor gives rise to a built-in electric field. This phenomenon is called the Seebeck effect or the thermoelectric effect. The Seebeck coefficient measures the magnitude of this effect. The thermoelectric voltage developed per unit temperature difference in a conductor is called the Seebeck coefficient. [5]

We measured the TEP value with the device explained below; the unit measure of TEP is $\left[\frac{nV}{°C}\right]$.

Consider an aluminum rod that is heated at one end and cooled at the other end as depicted in Figure 1:

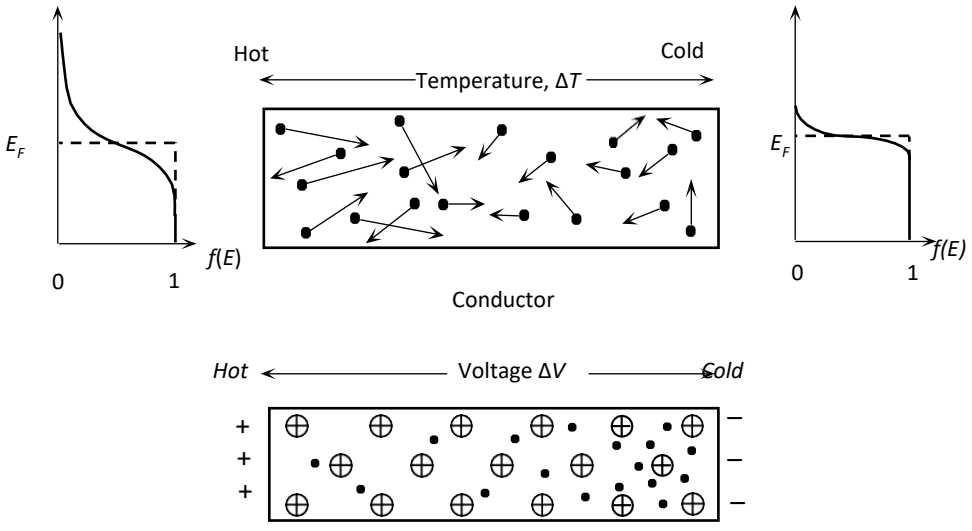

Figure 1. Seebeck effect

The electrons in the hot region are more energetic and therefore have greater velocities than those in the cold region. Consequently, there is a net diffusion of electrons from the hot end toward the cold end which leaves behind exposed positive metal ions in the hot region and accumulates electrons in the cold region.

This situation prevails until the electric field developed between the positive ions in the hot region and the excess electrons in the cold region prevents further electron motion from the hot to cold end. A voltage is therefore developed between the hot and cold ends with the hot end at positive potential. The potential difference ΔV across a piece of metal due to a temperature difference ΔT is called the Seebeck effect.

To value the magnitude of this effect we introduce a special coefficient which is defined as the

potential difference developed per unit temperature difference, called Seebeck coefficient:

$$S = \frac{dV}{dT} \qquad (1)$$

By convention, the sign of S represents the potential of the cold side with respect to the hot side. If electrons diffuse from hot to cold end, then the cold side is negative with respect to the hot side and the Seebeck coefficient is negative.

However, in a p-type semiconductor, on the other hand, holes would diffuse from the hot to the cold end. The cold side would be positive with respect to the hot side which would make S a positive quantity.

The coefficient S is widely referred to as the thermoelectric power even though this term is certainly misleading as it refers to a voltage difference rather than power. The definition, however, has remained the same and we will use this term even if improper.

S is a material property that depends on temperature, S = S(T). It is tabulated for many materials as a function of temperature. Given the Seebeck coefficient S(T) for a material, the voltage difference between two points where temperatures are To and T, from equation above, is given by:

$$\Delta V = \int_{T_0}^{T} S dT \qquad (2)$$

The voltage difference in Equation above is for the cold end with respect to hot as in the convention for *S*.

The average energy E_{av} per electron in a metal in which the density of states $g(E) \propto E1/2$ is given by:

$$E_{av}(T) = \frac{3}{5} E_{FO} \left[1 + \frac{5\pi^2}{12} \left(\frac{kT}{E_{FO}} \right)^2 \right] \qquad (3)$$

where E_{F0} is the Fermi energy at 0 K. It is clear from Equation that the Fermi-Dirac distribution actually extends to much higher energies when the temperature is raised, as showed in Figure 1, so that the average energy per electron, as determined by Equation above, is actually greater in the hot end.

Consequently, the more energetic electrons in the hot end diffuse toward the cold region until a potential difference ΔV is built up preventing further diffusion. We should also note that the average energy per electron as determined by Equation (3) also depends on the material in function of E_{FO}.

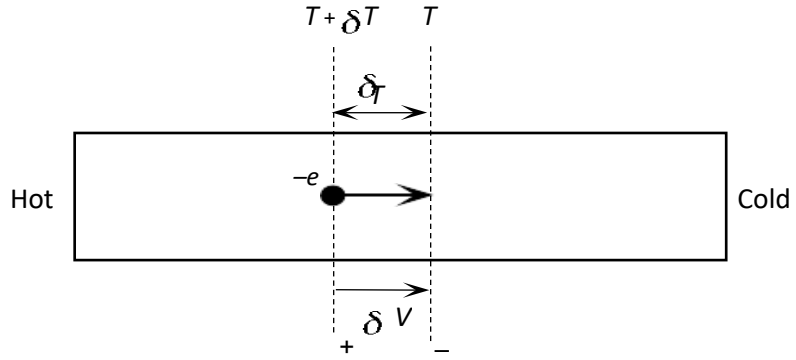

Figure 2. Electron movement in Seebeck effect

Consider a small length x over which the temperature difference is T and voltage difference is V. Suppose that one electron diffuses from hot to cold region across this potential difference. Suppose that a small temperature difference of δT results in a voltage difference δV between the accumulated electrons and exposed positive metal ions as depicted in Figure 2. Suppose that one electron manages to diffuse from the hot region to the cold region. It has to do work against the potential difference δV which is $-e\delta V$. This work done against δV decreases the average energy of the electron by δE_{av} from E_{av} (hot) to E_{av} (cold):

$$-e\delta V = E_{av}(T + \delta T) - E_{av}(T)$$

Substituting for $E_{av}(T)$ from Equation (3) and expanding $(T + \delta T)$ and neglecting δT^2 term we obtain:

$$-e\delta V \approx \frac{\pi^2 k^2 T \delta T}{2E_{FO}}$$

Since $S = \frac{\delta V}{\delta T}$, the Seebeck coefficient is given by the equation[1]:

$$S \approx -\frac{\pi^2 k^2 T}{2eE_{FO}} \qquad Seebeck\ coefficient\ for\ metals$$

While all materials have a nonzero thermoelectric effect, in most materials it is too small to be useful. [6]

However, low-cost materials that have a sufficiently strong thermoelectric effect (and other required properties) are also considered for some applications, including for example power generation and refrigeration.

TEP test

Name of the software = PTEacq

The device used is provided by the university and it works with 2 different sides with a temperature difference of 10°C (Left=15°C and Right=25°C); the temperature of the two sides is stabilized by a water-cooling system. In the initial phase it's important to wait some minutes for the device to reach the two correct temperatures in order to avoid errors of measuring.

The device is showed in the figure below:

Figure 3. TEP device

The unit measure of TEP is $\left[\frac{nV}{°C}\right]$.

The test has been done using 4 different positions for each sample, as showed in the figure 7 below, to have greater accuracy of the results with the average of the values obtained.

The average duration of the test for each position is about 60 seconds and this is useful to obtain a stable TEP value that doesn't change in time anymore.

During some measurements the acquisition times of the TEP values can vary from sample to sample and from position to position; therefore, the TEP value considered is the one obtained when it becomes stable and no longer varies over time.

During the switch of the fourth position, it is better to wait a few minutes to make the temperature on the specimen homogeneous, especially when changing part of the specimen from hot to cold (switch between the second position and the third); this is done to obtain more precise data.

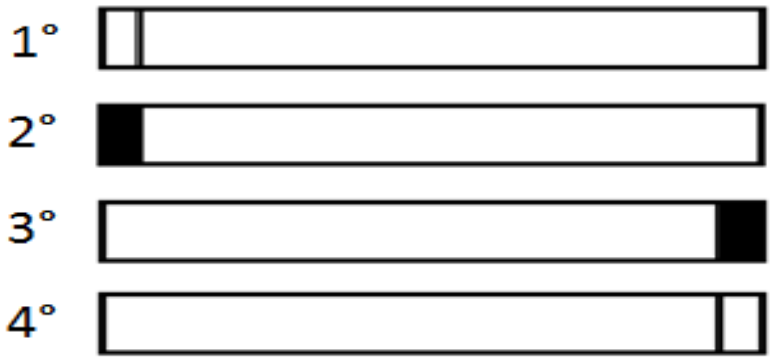

Figure 4. TEP position used for each measurement

Next to the measurement I obtained the average TEP value in a table and I used those values for the graphs.

The TEP value are used in the second chapter to see if there's an influences or correlation between this values and the different content of nitrogen inside of the samples.

In the third chapter we also measure this quantity before and after the various heat treatment in order to see the changes; then we compared this value with other quantities (magnetic and hardness Vickers) for check any correlation between them.

1.3 Magnetic investigation

In this paragraph the fundamentals of magnetism and the behaviour of materials will be explained. Particular attention is posed on the ferromagnetic materials because they are frequently used in industrial practices

All materials can be divided, considering their magnetic behaviour, into five categories: diamagnetism, paramagnetism, ferromagnetism, ferrimagnetism and antiferromagnetism. The two more common types of magnetic materials are the first two groups and they are generally defined as non-magnetic materials, whereas materials of the other groups are those that are none as magnetic materials because of their long-range magnetic behaviour.

Magnetism is that physical phenomenon generated by movements of electric charge. These motions originate a magnetic field that can create attraction or repulsion between two objects. Even different behaviours are possible such as the magnetization of a material after the application of a magnetic field or a non-visible interaction between two materials.

Theoretical considerations are necessary to describe these magnetic behaviours with the introduction of several parameters.

First, the concept of magnetic moment has to be introduced: this is intended as the orientation and strength of the magnetic field produced by several objects; It can be represented as a magnetic dipole. Furthermore, it is important to introduce other parameters: H is conventionally defined as the magnetic field, B is the field generated inside the material after the application of the magnetic field (H); B can be called with several names like magnetic flux density or magnetic induction; In vacuum, B and H are proportional to each other and they are related by the proportionality constant μ_0, the so-called vacuum permeability, as showed in the formula below:

$$B = \mu_0 \cdot H$$

In the case we consider the contribution of the material to the generated field, it is necessary to introduce a parameter known as the magnetization (M), that describes the magnetic properties of the material. Therefore, considering the application of H in a material, the previous equation become:

$$B = \mu_0 \cdot H + \mu_0 \cdot M$$

H is expressed in amperes on meter $[\frac{A}{m}]$, B is expressed in tesla $[T]$, M is expressed in amperes on meter $[\frac{A}{m}]$ and μ0 is expressed in Henries on $[\frac{H}{m}]$ or equivalently in newton on ampere squared $[\frac{N}{A^2}]$

In some well-defined instances, it is important to define the relationships:

$$B = \mu \cdot H = \mu_0 \cdot \mu_r \cdot H$$

$$M = \chi \cdot H$$

Where μ is the magnetic permeability $[\frac{H}{m}]$, μ_r is the relative magnetic permeability and χ is the susceptibility. The quantities μr and χ are linked by the equation:

$$\mu_r = 1 + \chi$$

The susceptibility (χ) is a measure of the magnetic properties and it can express the influence of the magnetic field in the material. χ is higher for soft magnetic materials and lower for hard magnetic materials. [7,8]

Diamagnetism is a form of magnetism that characterizes every type of material in presence of a magnetic field. This behaviour is characterized by a weak quantum mechanical effect and it can be identified in every material that does not show any ferromagnetic or paramagnetic properties. Materials in which diamagnetic behaviour is relevant are those where magnetization is the opposite of the magnetic field, therefore these materials are weakly repellent to each other. Magnetic permeability (μ) of diamagnetic materials is always less than vacuum permeability (μ_0); therefore, relative magnetic permeability (μ_r) is always <1 due to the relation $\mu_r = \mu/\mu_0$.

As a consequence of the relation between μ_r and χ, it is possible to say that susceptibility is always negative and this can find confirmation in the fact that M and H are characterized by opposite direction. Most important example of diamagnetic materials are, for example, water and silver and their typical values of susceptibility are respectively $-0.91 \cdot 10^{-5}$ and $-2.6 \cdot 10^{-5}$.

Paramagnetism is the second form of magnetism shown by those materials that, in presence of a magnetic field, are weakly attracted. This phenomenon is caused by the presence of unpaired electrons that, due to their spin, can behave like magnetic dipoles. Under the presence of a magnetic field they can alienate themselves to the field and cause a weak attraction.

As consequences, all those atoms that are characterized by uncomplete orbitals are paramagnetics. In paramagnetic materials, magnetization and external applied magnetic field are concordant. Therefore both, the magnetic susceptibility and relative magnetic permeability (μ_r) are always positive. Examples of paramagnetic materials are aluminium and magnesium and their typical values of susceptibility are respectively $2.3 \cdot 10^{-5}$ and $1.2 \cdot 10^{-5}$. Differently from ferromagnetic materials, the magnetization of paramagnetics material return to zero when the external magnetic field is turned off.

Ferromagnetic materials present completely different features in comparison with other materials and *ferromagnetism* is for sure the most interesting behaviour to study magnetism. To explain ferromagnetism is important to introduce the concept of a domain, a part of the typical structure of these materials.

A domain (also called Weiss domain) is a small region within the ferromagnetic material that, if exposed to a magnetic field, shows a magnetization in a uniform direction. Although within all domains the magnetic field is intense, it can be possible that the bulk material shows an unmagnetized behaviour due to the random orientation of domains. When an external magnetic field (H) is applied, the walls of these domains, that divide a domain from another one, start to move and the modification of the domain size begins. In this process there is an increasing in size of those domains that show a parallel magnetization to H and a decreasing in size of those domains that are not parallel. The material will saturate when all the domains will be aligned and it normally happens by increasing the external field. The saturation magnetization is the maximum magnetization that can be obtained with a magnetic field.

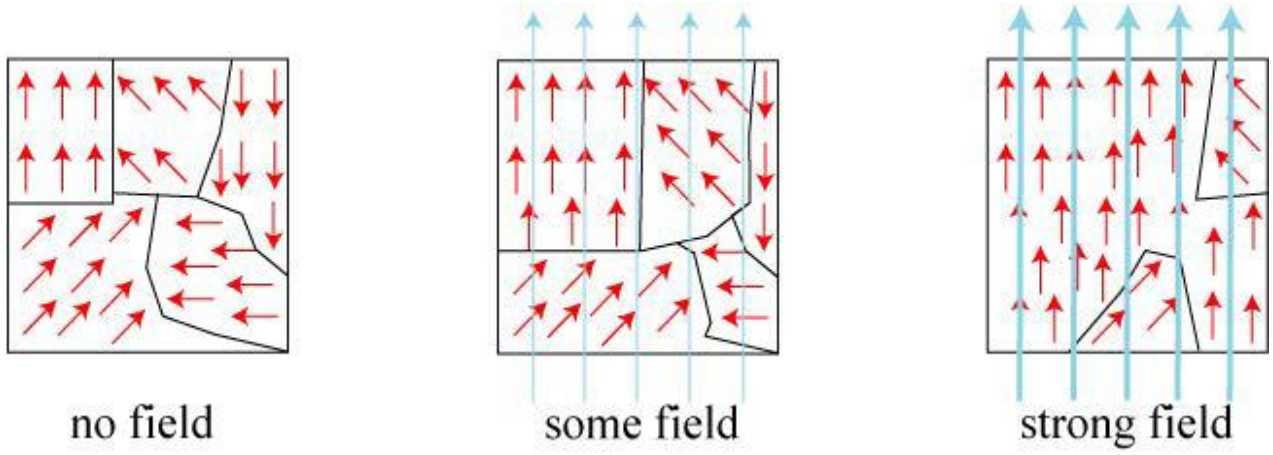

Figure 5. Domains without field (randomly orientated), Domains with the increasing of the field (weakly or strongly orientated)
Domain's walls also move with the increasing of the field.

The higher the density of defects, the harder movement of the domain's wall will be. In any case, once the external field H is turned off, a residual magnetization will remain inside of the material. This behaviour is also caused in this case by the presence of defects such as dislocations that avoid reversible movements of walls.

The susceptibility (χ) in ferromagnetic materials is positive and generally is a very high value. The magnetic relative permeability (μ_r) is also positive with a high value. The magnetic behaviour and magnetic properties, both magnetic relative permeability and susceptibility are connected to the value of H.

Differently from diamagnetic and paramagnetic materials, in ferromagnetic materials there is no linear correlation between H and B. Therefore, is important to measure the magnetisation induction B in function of H, with the function $B=B(H)$.

The graphical representation of this function is the so-called magnetic hysteresis loop showed in figure 6:

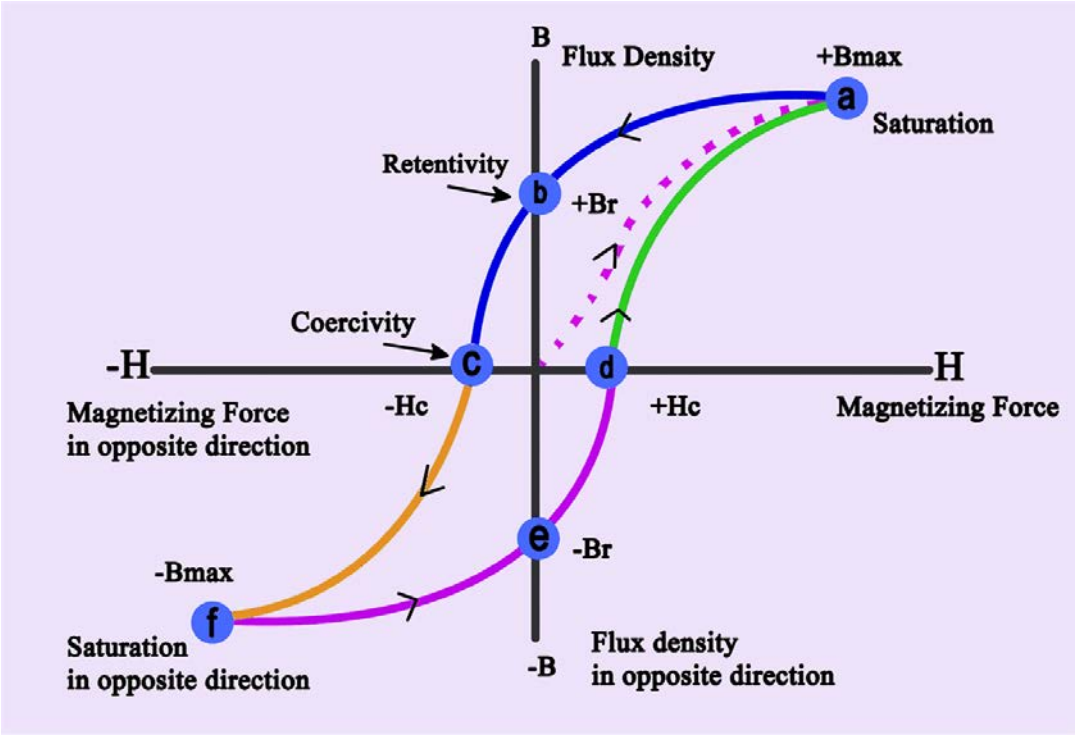

Figure 6. Saturation hysteresis loop of a ferromagnetic material

As shown in the figure above, an initial unmagnetized sample is characterized by values of H and B equal to 0. This curve from 0 rises till the maximum value of a called magnetisation saturation or saturation induction (Bsat≅Bmax) (a). After this value (Hm) an increase in H does not correspond to a significant increase of B. This magnetization process is possible thanks to the motion and growth of magnetic domains. When the applied field reaches zero again, the sample is still characterized by some magnetization due to the magnetic domains where the field is still oriented in the direction of the previous field (b). This point can be also called Br, the remnant induction. In this point the material is magnetized without the presence of H, therefore it is a permanent magnet. To reduce the magnetization to zero (c), a reverse field has to be applied. This field is called coercivity or coercive force (Hc). The negative part of the graph is specular to the positive part: with lower values of Hc it is possible to reach the negative saturation (f) and after that point a decrease of H values does not change significantly the values of B.

Then, the H values can rise till the value of Hm (a). Through the curve d-a it is possible to find a point in which there is some magnetization left even if the field is 0 (e) and a point in which the magnetization is zero, where the value of H corresponds to the coercivity force (d).

The saturation hysteresis loop is the biggest curve possible but also internal loop can be obtained stopping H before it reaches the value of Hm. [9]

It is possible to extrapolate several information from the hysteresis loop; regarding the saturation magnetization, it is proportional to the ferromagnetic phase. Therefore, an increase in the value of

saturation magnetization corresponds to an increase of ferromagnetic phase. Soft magnetic materials are characterized by small values of Hc, hard magnetic materials by high values of Hc. The coercivity (Hc) is also proportional to the hardness.

All these consideration on ferromagnetic materials are true under a certain and well defined temperature, the Curie temperature. Above this value of temperature, a ferromagnetic material loses its tendency for dipoles to align, therefore a paramagnetic material is obtained. This temperature can change a lot between a material and another one. Example of ferromagnetic materials are Iron, Cobalt or Nickel and their Curie temperatures are respectively 1043 K, 1399 K and 627K.

Also, *antiferromagnetism* and *ferrimagnetism* behaviours are possible, even if they are less common to be found in materials. In antiferromagnetic materials, the magnetic moments of neighbouring valence electrons tend to point in opposite directions. Examples of these kind of materials is chromium. In ferrimagnetic materials, like in antiferromagnetic materials, neighbouring valence electrons tend to point in opposite directions, but layers of magnetic moments are unequal, as shown in figure 7 below:

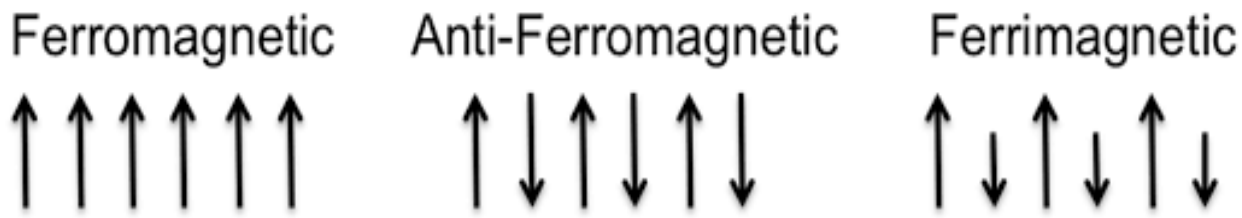

Figure 7. Representation of magnetic moments in ferromagnetic, antiferromagnetic and ferrimagnetic materials

Like ferromagnetism, even antiferromagnetic and ferrimagnetic materials maintain their magnetization when the applied field becomes zero.

Phases in the same material can have a different behaviour. It is the case of austenitic and ferritic phase that are respectively paramagnetic and ferromagnetic and ε-martensite and α'-martensite that are respectively paramagnetic and ferromagnetic. Thanks to their behaviour it is possible to carry out several magnetic tests, like AC magnetization curves test, that will be explained in the following paragraphs.

AC magnetization test

An alternating current single sheet magnetic tester is used to measure different values from hysteresis loop such as saturation induction (Bsat), remanence induction (Br), coercivity (Hc) and maximum relative permeability (μmax).

The instrument consists of two symmetrical U-shaped laminated Fe-Si iron yokes that close the magnetic circuit.

The whole system is connected to a function generator that supplies a sinusoidal current which induces the magnetic field in the sample and a power amplifier. Both the driving and the pick-up coil surrounded the middle part of the sample.

The magnetic tester is controlled by a PC computer connected with a 16 bit data acquisition card in order to collect the measured data.

About the methodology of the test the parameters used are:

- The maximum applied field Hmax 5000 A / m, because it is sufficient to reach the saturation of the normal curve and the hysteresis cycle
- The thickness (A) and width (B) of each specimen used, measured by the calibre, have been inserted so that the software is able to calculate the cross-section area useful for obtaining the magnetic quantities
- The supplied current has a frequency of 5 Hz, to avoid the formation of eddy's current

The device is set to ON and then the specimen is demagnetized (100 cycles).

Next the software for magnetizing and forming the hysteresis curve is started (100 cycles); we noticed that the delay time for the magnetization (seconds between an increase and the other of the magnetization) is equal to 2 sec, so we need more or less 200 sec for each test.

This to ensure the perfect magnetic accommodation within the samples.

This process was repeated for each sample. Various magnetic quantities are obtained in a table and then used in the graphs.

The graphs obtained will be both those of comparison with the TEP values and with HV and both the graph of the hysteresis cycle and the normal curve.

The figure 8 shown in the next page is a schematic operation of used equipment:

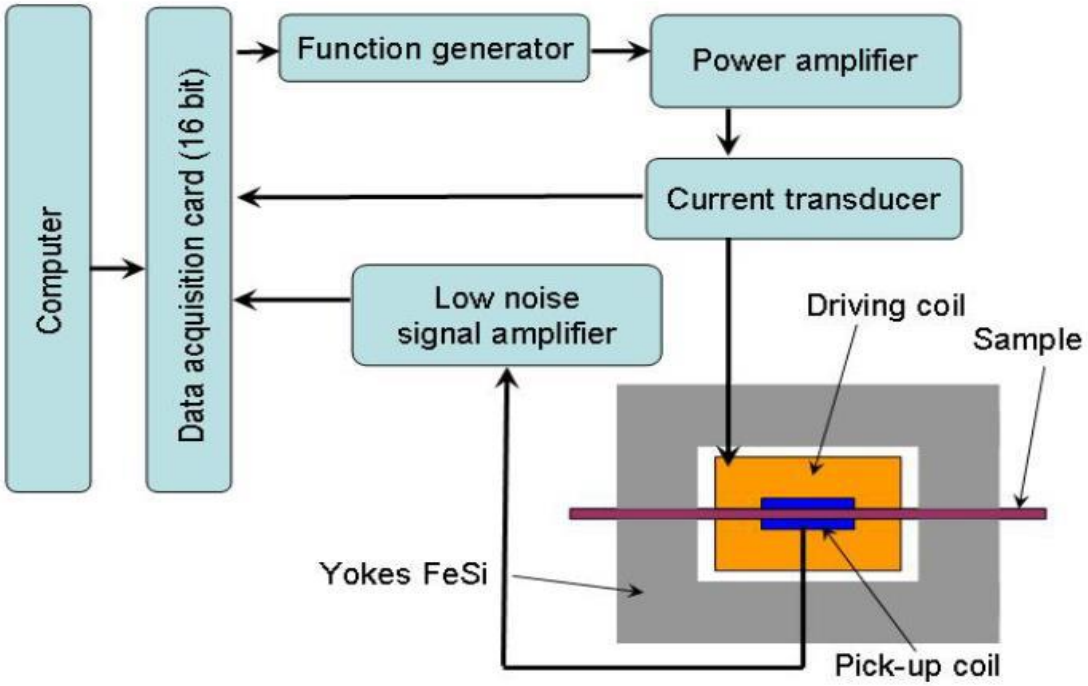

Figure 8. Set-up of AC single sheet magnetic tester [9]

In general, the Bmax is determined only by the chemical composition, so it's not influenced by the microstructure (intrinsic property); so this value doesn't change for the heat treatment.

Instead Br and Hc are influenced by the microstructure, the defects and the stress state like compression (estrinsic property) so they are strictly correlated to the type of heat treatment applied.

For the reasons mentioned before Bmax values are usually used in the graphs with the samples, for the samples that were heat treated, because the changes of values that we noticed are made by measurement error, due to limited excitement and not by the changes of the microstructure; however, in some cases the Bmax values are used in the comparison between other quantities measured because this graphs can show some correlations.

1.4 Hardness Vickers test

Hardness is defined as the property of the material which enables it to resist plastic deformation, usually induced by indentation or penetration. This property can be measured considering how resistant is a solid material exposed to a compressive force applied on it.

For this work, all the hardness tests are done using a microhardness testing machine (including electron microscope) made by Buehler company; an image of it is shown in the image below:

Figure 9. Micro hardness machine with electron microscope (Buehler company)

The indenter shape determines the hardness type test so a square base pyramid shaped indenter is used for testing in the Vickers scale; therefore, this testing method is called Vickers hardness test

In general, the Vickers method has two range of forces: micro and macro, respectively from 10g to 1000g and from 1kg to 100kg. In this work the micro hardness Vickers test is carried out with a load of 100g force because the thickness of the samples doesn't allow the use of larger loads; moreover, the load application time is 15 seconds per test and the zoom used is 40x.

The test is done on 5 different points for each side of the sample and then an average of the values obtained is considered; an exception is made for samples that present bending after heat treatment, because of the induced stress; in those cases only one face of the sample is measured, that is the one with the ends upwards, since the other side would lead to invalid results.

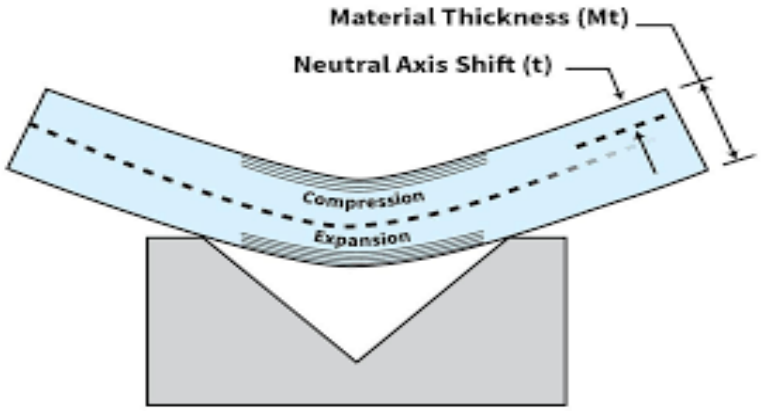

Figure 10. Sample subject to bending

An important precaution to have before carrying out the hardness test is to clean the surface of the sample with fine abrasive paper so as to make the result of HV as reliable as possible; this process is essential to be applied to the pieces after the various heat treatments given the oxidation formed.

The test consists in measuring the diagonals of the indentation shape made by the indenter and, knowing the load, it is possible to calculate the value of Vickers hardness with the following equation:

$$HV = 0.1891 \cdot \frac{F}{d^2}$$

Where F is the load in kilograms and d is the average length of the diagonals left by the indenter in millimetres, so the unit measure will be $\left[\frac{N}{mm^2}\right]$.

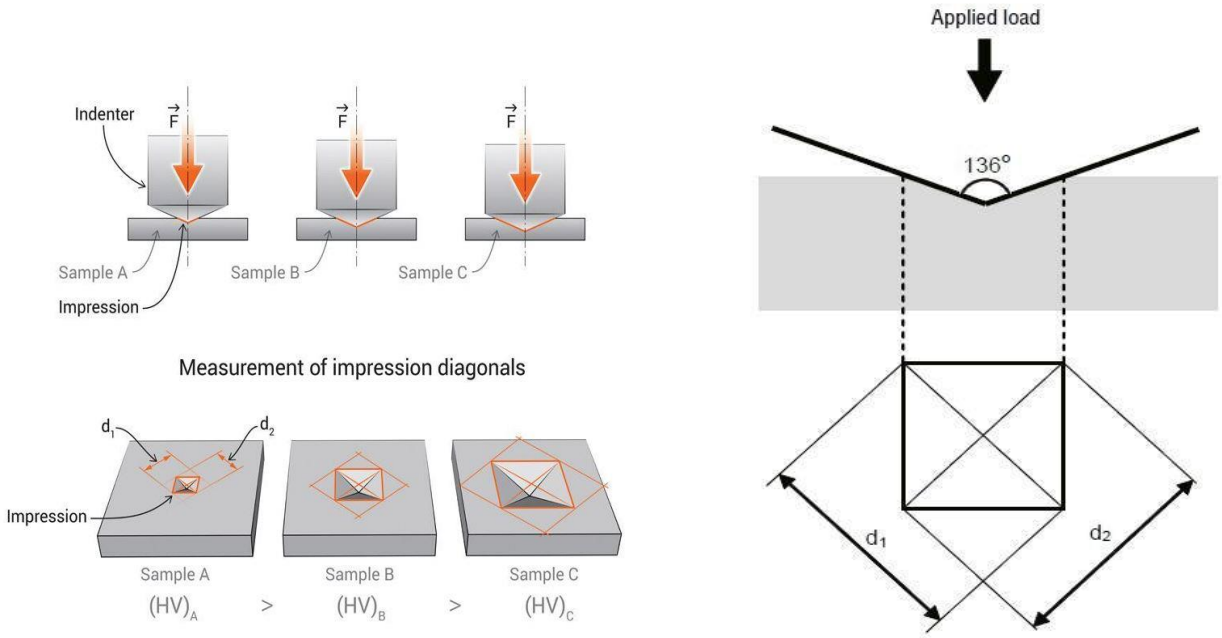

Figure 11. Shematic representation of Vickers test and indenter

1.5 Introduction to heat treatments

The definition of a heat treatment is an operation by which an alloy or a metal are subjected, below the melting point or in their melting range, in a certain ambient, to one or more thermal cycles, in order to give them some properties. The structure of a metal is then modified, obtained by heating to a certain defined T maintained for a certain time and a subsequent cooling; there are also side effects like change of geometric (distortion) and surface (oxidation, decarburization) conditions, and of the solid state of internal tensions of the pieces (cracks).

Austenitizing

The initial phase (heating + maintenance) is called austenitization; this process consists of heating completely or partially, depending on the chemical composition of the steel. In the figure 12 below the Fe-C diagram will be showed, which is the reference point to be taken into consideration during thermal treatments; it describes the equilibrium structures of iron carbon and cast iron alloys:

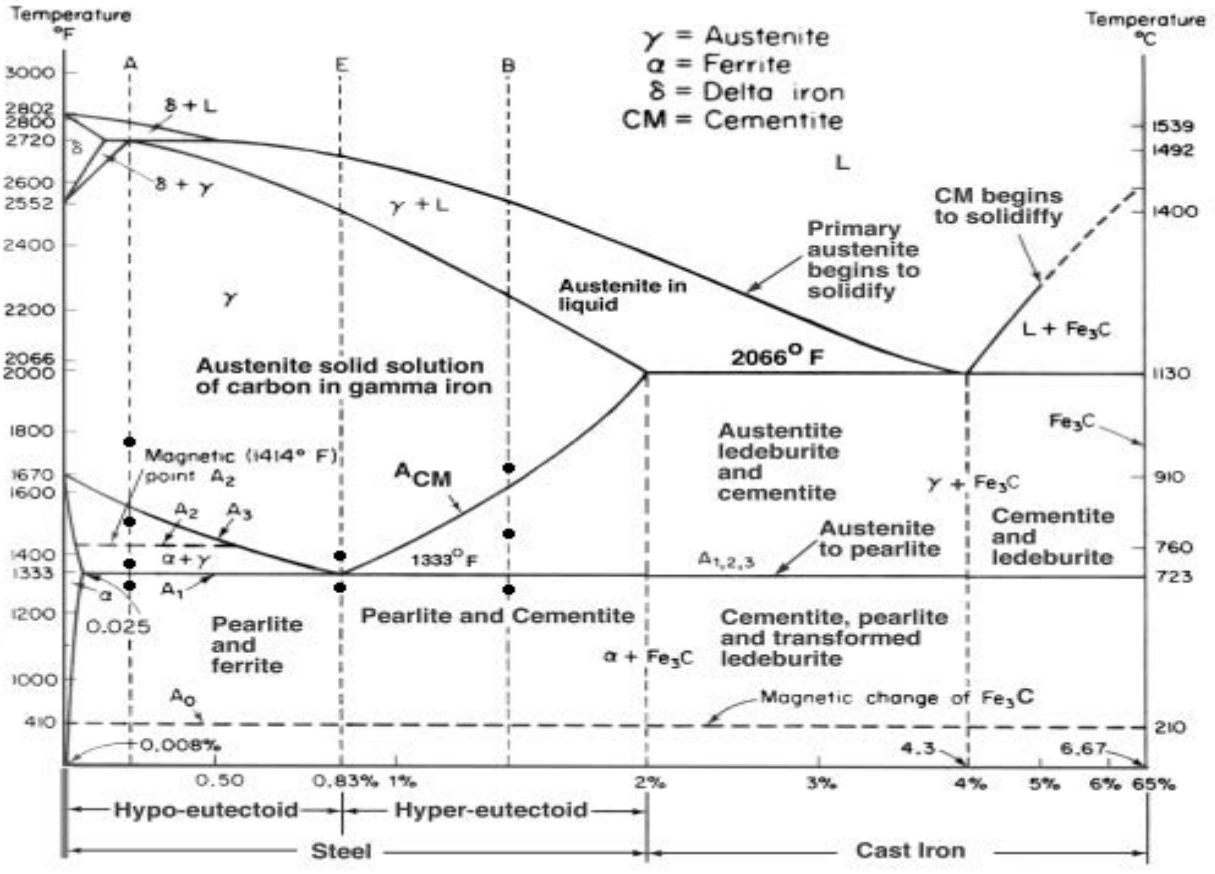

Figure 12. Iron carbon diagram for steels and cast iron

A short summary of the microstructural constituents in a state of equilibrium is listed:

- *Ferrite (α):* Interstitial solid solution of very small percentages of carbon in α iron; structure BFC. It is ferromagnetic up to T = 769 ° C but at T> it becomes paramagnetic.

- *Austenite (γ):* Interstitial solid solution of carbon in the iron γ. It has a Paramagnetic phase.
- *Cementite (Fe_3C):* Intermediate phase of Fe_3C composition which has the characteristics of hardness and fragility
- *Pearlite:* Aggregate consisting of ferrite and iron carbide obtained by direct transformation of austenite by cooling below the critical point A_1. Perlite is obtained with coarse-sized lamellas if its formation occurs at a temperature just below the critical point A1, or very fine, solvable at high magnifications, if it occurs at lower temperatures. It is called globular perlite, a structure characterized by an aggregate of ferrite and cement with a spherical shape, obtained by globulization.
- *Bainite:* Aggregate of ferrite and cementite with acicular forms. The diffusion of carbon atoms at intermediate T is still possible, but the carbides that are formed consist of ever finer clusters.
- *Martensite:* The formation of martensite occurs within the austenitic grain as a solid supersaturated solution of the Carbon in the Ferrite. The process takes place almost instantly, through a coordinated movement of atoms and not by diffusion, prevented by the low temperature; the chemical composition of martensite coincides with the austenite one. Nucleation starts from the inside, not from the grain boundary.

  The formation start temperature is usually indicated with Ms and the formation termination temperature with Mf. The remarkable reticular deformations, which hinder the movement of the dislocations, are the first cause of the hardening.

More informations about the different microstructures will be explained in the next paragraphs of this chapter in reference to the microstructure obtained based on the heat treatment. About austenitization the fundamental parameters are the T_a=austenitization temperature and the t_a=austenitization time; austenitization is necessary in hardening and normalization treatments and can be complete or partial with the coexistence of several phases (austenite + carbides).

The T necessary to completely austenize a steel can be determined from the phase diagram:

- Hypereutectoid steels are heated to $T > A_3$
- Eutectoid steels are heated to $T > A_1$ →<u>High carbon steel C75</u>
- Hypereutectoid steels are heated to $T > A_{cm}$

The austenitization is formed by nucleation + growth process; Upon reaching T_a I have a homogeneous structure of austenite.

The areas coming from the ferrite result with a low concentration of C while the areas coming from the carbides have a high concentration of C; It takes some time for a homogeneous structure to form.

The effect of temperature on austenitization, if there is more overheating, are: less critical core diameter, higher nucleation rate and Increased core growth rate; a too low T doesn't allow the complete dissolution of the carbides while a too high T leads to the formation of a coarse austenitic grain.

Grain growth is blocked by cementite and ferrite, and by the presence of carbides. In addition, the higher is the C content, the greater the austenitic grain growth tendency.

A prolonged heating to T >> A_{c3} / A_{cm} causes an excessive enlargement of the crystalline grain known as overheating.

In conclusion it is good to obtain an austenitic structure and a homogeneous structure and to avoid an enlargement of the grains (creates residual austenite), oxidation, decarburization, carburation of the surface layers and partial fusion.

For each steel the appropriate temperature and retention time must be found.

Phase transformations

Metallic materials, in general, have a wide range of mechanical properties; the mechanical properties are reliant on the characteristics of the microstructure. The development of microstructure involves some type of phase transformation, so it is an alteration in the number and/or character of the phases.

These transformations are divided into three classifications:

1. The first group of transformations are simple diffusion-dependent transformations in which there is no change in either the number or composition of the phases present. These includes solidification of a pure metal, allotropic transformations, and, recrystallization and grain growth
2. In the second type of diffusion-dependent transformation, there is some alteration in phase compositions and often in the number of phases present; the final microstructure ordinarily consists of two phases
3. The third kind of transformation is diffusionless, wherein a metastable phase is produced.
   A martensitic transformation, which may be induced in some steel alloys, belongs to this category.

Speaking of phase transformation kinetics, we can say that with phase transformations, normally at least one new phase is formed that has different physical/chemical characteristics and/or a different structure than starting phase; furthermore, most phase transformations don't happen instantaneously. Rather, they begin by the formation of numerous small particles of the new phases, which increase in size until the transformation is finished.

The progress of a phase transformation can be distinguished into two distinct stages: *nucleation* and *growth*.

Nucleation involves the appearance of very small particles, or nuclei of the new phase (often consisting of only a few hundred atoms), which are capable of growing; during the growth stage these nuclei increase in size, which results in the disappearance of some (or all) of the starting phase. The transformation reaches completion if the growth of these new phase particles is allowed to proceed until the equilibrium fraction is attained.

There are two types of nucleation: homogeneous and heterogeneous. The distinction between them is made according to the site at which nucleating events occur. For the homogeneous type, nuclei of the new phase form uniformly throughout the parent phase; whereas for the heterogeneous type, nuclei form preferentially at structural inhomogeneities, such as container surfaces, insoluble impurities, grain boundaries, dislocations, and other cases.

Homogeneous Nucleation

A discussion of the theory of nucleation involves a thermodynamic parameter called free energy (or Gibbs free energy), G; free energy is a function of other thermodynamic parameters, one of which is the internal energy of the system (the enthalpy, H), and another is a measurement of the randomness or disorder of the atoms or molecules (the entropy, S). However, relative to phase transformations, an important thermodynamic parameter is the change in free energy, ΔG; a transformation will occur spontaneously only when ΔG has a negative value.

We can consider the solidification of a pure material, assuming that nuclei of the solid phase form in the interior of the liquid as atoms cluster together so as to form a packing arrangement similar to that found in the solid phase. Furthermore, it will be assumed that each nucleus is spherical in geometry and has a radius r.

This situation is represented schematically in Figure 13:

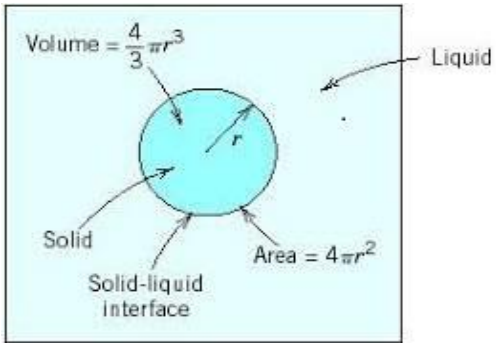

Figure 13. Schematic diagram showing the nucleation of a spherical solid particle in a liquid

There are two contributions to the total free energy change that accompany a solidification transformation. The first is the free energy difference between the solid and liquid phases, or the volume free energy, $\boldsymbol{\Delta G_v}$. Its value will be negative if the temperature is below the equilibrium

solidification temperature, and the magnitude of its contribution is the product of $\boldsymbol{\Delta G_v}$ and the volume of the spherical nucleus ($\boldsymbol{\frac{4}{3}\pi r^3}$).

The second energy contribution results from the formation of the solid–liquid phase boundary during the solidification transformation. Associated with this boundary is a surface free energy, γ, which is positive; furthermore, the magnitude of this contribution is the product of and the surface area of the nucleus ($4\pi r^2$).

So the *total free energy* change is equal to the sum of these two contributions:

$$\Delta G = \frac{4}{3}\pi r^3 \Delta G_v + 4\pi r^2 \gamma$$

These volume, surface, and total free energy contributions are plotted schematically as a function of nucleus radius in Figure 14:

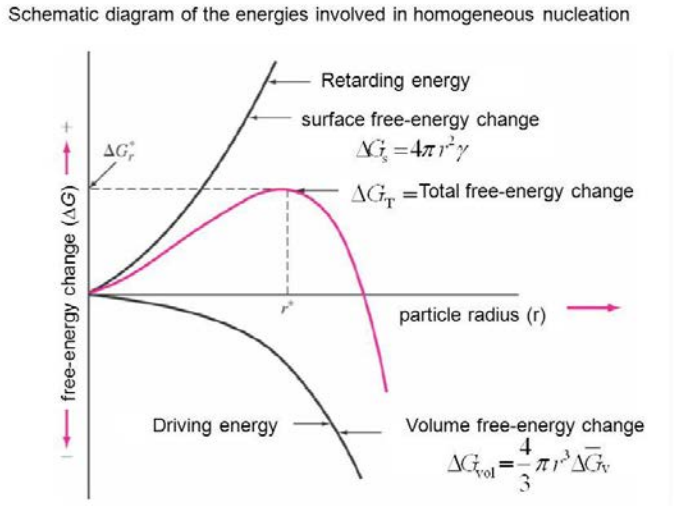

Figure 14. Schematic diagram of the energies involved in homogeneus nucleation

It can be noted from the figure 14 that the curve associated with the sum of both terms, increases first, then passes through a maximum, and finally decreases. In a physical sense, this means that as a solid particle begins to form as atoms in the liquid cluster together, its free energy first increases. If this cluster reaches a size corresponding to the critical radius r*, then growth will continue with the accompaniment of a decrease in free energy. On the other hand, a cluster of radius less than the critical will shrink and redissolve. This subcritical particle is an *embryo,* whereas the particle of radius greater than r* is termed a *nucleus*. A critical free energy, ΔG^*, occurs at the critical radius and, consequently, at the maximum of the curve.

This ΔG^* corresponds to an *activation free energy,* which is the free energy required for the formation of a stable nucleus. Equivalently, it may be considered an energy barrier to the nucleation process.

Since r* and ΔG^*appear at the maximum on the free energy versus radius curve
of figure 16, the derivate give us the equation that searched. For obtain r* we differentiate the ΔG equation with respect to *r*, set the resulting expression equal to zero, and then solve for r= r*:

$$\frac{d\Delta G}{dr} = \frac{4}{3}\pi\Delta G_v(3r^2) + 4\pi\gamma(2r) = 0$$

So it is obtained:

$$r^* = -\frac{2\gamma}{\Delta G_v}$$

At the end it is possible to obtain the critical free energy replacing the expression of r* into the ΔG equation:

$$\Delta G^* = \frac{16\pi\gamma^3}{3(\Delta G_v)^2}$$

Heterogeneous Nucleation

Levels of supercooling for homogeneous nucleation may be significant (on occasion several hundred degrees Celsius), in practical situations they are often on the order of only several degrees Celsius. The reason for this is that the activation energy (energy barrier) for nucleation (ΔG^*) is lowered when nuclei form on preexisting surfaces or interfaces, since the surface free energy (γ of ΔG^* equation) is reduced. In other words, it is easier for nucleation to occur at surfaces and interfaces than at other sites; this type of nucleation is called heterogeneous.

In order to understand this phenomenon, let's consider the nucleation, on a flat surface, of a solid particle from a liquid phase. It is assumed that both the liquid and solid phases "wet" this flat surface, that is, both of these phases spread out and cover the surface; this configuration is showed schematically in Figure 15 below:

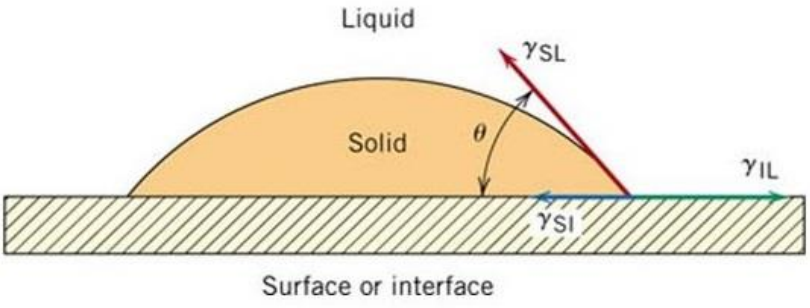

Figure 15. Heterogeneous nucleation of a solid from a liquid

In the figure above there are three interfacial energies (represented as vectors) that exist at two-phase boundaries (solid liquid γ_{SL}, solid surface γ_{SI} and liquid surface γ_{IL}) as well as the wetting

angle θ (the angle between the γ_{SI} and γ_{SL} vectors). Taking a surface tension force balance in the plane of the flat surface leads to the following expression:

$$\gamma_{IL} = \gamma_{SI} + \gamma_{SL} \cos\theta$$

Using the same procedure used in homogeneous nucleation we obtain the following expressions:

$$r^* = -\frac{2\gamma_{SL}}{\Delta G_v}$$

$$\Delta G^* = \left(\frac{16\pi\gamma_{SL}{}^3}{3(\Delta G_v)^2}\right) S(\theta)$$

The term $S(\theta)$ of this equation is a function only of θ (the shape of the nucleus), which will have a numerical value between zero and unity.

From Equation 10.13, it is important to note that the critical radius r^* for heterogeneous nucleation is the same as for homogeneous, inasmuch γ_{SL} as is the same surface energy as in the equation in the Homogeneous Nucleation.

It is also evident that the activation energy barrier for heterogeneous nucleation (Equation ΔG^*) is smaller than the homogeneous barrier (Equation ΔG^* for the homogeneous nucleation) by an amount corresponding to the value of this $S(\theta)$ function:

$$\Delta G^*_{het} = \Delta G^*_{hom} S(\theta)$$

The figure 16 is a schematic graph of ΔG versus nucleus radius, plots curves for both types of nucleation, and indicates the difference in the magnitudes of ΔG^*_{het} and ΔG^*_{hom} in addition to the constancy of r^*.

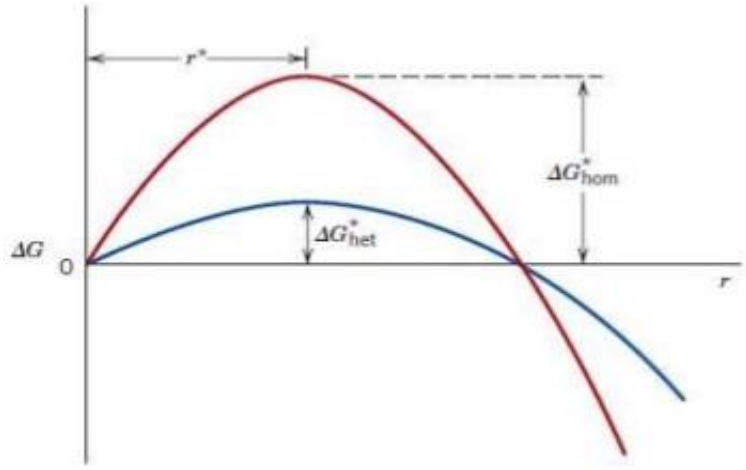

Figure 16. Schematic free energy versus-embryo/nucleus radius plot both (homogeneous and heterogeneous nucleation). Critical free energies and the critical radius are also shown.

This lower for heterogeneous means that a smaller energy must be overcome during the nucleation process (than for homogeneous), and therefore heterogeneous nucleation occurs more easily.

Growth

In terms of the nucleation rate, the $\dot{N}$ versus T curve is shifted to higher temperatures for heterogeneous.; this effect is represented in figure 17, which also shows that a much smaller degree of supercooling is required for heterogeneous nucleation:

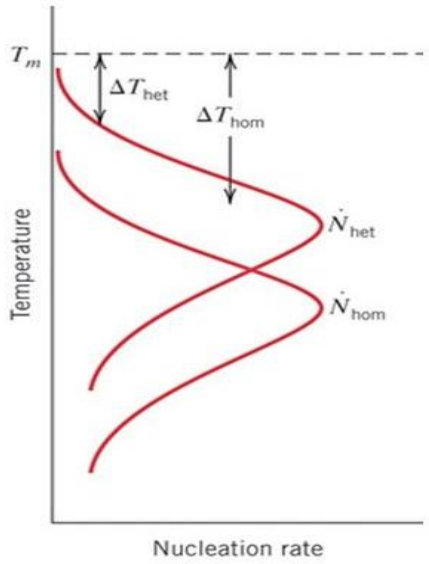

Figure 17. Nucleation rate versus temperature for both homogeneous and heterogeneous nucleation. Degree of supercooling (ΔT) for each is also shown.

The growth step in a transformation phase begins once an embryo has exceeded the critical size, r*, and becomes a stable nucleus. Note that nucleation will continue to occur simultaneously with growth of the new phase particles; of course, nucleation cannot occur in regions that have already transformed to the new phase. Furthermore, the growth process will stop in any region where particles of the new phase meet, since here the transformation will have reached completion. Particle growth occurs by long-range atomic diffusion, which normally involves several steps—for example, diffusion through the parent phase, across a phase boundary, and then into the nucleus. Consequently, the growth rate is determined by the rate of diffusion, and its temperature dependence is the same as for the diffusion coefficient:

$$\dot{G} = C \exp\left(-\frac{Q}{kT}\right)$$

where Q (the activation energy) and C (a pre-exponential) are independent of temperature. The temperature dependence of $\dot{G}$ is represented by one of the curves in figure 18; also shown is a curve for the nucleation rate:

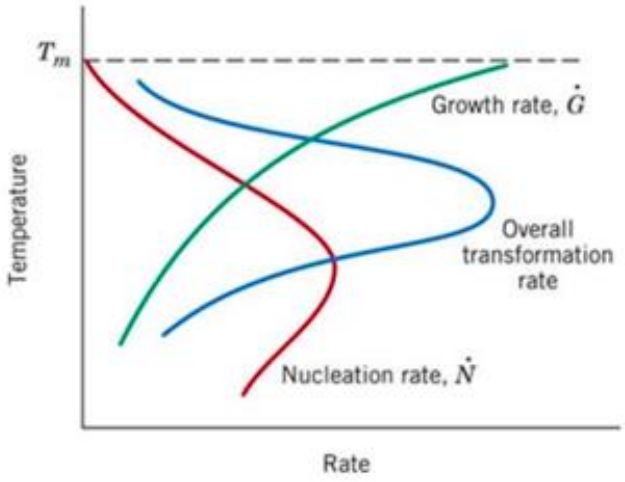

Figure 18. Schematic plot showing curves for nucleation rate ($\dot{N}$), growth rate ($\dot{G}$), and transformation rate versus temperature

The total rate showed in figure 18 represents this combined effect. The general shape of this curve is the same as for the nucleation rate, in that it has a peak or maximum that has been moved upwards with respect to the curve. [8]

TTT diagram

The TTT (Time Temperature transformation) diagram is a representation of the austenite decomposition kinetics obtained by isothermal cooling (constant T that depends on the process and from what we want to obtain) for different durations up to the complete reaction:

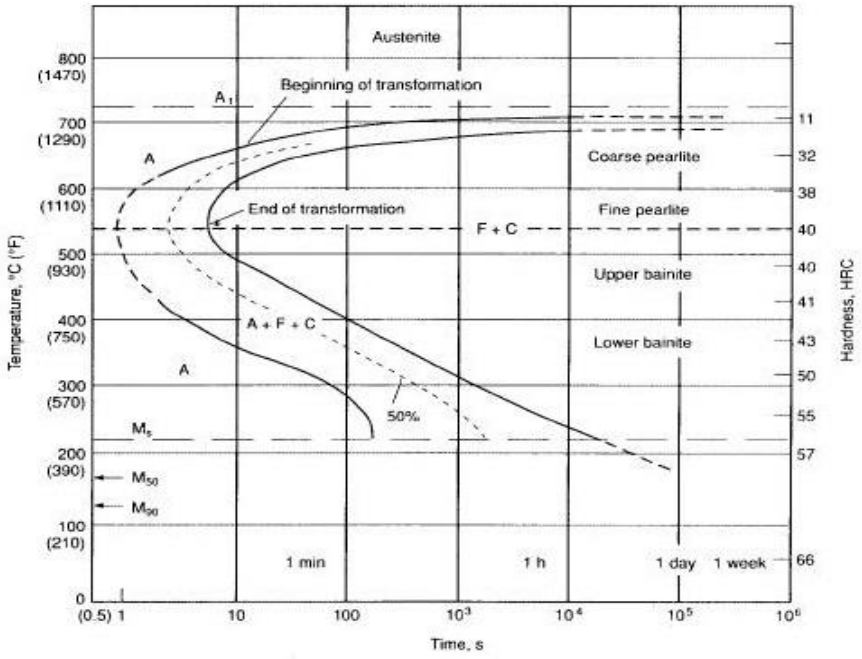

Figure 19. TTT, Time Temperature Transformation (isothermal) diagram for eutectoid steel

This particular diagram is valid only for an iron-carbon alloy of eutectoid composition and the used C75 belongs to this category ; for other compositions, the curves will have different configurations. In addition, these plots are accurate only for transformations in which the temperature of the alloy is held in the duration of the reaction. Conditions of constant temperature are termed isothermal; thus, plots such as Figure 19 are referred to as isothermal transformation diagrams.

This diagram has been taken as a reference for the subsequent successive paragraphs 3.4 (pearlite transformation) and 3.5 (bainite transformation) for the choice of the temperature to be kept constant so as to obtain the desired microstructure to carry out the tests; more information about this microstructure will be explained in these paragraphs.

Considering the cooling at constant temperatures from the graph we have that at higher temperatures (700 ° C) we obtain a coarse perlite, choosing a lower T (600 ° C) to obtain a fine perlite; for temperatures below 500 ° C higher bainite is obtained while for temperatures around 300 ° C there is lower banite. It is also noted that just above 200 ° C there is the beginning of the formation of martensite (Ms), while just above 100 ° C there is complete martensite or martensite finish (Mf).

CCT diagram

Unlike the previous diagram, reference is made to the CCT (continuos cooling transformations) diagram when cooling occurs at increasing speeds as shown in Figure 20:

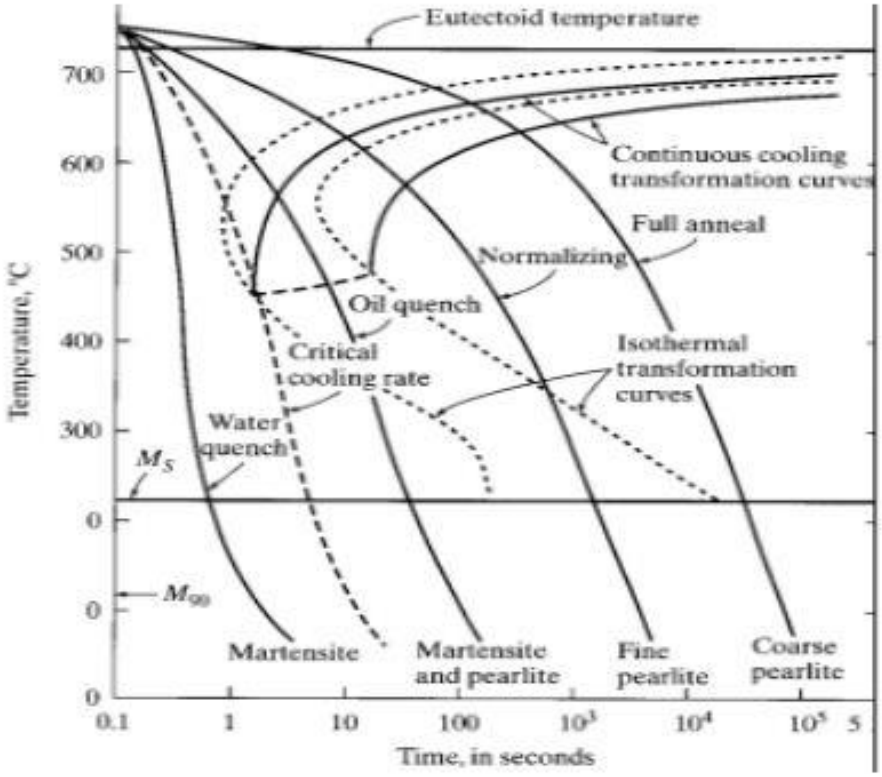

Figure 20. CCT, Continuos Cooling Transformations diagram for eutectoid steel

In the diagram it is possible to see the different heat treatment that we can apply to the samples to obtain certain results; with this conditions, for this type of material (eutectoid carbon steel, C75) we noticed that it is possible to obtain, starting from austenite, martensite or pearlite depending on the heat treatment and type of cooling used.

It is important to mention *the critical cooling rate* which is defined as the minimum cooling speed such that in ambient temperature there is only martensitic structure.

This diagram will be taken as a reference for the following paragraphs 3.2 (hardening and annealing) and 3.3 (hardening and double tempering); in the following paragraphs, the types of heat treatment performed and the parameters used during the test will be analysed with more precision.

CHAPTER 2

INFLUENCES OF NITROGEN CONTENT ON PROPERTIES

2.1 Characteristic, samples used and applications of carbon steel C75

Characteristic of carbon steel C75

The steel used during all the tests is an unalloyed high carbon steel, or spring steel, indicated by designation with C75 (0,75 %); this type of material is the hardest, strongest, and yet least ductile of the carbon steels. Seventy-Five Carbon is obtained by cold rolled annealed strip steel and put in the coils as showed in the figure 21:

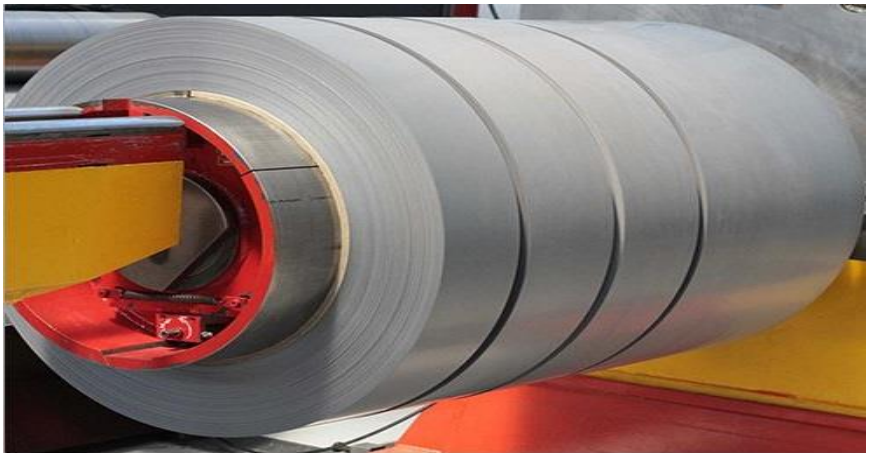

Figure 21. Example of carbon steel coil

C75 carbon spring steel can be easily formed and heat treated, tonnages stocked in a wide thickness range available for immediate processing to widths as required.

From this coil it is possible to obtain carbon steel sheets with a required thickness and width. The range content of the main elements that are present inside, given by the normative, are showed in the table below:

Grade	Carbon Percent	Silicon Percent	Manganese Max Percent	Sulphur Max Percent	Phosphorous Max Percent	Copper Max Percent
(1)	(2)	(3)	(4)	(5)	(6)	(7)
1	0.50--0.75	0.10--0.35	1.0	0.050	0.040	0.20
2	0.60--0.85	0.10--0.35	0.8	0.040	0.040	0.20
3	0.75--1.00	0.10--0.35	0.8	0.030	0.030	0.12
4	0.75--1.00	0.10--0.35	0.8	0.025	0.025	0.12

Table 1 - C75 range content of the main elements [%]

Sample used

In this test we used laminated carbon steel C75 samples with a thickness of the order of millimetre and a width of 5÷6 mm.

As regards the analysis of the influence of the nitrogen content, analysed in the second chapter, 12 samples, marked with a number to allow recognition, selected from 300 samples (some samples are showed in figure 22 below) all from the same coil were chosen:

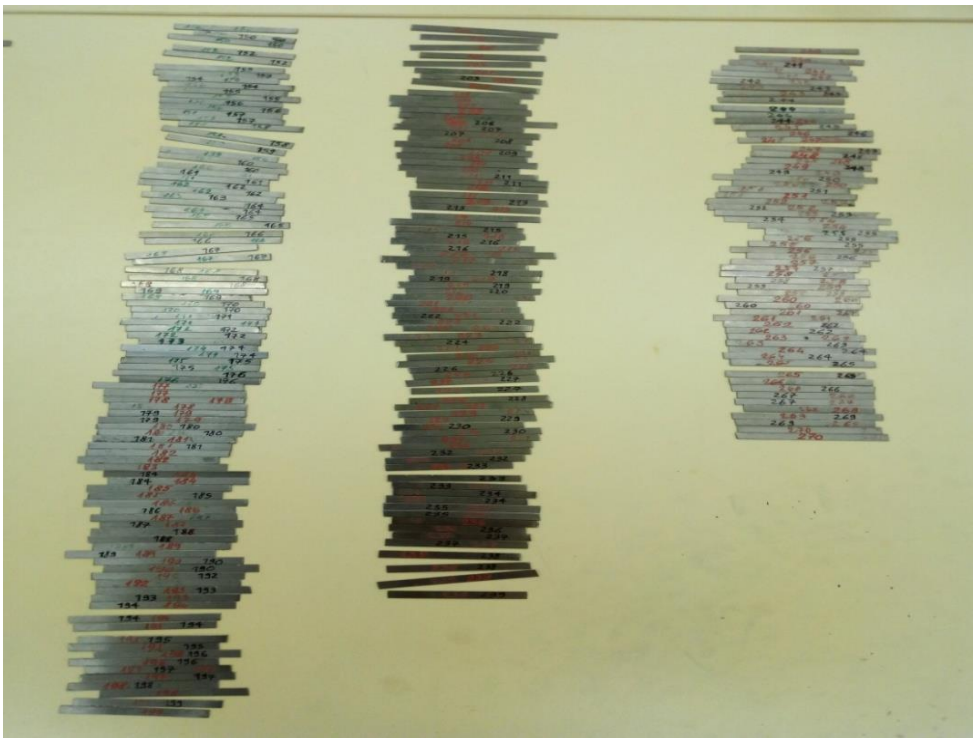

Figure 22. Selection of the samples used

More precisely 24 samples in total were used for this chapter because each of the 12 samples had a copy that was send to an external company to measure the nitrogen content (this process analysis is destructive).

The choice was made based on the nominal values of TEP in order to have a wide range of different values (from 3500 to more than 7000) as to allow for better comparison with the other quantities analysed, each of them having a different content of nitrogen.

As regards to the analysis of the effect of the heat treatments on the different quantities that will be mentioned in the chapter, three the samples used have more or less the same dimension of the samples used before but they came from different boxes, produced by different coil.

More precisely the sample used are categorized per boxes/heat treatments applied, as showed below (the process of heat treatment will be explained better in the third chapter):

- *BOX 0* = 6 different samples from the same coil produced in Austria (good production quality); 2 of this samples were annealed and 4 of them were quenched in water.

- *BOX 1* = 4 different samples from the same coil produced in Austria (bad quality because of some problems in the mechanical deformation that have been noticed by the producing company) were quenched in water and next tempered for two times.
- *BOX 2* = 6 different samples from the same coil produced in Austria (good production quality) were heat treated for obtain a Perlitic structure.
- *BOX 3* = 6 different samples from the same coil produced in Italy (good production quality) were heat treated for obtain a Bainitic structure.

Applications

As a general use steel, spring steel has a wide range of commercial applications.

It is a common material used for manufacturing objects like springs, washers, saw blades, lock picks, antennas, and scrapers.

Figure 23. Examples of washer and springs

Figure 24. Example of a saw by Irwin company and an antenna

2.2 Nitrogen content

The purpose of chapter 2 is to verify any correlations between the different nitrogen content present in the various samples and the properties, specifically the TEP, the magnetic quantities and the Vickers hardness.

As described in chapter 1, 12 samples with different nitrogen contents were available, but they were in double copy (indicated with a *b*) or rather having the same nitrogen content (24 total of which 12 with different nitrogen content); the second copies of each samples were sent to a Hungarian company, the Dunaferr laboratory, for the analysis of the exact nitrogen content. This nitrogen content test is destructive so the remaining 12 samples (indicated with an *a*) were used for tests and evaluations.

The table 2 below shows the 3 nitrogen values obtained from the test for each selected specimen; an average of these values is made, in some cases omitting values that are very discontinuous from the other two, in such a way as to have a more relevant response to reality:

	Content of Nitrogen (%)			
n° sample	1	2	3	**Average**
2b	0.01	0.0109	0.0099	0.01
6b	0.0128	0.0129	0.013	0.0129
17b	0.0083	0.008	0.0085	0.0083
18b	0.012	0.0118	0.0128	0.0119
24b	0.0094	0.0099	0.0091	0.0095
44b	0.0113	0.0108	0.0109	0.011
73b	0.0091	0.0087	0.0092	0.009
186b	0.0083	0.0084	0.0104	0.0084
203b	0.0107	0.0105	0.0111	0.0108
215b	0.01	0.0098	0.0104	0.0101
259b	0.0093	0.0087	0.009	0.009
261b	0.0112	0.0105	0.0115	0.0114

Table 2 – Content of Nitrogen and TEP values

We then proceed to the description of the results as regards the various tests comparing them with the content of Nitrogen (expressed in %) obtained and next we make a final comparison between the quantities.

2.3 TEP results

Tests were performed on the thermoelectric power value of the 12 samples with the procedure and precautions described in chapter 1 (*Section 1.2 – TEP test*).

Thus, obtained the 4 values of TEP [nV/°C], one for each position, for each sample, an average of these values was made; this average was used in the graph 1 with the values of the nitrogen content to check if there is any correlation:

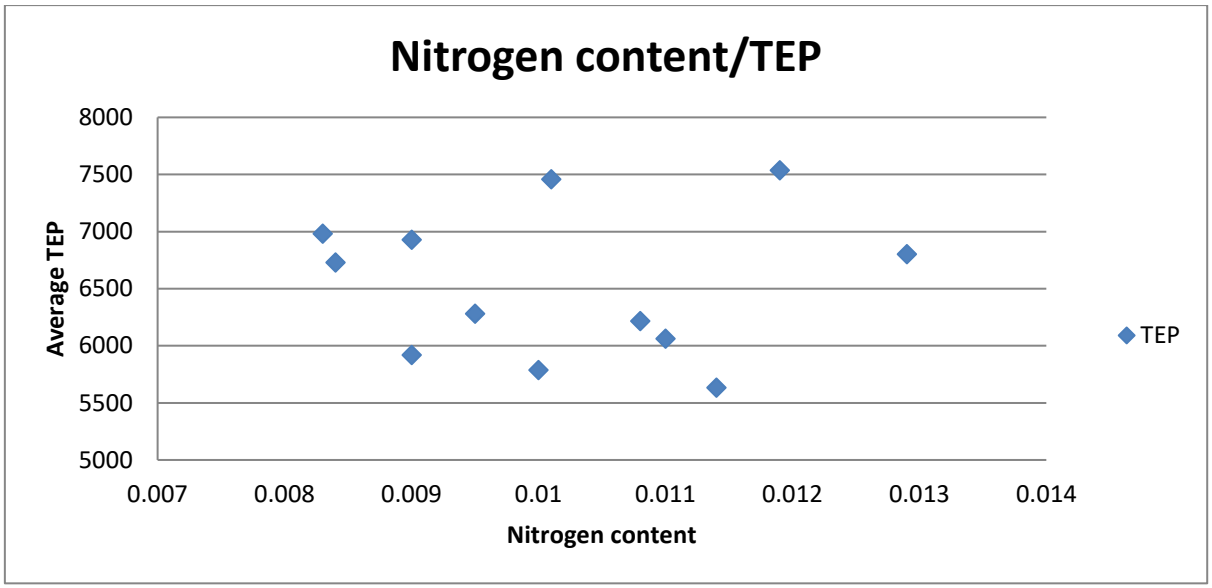

Graph 1 – Nitrogen content and TEP

As it can be seen, the TEP values obtained vary a lot from sample to sample; this happens because the samples come from the same production reel but they were cut in different points. The fact that the TEP values are so different helps us in the analysis of comparison with the different nitrogen contents present in the samples.

Analyzing the graph, we note that no correlation was found between the nitrogen content and the TEP values.

2.4 Magnetic results

Magnetic size tests were performed on the 12 samples with the procedure and precautions described in chapter 1 (*Section 1.3 - AC magnetization test*).

Values of various magnitudes have been obtained such as $B_r[T]$, $B_{max}[T]$, $Hc[A/m]$, μ_i and μ_{max} $[H/m]$ o $[N/A^2]$ in the graphs below:

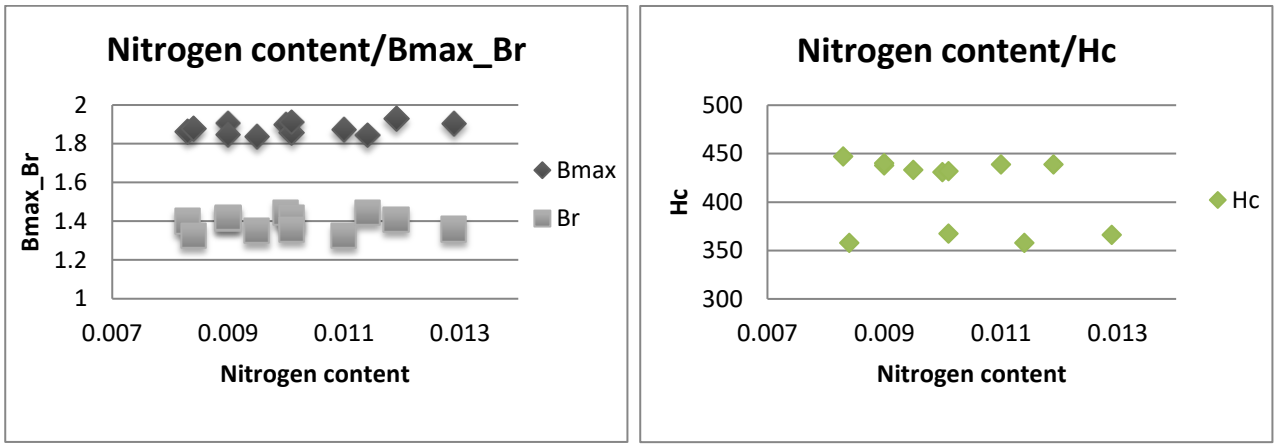

Graph 2 – Nitrogen content compared to Bmax_Br and Hc

From the graph above we note that there is no correlation of the nitrogen content with the coercivity, Hc, while we observe a linear connection between nitrogen content and Bmax and the residual induction, Br.

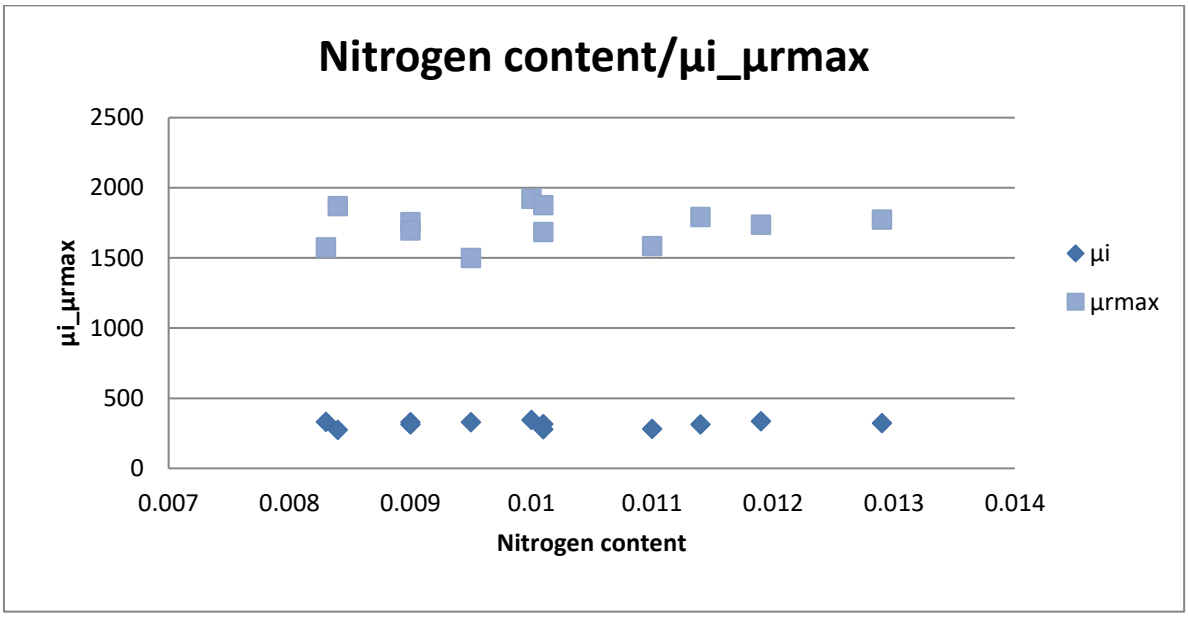

Graph 3 – Nitrogen content compared to µi and µrmax

From graph 3 we note a linear connection of the values between the nitrogen content and the μ_i while there is no correlation with the μ_{max}.

2.5 Hardness HV results

Regarding the hardness tests, it was done using a microhardness testing machine from Buehler company with the parameter described in chapter 1 (*Section 1.4*).

The test is done on 5 different points for each side of each samples and then an average of the values obtained is used in the graph 4 below; each point on the graph therefore corresponds to the average of the Vickers hardness values compared with the nitrogen content present in the sample.

Furthermore, the point of the sample where to apply the indenter to carry out the hardness test was chosen by trying to have the cleanest possible starting surface so as to invalidate the results as little as possible.

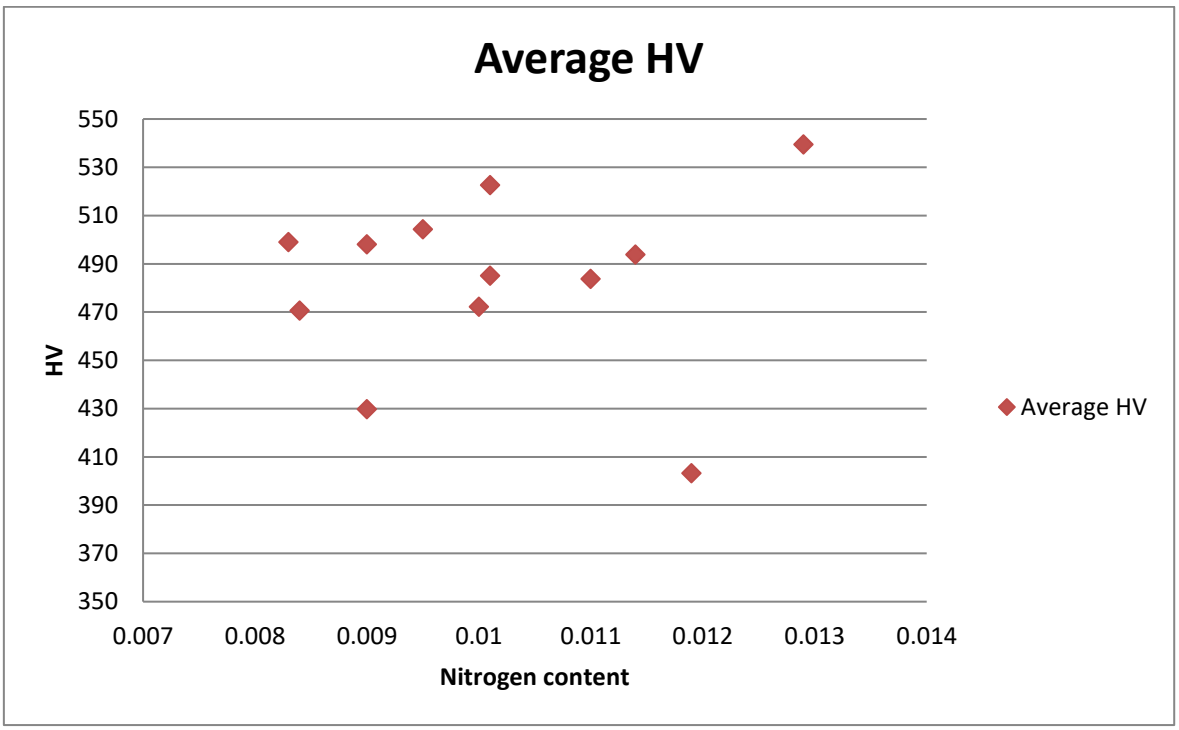

Graph 4 – Nitrogen content compared to hardness Vickers

As it can be seen, the HV $\left[\frac{N}{mm^2}\right]$ values obtained vary a lot from sample to sample; this happens because the samples come from the same production reel but they were cut in different points. The fact that the HV values are so different is useful for the analysis of comparison with the different nitrogen contents present in the samples.

Analyzing the graph, we note that no correlation was found between the nitrogen content and the HV values.

2.6 Comparative results with TEP values

In the last paragraph of chapter 2 some comparisons have been made between the quantities obtained from the tests done previously.

Specifically, the magnetic quantities and the Vickers hardness value will be compared with the TEP values; the comparison will be shown in the following graphs:

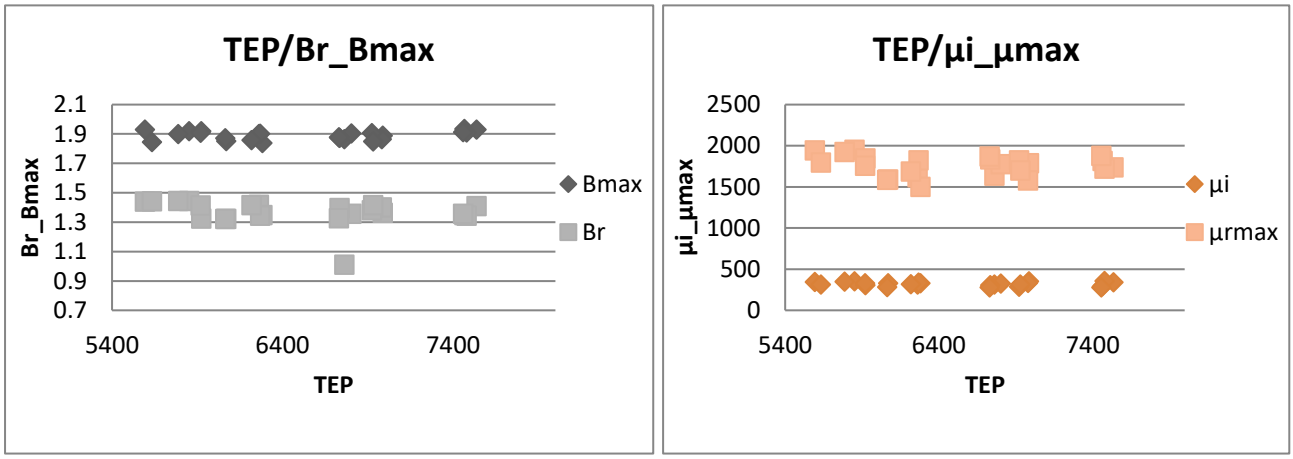

Graph 5 – Correlation between TEP values and Bmax/Br and µi/µmax

Regarding the graph 5 above there is substantial linear connection between the TEP values and the values of Br, Bmax and μ_i, excepted for 1 value of Br (around 1 Tesla) that can be avoided.

The linear connection of the quantities is valid because the differences between this magnetic values are minimal; these differences can be transcended given the use of averages values in the analysis and also possible accidental measurement errors during the tests due to the process or for problems related to the devices used. As far as the μ_{max} is concerned, on the other hand we note that there is no correlation with the values of TEP.

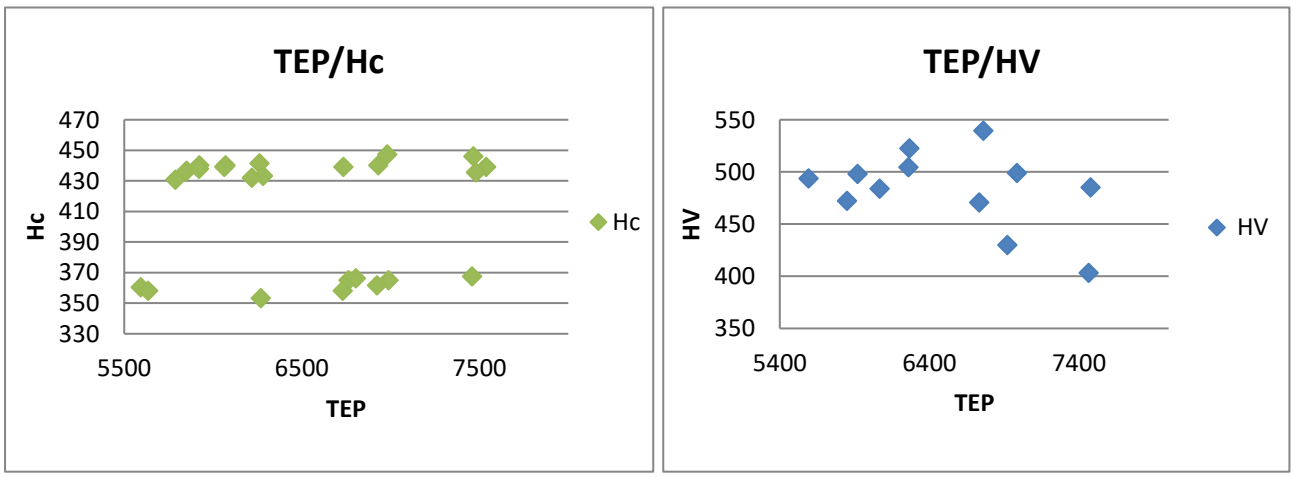

Graph 6 – Correlation between TEP values and Hc and HV

Graph 6 shows a non-correlation between TEP values with coercivity and hardness.

CHAPTER 3
CHANGE OF PROPERTIES AFTER HEAT TREATMENTS

3.1 Quenching and annealing – Box 0

In this paragraph six samples of the BOX 0 are considered (produced in Austria with a good production quality) for the heat treatment; 4 of them have been quenched in water (samples from 0.1 to 0.4) and 2 of them have been annealed (samples 0.5 and 0.6).

Before making the heat treatments on the samples, preliminary TEP and hardness Vickers tests are performed.

The heat treatments used will be discussed below, then the process parameters will be defined; subsequently the test results will be graphed (before and after the heat treatments), the quantities discussed and compared.

Finally, general comparisons have been made between the quantities analysed.

Quenching

The quenching (hardening) heat treatment consists of bringing steel samples at a temperature in the austenitic area and then operating a rapid cooling of the workpieces in water, oil or air to obtain certain material properties. A type of heat treating like quenching prevents undesired low-temperature processes, such as phase transformations. It does this by reducing the timing during which these undesired reactions are both thermodynamically favourable, and kinetically accessible; for example, quenching can reduce the crystal grain size of the metals, increasing their hardness a lot.

In general quenching is most commonly used to harden steel by introducing martensite; in which case the steel must be rapidly cooled through its eutectoid point, the temperature at which austenite becomes unstable.

Of the various microstructures that may be produced for a given steel alloy, martensite is the hardest and strongest and the most brittle; In fact, it has negligible ductility.

To obtain this type of microstructure (martensite) we will refer to the CCT diagram mentioned previously (pieces kept above 723 °C and and cooled quickly in water).

Its hardness is dependent on the carbon content, up to about 0.6 wt%, which plots the hardness of martensite and fine pearlite as a function of weight percent carbon. In contrast to pearlitic steels, strength and hardness of martensite are not thought to be related to microstructure.

Rather, these properties are attributed to the effectiveness of the interstitial carbon atoms in hindering dislocation, and to the relatively few slip systems (along which dislocations move) for the BCT (body-centered tetragonal) structure, whereas austenite has a face-centered cubic (FCC) structure.

Austenite is slightly denser than martensite, and therefore, during the phase transformation upon quenching, there is a net volume increase. Consequently, relatively large pieces that are rapidly quenched may crack as a result of internal stresses; this becomes a problem especially when the carbon content is greater than about 0.5 wt%, as in our case where it is 0,75 wt%.

As regards to the parameter of the heat treatment used, quenching will then be carried out on the 4 samples (from 0.1 to 0.4) with the following parameters:

1. Heating the furnace at T = 800°C (austenitic zone) and putting the samples inside for 6 min
2. Samples Cooled directly in water

Therefore, the total duration of the quenching process is very short, the longer time is spent waiting for the oven to reach the desired temperature.

Annealing

The exposure to an elevated temperature for an extended time period followed by cooling to room temperature at a relatively slow rate is termed annealing; the reason for slow cooling is to allow the carbon in the steel to diffuse out of the austenite and form perlite microstructure, which is soft compared to the martensitic structure obtained with quenching, or cementite.

Ordinarily, annealing is carried out to relieve stresses and increase softness, ductility, and toughness. A variety of annealing heat treatments are possible; they are characterized by the changes that are induced, which many times are microstructural and are responsible for the alteration of the mechanical properties. Any annealing process consists of three stages: heating to a desired temperature, holding at a certain temperature and cooling (usually to room temperature); in this case we also referred to the CCT diagram.

Time is an important parameter in these procedures. During heating and cooling, there exist temperature gradients between the outside and interior portions of the piece; their magnitudes depend on the size and geometry of the piece. If the rate of temperature change is too great, temperature gradients and internal stresses may be induced that may lead to warping or even cracking.

Also, the actual annealing time must be long enough to allow for any necessary transformation reactions; annealing temperature is also an important consideration; annealing may be accelerated by increasing the temperature, since diffusional processes are normally involved. [10]

About the parameters of the heat treatment used, annealing will then be carried out on samples 0.5 and 0.6 with the following parameters:

1) Heating the furnace at T = 800°C (austenitic zone) and putting the samples for 6 min
2) Holding the samples inside of the same furnace with a temperature from 800°C to 350°C for 4h and 30 minutes
3) Cooling them at room temperature for 30 minutes

Therefore, the total duration of the annealing process is about 5h.

Results and comparisons

After the heat treatments the TEP and HV tests were repeated and also the AC magnetic measurement (only after the thermal treatments) were carried out; so about the magnetic measurement, for this box, we will use the values measured after the heat treatments only for the comparison between the other quantities.

It is important to mention the fact that after the heat treatments there was oxidation on the samples, so in order to have a usable surface to perform the tests again an abrasive paper to remove the oxide was used; this process was also carried out after the heat treatments described in the following paragraphs.

The results obtained for the different quantities will be shown below in the graphs comparing with the samples considered, before and after the heat treatments:

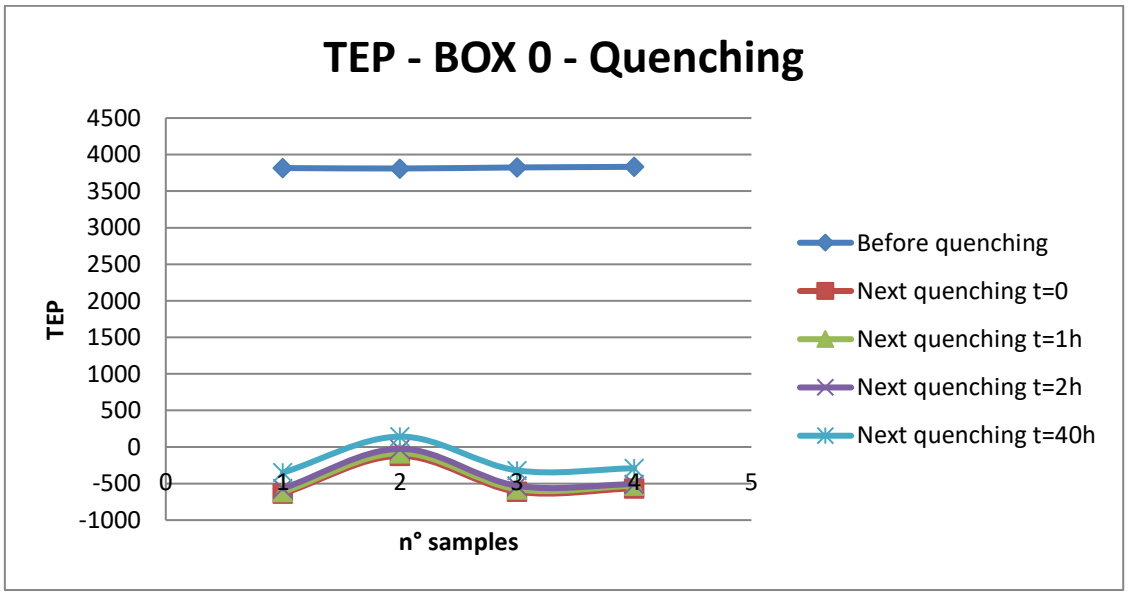

Graph 7 – TEP values about quenching

It has been noticed that after the quenching the TEP value decreases a lot until it reaches negative values; the negative values of the TEP means that the polarity changed.

These major changes are given by the stresses induced by quenching and microstructural changes. After some hours (1h, 2h and 40h) the test has been done again and it is possible to note that the tendency of the TEP values is to grow up. This could be due to slow diffusion and the reverse transformation phenomenon.

We noticed that the 2th sample value can be considered abnormal and not in line with other values so it can be discarded.

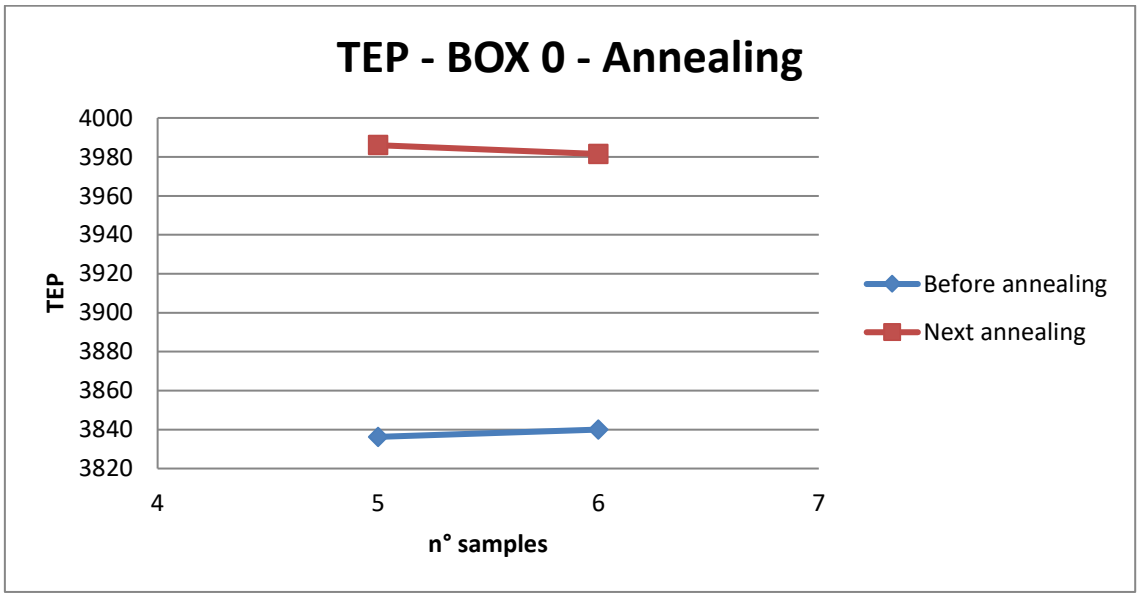

Graph 8 – TEP values about annealing

It has been noticed that after the annealing the TEP value increase a bit.

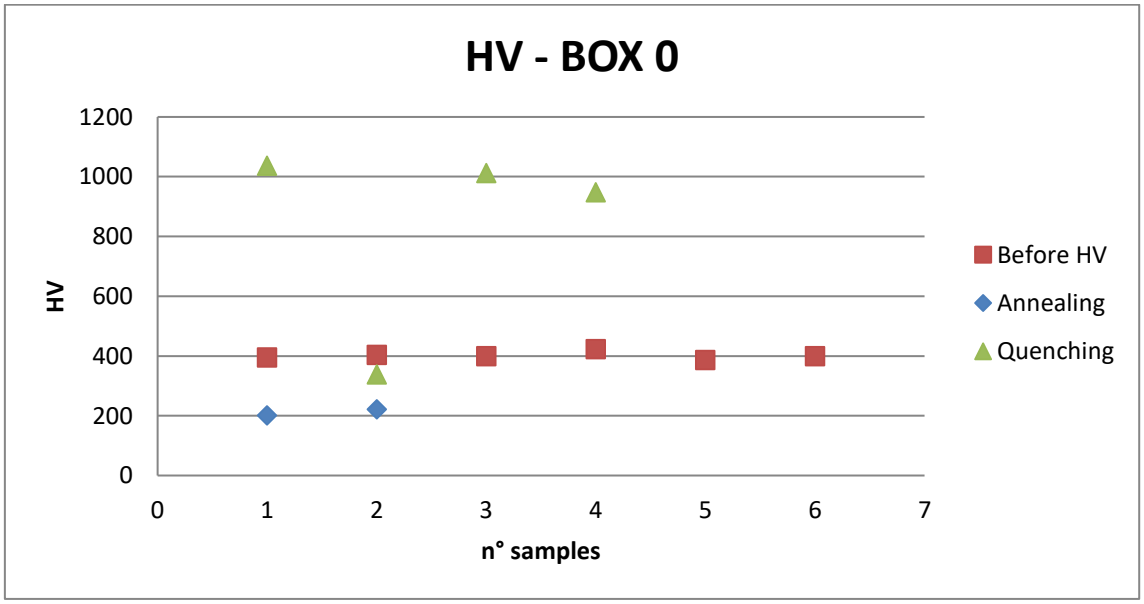

Graph 9 – HV values about quenching and annealing

As reported in the descriptive part of the theory, the results obtained for the Vickers hardness test tell us that after hardening the values increase dramatically and after annealing the values decrease with respect to the starting value.

As in the case of TEP measurements we can discard the 2th samples given the total inconsistency of results with the other 3 samples.

Some comparisons between the magnetic quantities, measured after the quenching, are shown below to verify any correlations with TEP values after the heat treatment; In the evaluation only the quenching values are considered because the annealing was done only for 2 pieces.

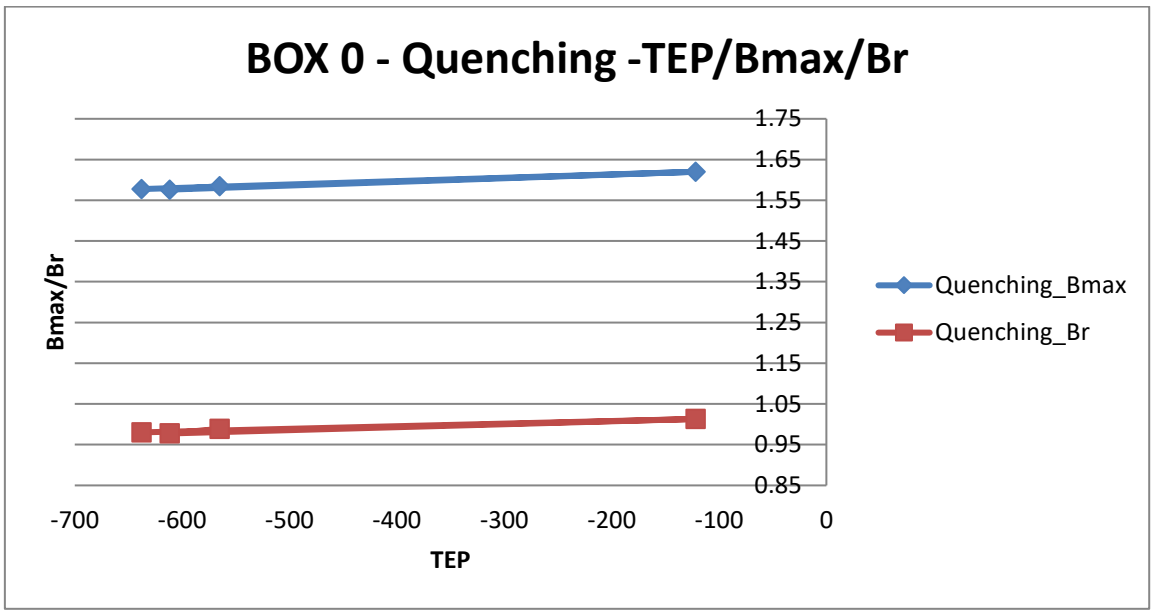

Graph 10 – Quenching Bmax and Br values compared to TEP

In the graph 10 a linear connection between Bmax/Br and TEP values is clearly visible.

It was also verified through the graphs that there are no correlations between the Hc values and the TEP values.

In the graph 11 below it is interesting to see that there is a linear connection between the hardness Vickers and the TEP values:

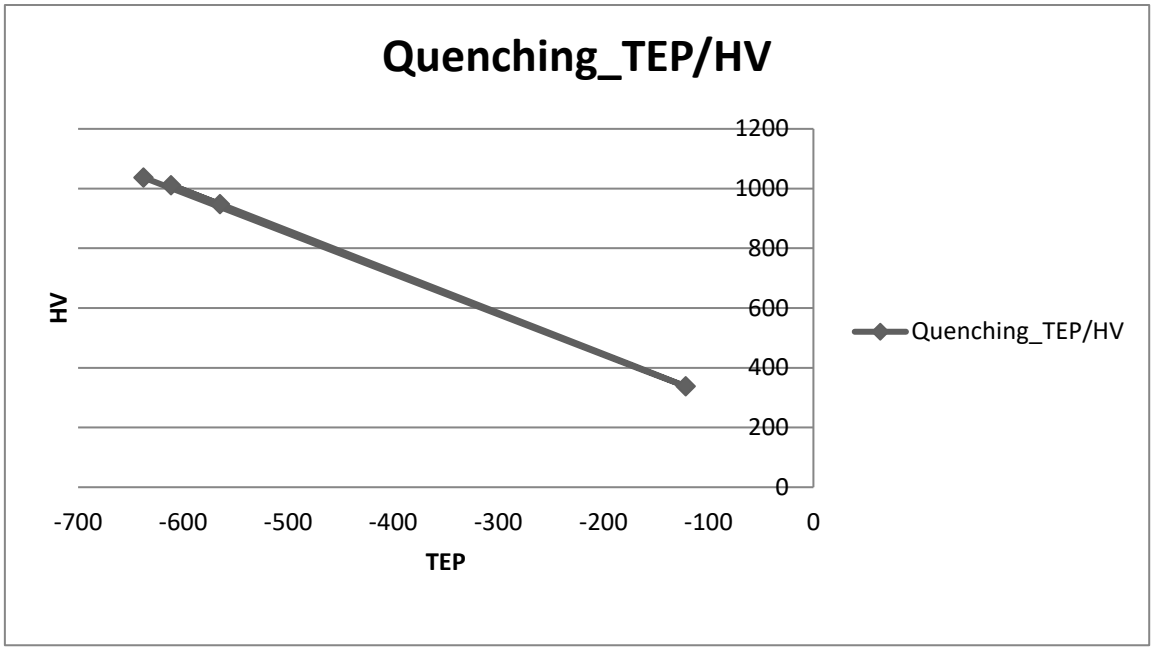

Graph 11 – Quenching HV values compared to TEP

Finally, comparisons have been made between the magnetic quantities Hc and Br measured after the hardening and the Vickers hardness values obtained after the heat treatment:

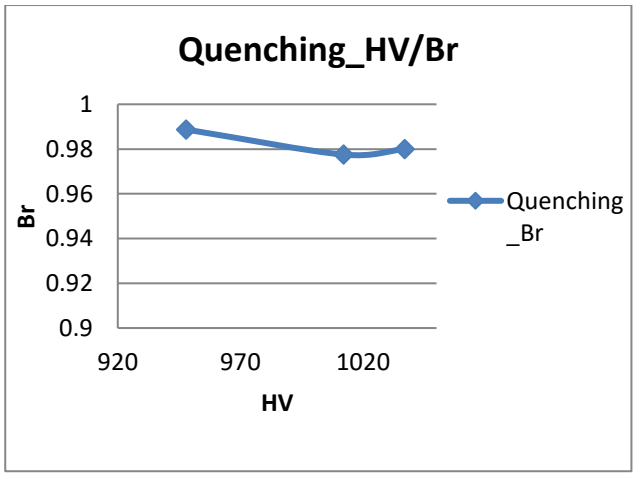

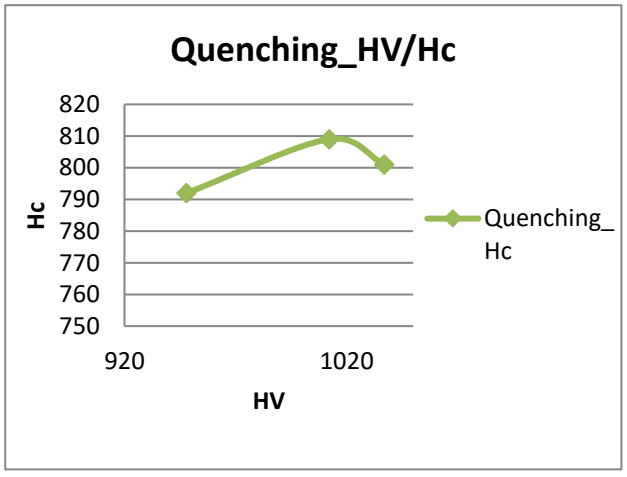

Graph 12 – Quenching HV values compared to Br and Hc

In both cases we note that we can consider that there is a linear connection between Hc and Br and the Vickers Hardness values because the scales used are very short and the values are close.

3.2 Quenching and double tempering – Box 1

In this paragraph four samples of the BOX 1 are considered (produced in Austria with a bad quality because of some problems in the mechanical deformation that have been noticed by the producing company) for the heat treatment; the 4 samples (from 1.1 to 1.4) have been quenched in water and next tempered twice with the process parameters described next.

Before making the heat treatments on the samples, TEP and Vickers hardness tests quantities are measured.

The TEP values are also measured after the quenching, the first tempering and the second tempering to notice what kind of changes are visible; about the other quantities we measured them again at the end of the process, so after the second tempering.

The test results will be graphed (before and after the heat treatments), the quantities discussed and compared.

Later general comparisons have been made between the quantities analysed.

Quenching and tempering

In the quenched state, martensite, in addition to being very hard, is so brittle that it cannot be used for a lot of applications; also, any internal stresses that may have been introduced during quenching have a weakening effect. The ductility and toughness of martensite may be enhanced and these internal stresses relieved by a heat treatment known as tempering.

Tempering is accomplished by heating a martensitic steel to a temperature below the eutectoid for a specified time period; normally, tempering is carried out at temperatures between 250 and 650°C; only internal stresses may be relieved at temperatures as low as 200°C.

This tempering heat treatment allows, by diffusional processes, the formation of tempered martensite, according to the reaction where the single-phase BCT martensite, which is supersaturated with carbon as mentioned before, transforms to the tempered martensite, composed of the stable ferrite and cementite phases.

The microstructure of tempered martensite consists of extremely small and uniformly dispersed cementite particles embedded within a continuous ferrite matrix. This is similar to the microstructure of spheroidite except that the cementite particles are much smaller. Tempered martensite may be nearly as hard and strong as martensite, but with substantially enhanced ductility and toughness.

The hard cementite phase reinforces the ferrite matrix along the boundaries, and these boundaries also act as barriers to dislocation motion during plastic deformation. The continuous ferrite phase is

also very ductile and relatively tough, which accounts for the improvement of these two properties for tempered martensite.

The size of the cementite particles influences the mechanical behaviour of tempered martensite:

- increasing the particle size
- decreases the ferrite–cementite phase boundary area

Consequently, a softer and weaker material is obtained, but harder and more ductile; furthermore, the tempering heat treatment determines the size of the cementite particles.

Heat treatment variables are temperature and time, and most treatments are constant-temperature processes.

Since carbon diffusion is involved in the martensite-tempered martensite transformation, increasing the temperature will accelerate diffusion, the rate of cementite particle growth and subsequently the rate of softening. [11]

As regards the parameter of the heat treatment used, quenching will then be carried out on the 4 samples with the following parameters:

A. Heating the furnace at T = 800°C (austenitic zone), putting the samples for 6 min, next cooling directly in water and TEP measuring
B. 1° tempering at T = 600°C for 30 min, next cooling the samples in water and still measuring TEP
C. 2° tempering at T = 600°C for 30 min, next cooling the samples in water and last TEP measuring are done

Results and comparisons

The tempering test was repeated twice to check if and how changes in the TEP values occur; as regards the other tests carried out it is assumed that the final values of hardness and magnetic quantities of the samples do not change between the first finding and the second.

Also, for this box the AC measurement were made only after heat treatments and therefore these values will be used only for comparisons with other quantities at the end of the paragraph.

The results obtained for the TEP and the hardness Vickers values will be shown in the next page in the graphs 13 and 14 comparing with the samples of the BOX 1 considered, before and after the heat treatments.

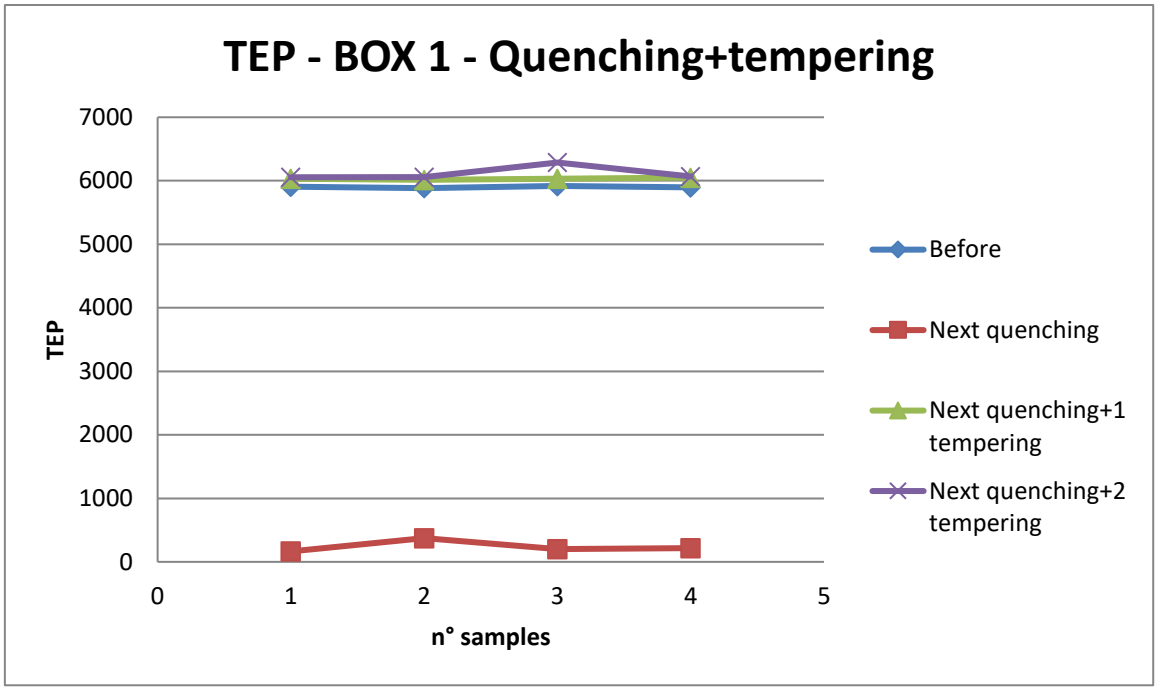

Graph 13 – TEP values about quenching and tempering

We noticed, as before, that after the quenching the TEP values decreases a lot, but it is interesting in this case to notice that after the 1° tempering we obtained the same level of TEP of the beginning before the heat treatment. So we can consider the tempering like a heat treatment that restores the initial TEP values; it is visible from the graph that after the 2° tempering the TEP values are more or less the same after the first tempering so there is no influence of the second tempering on the TEP values.

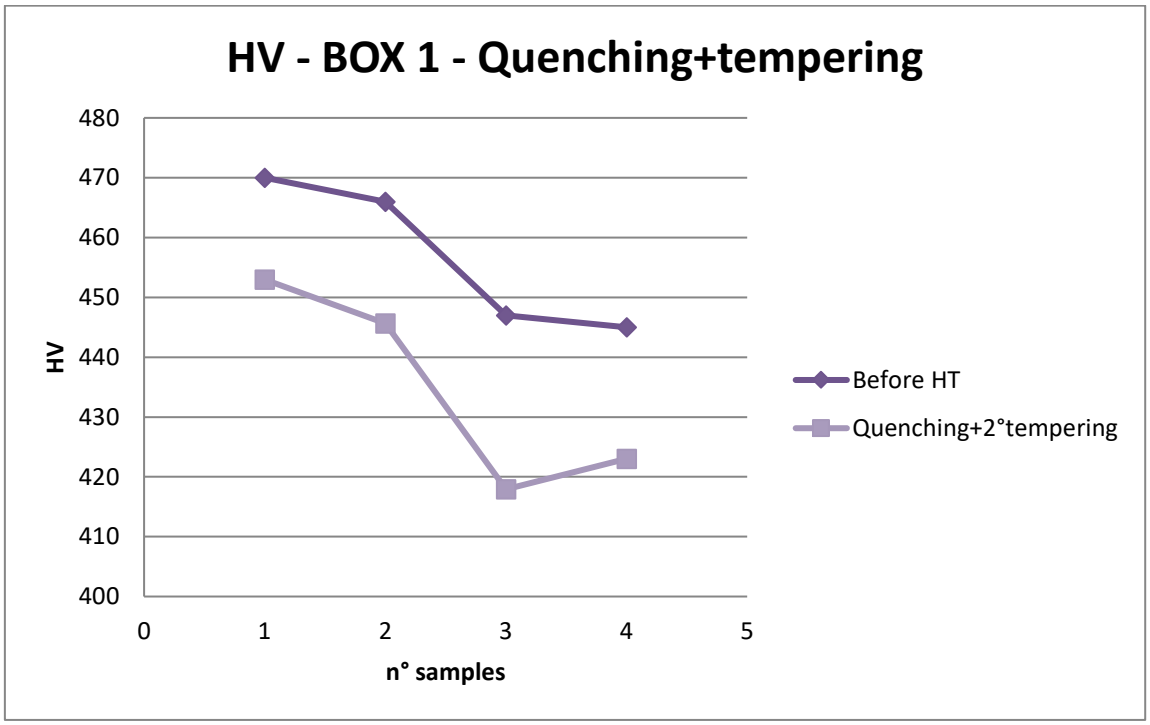

Graph 14 – HV values before the heat treatment and after quenching and 2° tempering

Next to the heat treatment it is possible to say that the values of hardness HV decrease a bit compared to the initial values (because the scale used has neighbouring values); this results respect the literature theory mentioned before. About this evaluation, as the other quantities, we have to consider that the graphs are done using an average values of data collects so the results are always an approximation.

Some comparisons between the magnetic quantities, measured after the heat treatment, are shown below to verify any correlations with TEP and HC values after the heat treatment:

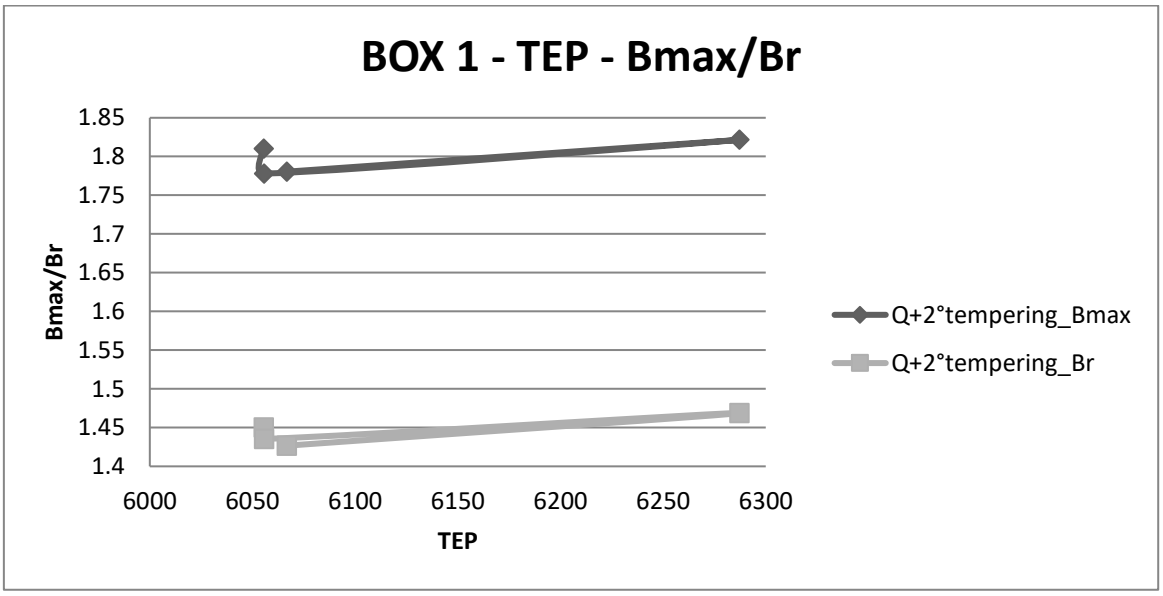

Graph 15 – TEP values compared with Bmax and Br

The values of Bmax and Br show a linear connection with the TEP values measured because of the short scale used in the graph 15; about the TEP values compared with the coercivity Hc there is absolutely no correlation between the quantities as showed in the graph 16:

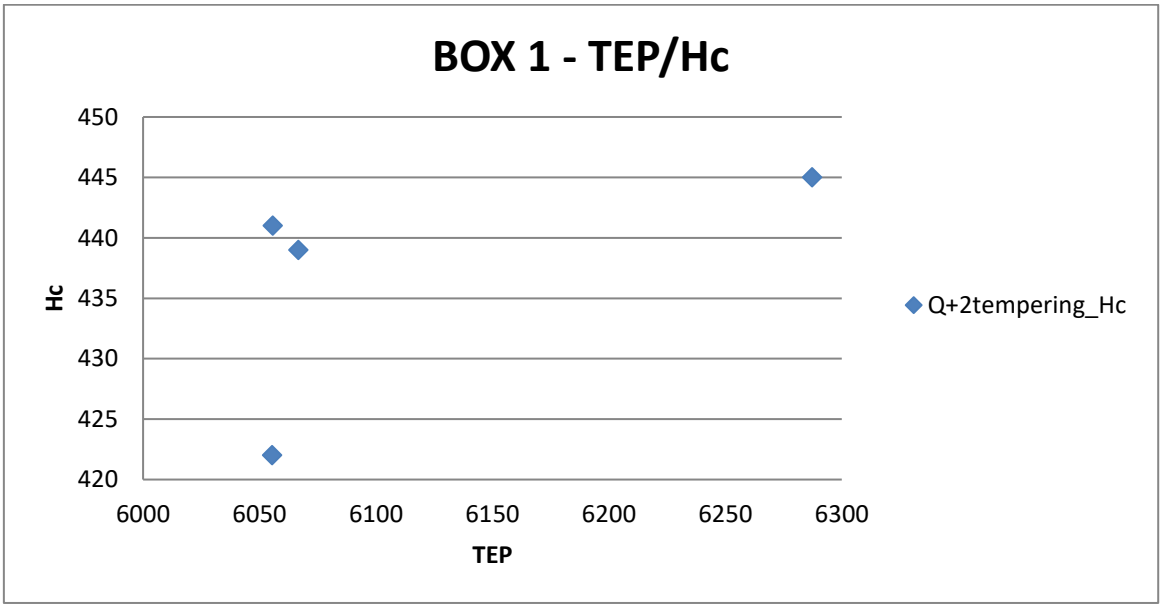

Graph 16 – TEP values compared with Hc

Talking about the hardness values compared to the magnetic quantities Bmax and Br, the results are shown below in graph 17:

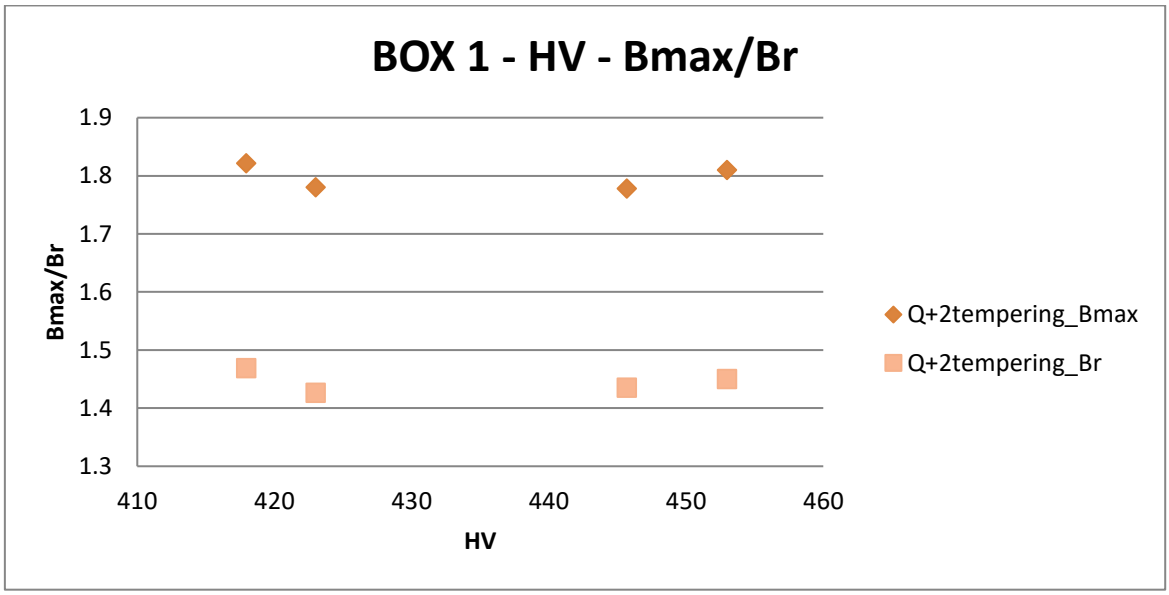

Graph 17 – HV values compared with Bmax and Br

By the graph 17 linear connection between the quantities reported can be noticed.

Once more, concerning the comparison between HV and coercivity Hc, the acquired data showns no correlation between the quantities therefore it was decided not to report the chart to avoid overloading the discussion.

At the end a last comparison is made between TEP and HV values as reported in the graph 18:

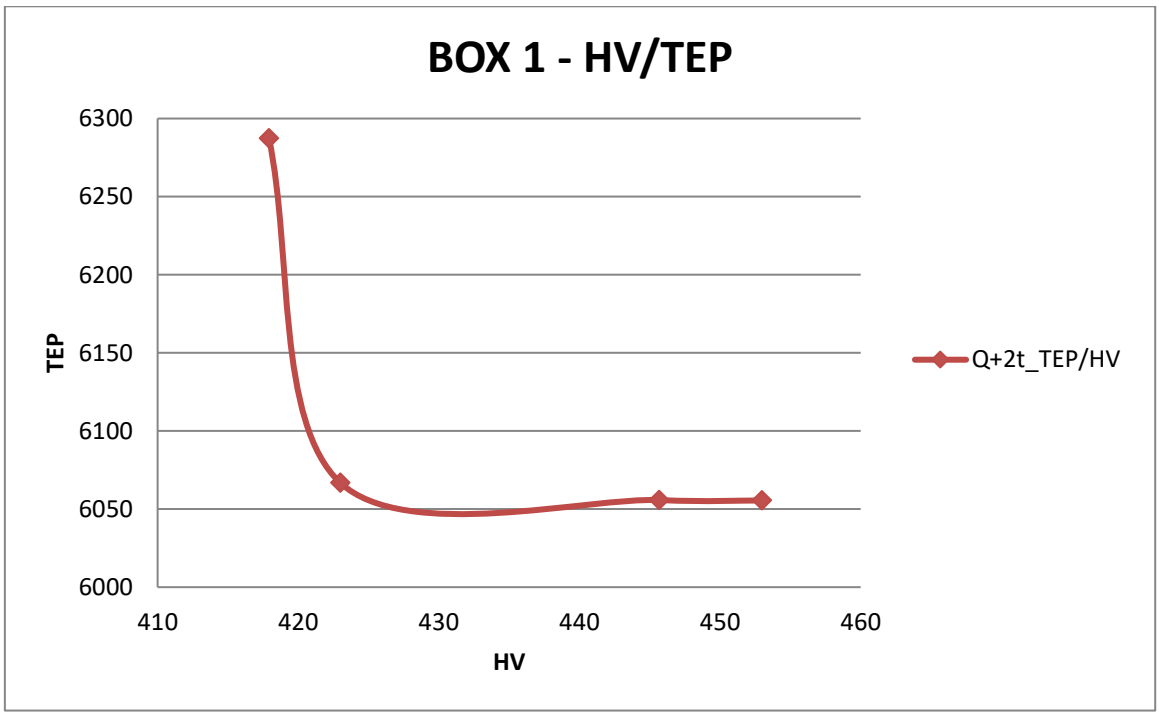

Graph 18 – TEP and HV values compared

In this case it is interesting to note how the two quantities would seem to form a pattern of hyperboles; we can say that a high value of TEP responds to a low value of HV until a certain value of HV where the TEP decreases a lot and tends to remain in this condition even with progressively increasing values of HV.

However this type of result would require many more specimens to be analysed, with different TEP and HV values (for this materials, as we have seen, there are differences in the order of thousands for the TEP values and the hundreds for the Vickers hardness) so as to check whether this trend is respected or not; in this case there are only 4 specimens and the results are not very reliable but it may be interesting for future studies, also for other materials.

3.3 Pearlitic transformation – Box 2

In this paragraph six samples (from 2.1 to 2.6) of the BOX 2 are considered (produced in Austria with a good production quality) for the heat treatment.

Before making the heat treatments on the samples, preliminary TEP, AC measurement for the magnetic quantities and hardness Vickers tests are performed.

In this type of heat treatment, unlike the previous ones, one needs to use two furnaces at the same time, given the desire to obtain a pearlitic structure.

The heat treatment used will be discussed below, then the process parameters will be defined; subsequently the test results will be graphed (before and after the heat treatments), the quantities discussed and compared.

At least general comparisons have been made between the quantities analysed.

Pearlitic transformation

Pearlite is a microstructure which contains a ferrite aggregate, specifically ferrite and iron carbide (cementite), obtained from the direct transformation of austenite by cooling it below the critical point A1 shown previously in the iron carbon diagram (723 °C).

To obtain this type of microstructure we will refer to the TTT diagram mentioned previously (pieces kept at a constant temperature for a different time).

The microstructure of perlite or an eutectoidal alloy is characterized by the regular alternation of lamellas. In the case of perlite, ferrite and cementite alternate.

Perlite starts to form on the edge of austenitic grains with the nucleation of a ferrite crystal. The carbon present is expelled from the ferrite core and the surrounding space is therefore richer. This will then give rise to cementite nuclei that flank the ferritic nucleus.

In the case of coarse perlite lamellae of rough dimensions are obtained if their formation occurs at a temperature just below the critical point A1; It is also possible to obtain very fine grain, termed fine pearlite , if it occurs at lower temperatures.

Cementite generally is much harder but more brittle than ferrite; thus, increasing the fraction of Fe3C in a steel alloy while holding other microstructural elements constant will result in a harder and stronger material; as cementite is more brittle, increasing its content will result in a decrease in both ductility and toughness (or impact energy). The layer thickness of each of the ferrite and cementite phases in the microstructure also influences the mechanical behaviour of the material.

Fine pearlite is harder and stronger than coarse pearlite. Therefore, the strong and rigid cementite phase severely restricts deformation of the softer ferrite phase in the regions adjacent to the boundary; thus, the cementite may be said to reinforce the ferrite. The degree of this reinforcement

is substantially higher in fine pearlite because of the greater phase boundary area per unit volume of material. In addition, phase boundaries serve as barriers to dislocation motion in much the same way as grain boundaries. For fine pearlite there are more boundaries through which a dislocation must pass during plastic deformation; so the greater reinforcement and restriction of dislocation motion in fine pearlite account for its greater hardness and strength.
Coarse pearlite is more ductile than fine pearlite which plots percentage reduction in area versus carbon concentration for both microstructure types. This behaviour results from the greater restriction to plastic deformation of the fine pearlite. [11]

In regards to the parameter of the heat treatment used, we used 2 ovens at the reported temperature and times:

1) Heating the first furnace at T = 800°C (austenitic zone) and putting the samples inside for 6 min
2) Stepping quickly to the second oven that has a temperature of 650 °C; the residence time of each sample is different:
    a. Time sample 2.1→5 min
    b. Time sample 2.2→10 min
    c. Time sample 2.3→15 min
    d. Time sample 2.4→20 min
    e. Time sample 2.5→25 min
    f. Time sample 2.6→30 min
3) Cooling all the pieces in air, at room temperature

Results and comparisons

After the heat treatments the TEP, AC measurement and HV tests were repeated; so about the magnetic measurement, for this box, we will use the values measured also for evaluating the changes before and after the heat treatment, not only for the comparison with TEP and HV values.
Especially after this heat treatment it is important to remove the oxide formed by using abrasive paper; concerning the oxidation of the samples, it was noted that the last samples, those remaining longer in the second oven, have a higher level of surface oxidation compared to the oxidation of the first samples left only a few minutes in the second oven.
Given the process temperatures used, a microstructure with a coarser than fine perlite was obtained, but this will then be better shown in the chapter 4 concerning metallography.
The results obtained for the different quantities will be shown below in the graphs comparing with the samples considered, before and after the heat treatments:

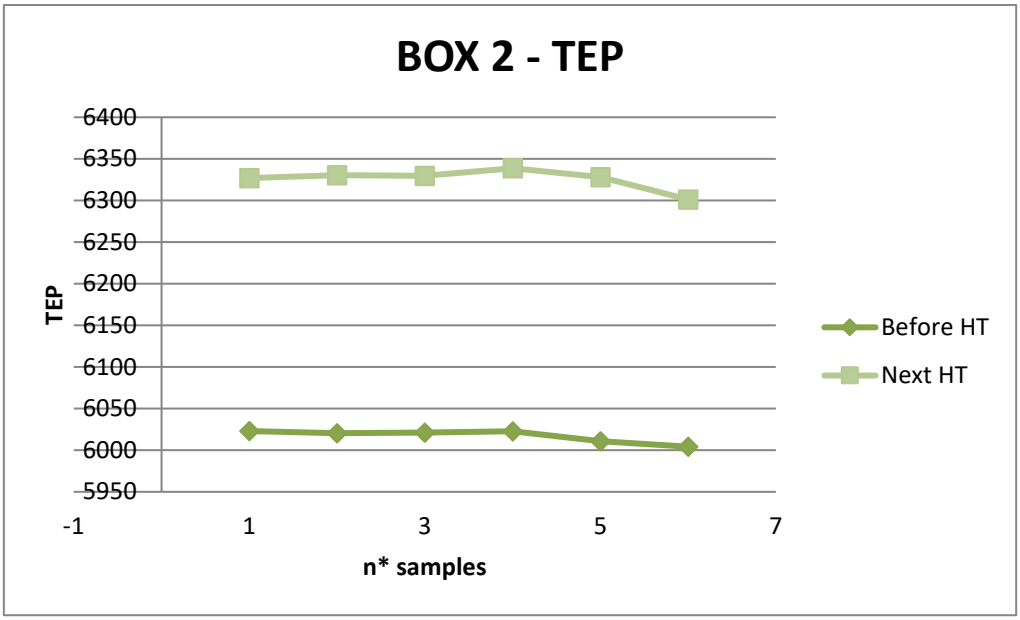

Graph 19 – TEP values before and after the heat treatment

Analysing the graph 19 containing the TEP values obtained before and after the heat treatment we note an increase in the values of the order of a few hundred.

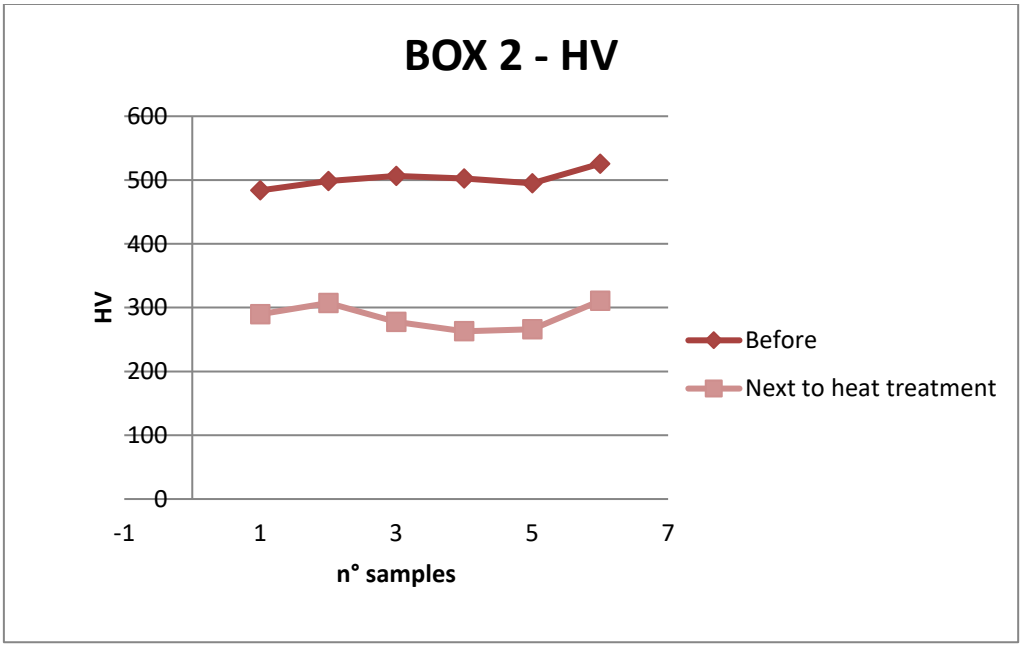

Graph 20 – HV values before and after the heat treatment

On the contrary, however, regarding the Vickers hardness values, a decrease in values is noted after the heat treatment.

Concerning the magnetic quantities, the Bmax values before and after the thermal treatment have not been reported because they are not influenced by the microstructure changes due to the thermal treatment.

Instead, for the residual induction, Br, it depends on the variation of the microstructure and from the graph 21 it can be seen how the values decrease after the thermal treatment.

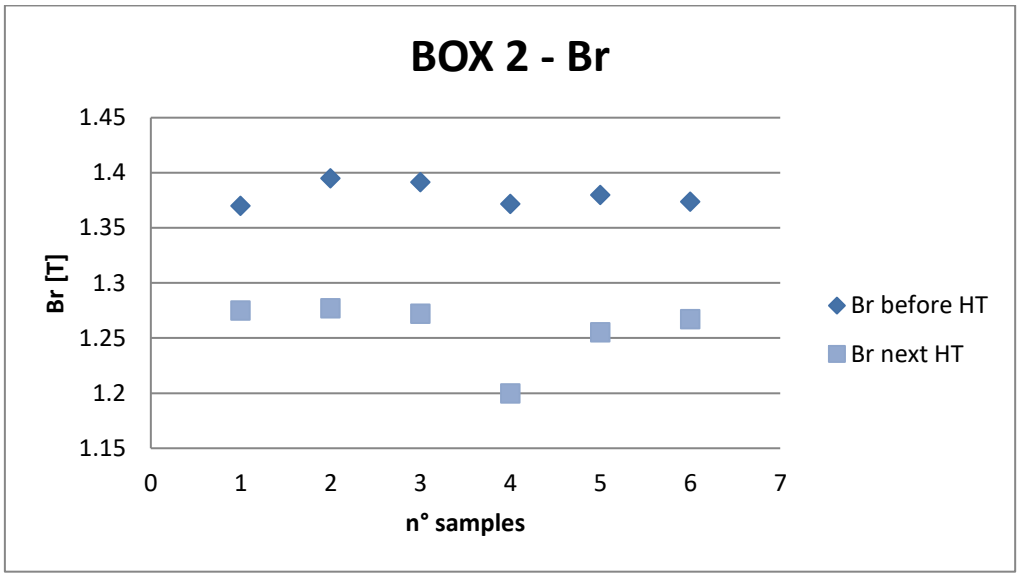

Graph 21 – Br values after and before the heat treatment

A consideration that is useful to make is that in the samples before the heat treatment is present a lot of ferrite and little austenite; after the heat treatment, there is instead a lot of residual austenite which leads to the lowering of the Br. Therefore, the material becomes more paramagnetic after the thermal treatment.

The following graph 22 shows the values of the Hc coercivity:

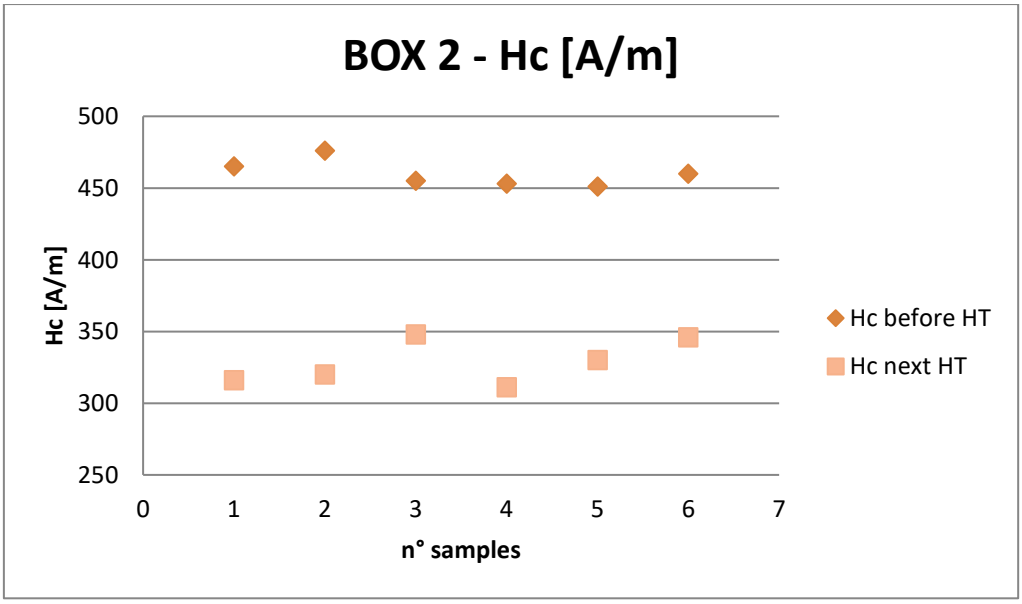

Graph 22– Hc values before and after the heat treatment

It is visible that also the Hc values decrease next to the heat treatment; in this case the decrease is correlated to the decrease of the HV values measured before.

We then move on to the comparisons between the measured quantities, namely the TEP and the HV compared with the 3 magnetic quantities (Bmax, Br and Hc):

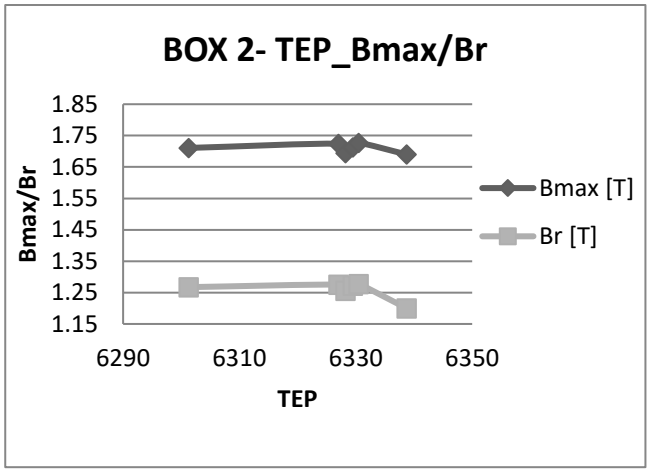

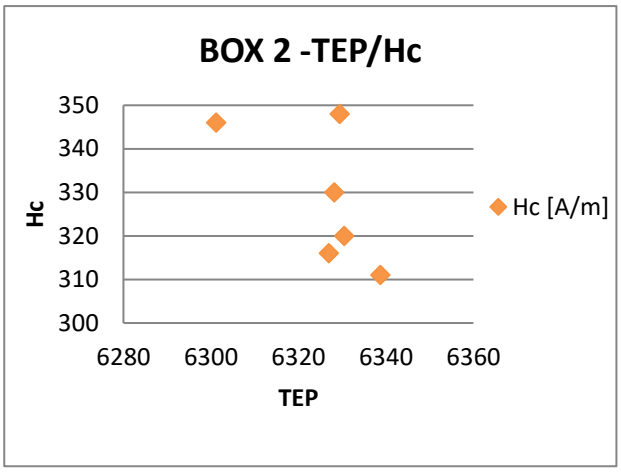

Graphs 23 – TEP values compared with magnetic quantities

We note linear connection between the Bmax and Br values (although some values deviate more from the constant line) and TEP values while there is no relation with the coercivity Hc.

In regards to the HV hardness shown below in graphs 24, there is a linear connection between Bmax and Br compared to hardness Vickers, while an almost sinusoidal trend between coercivity and hardness values is found.

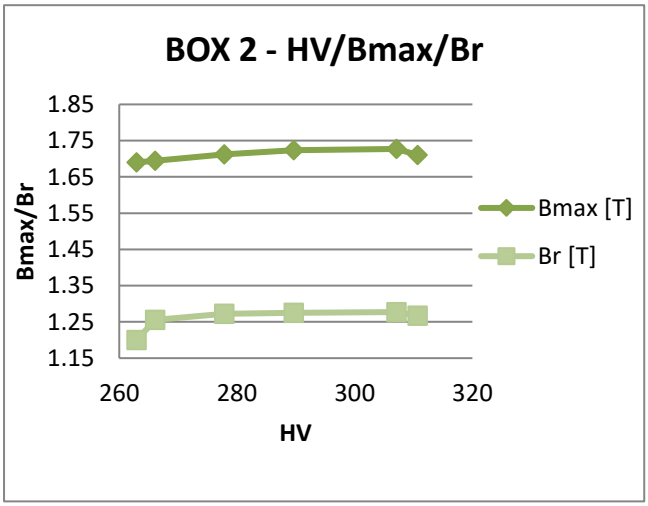

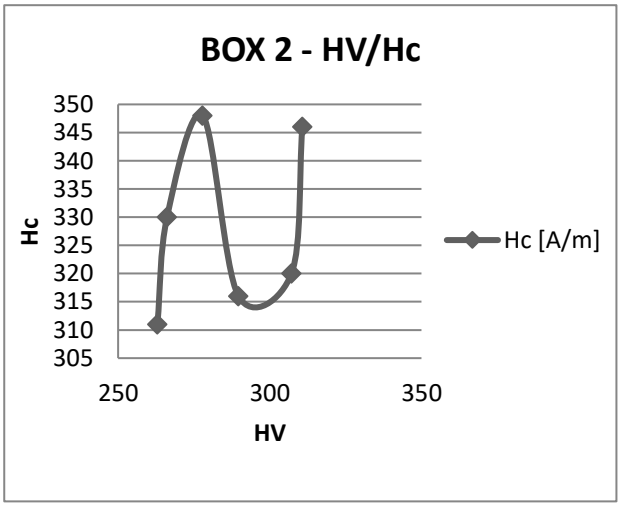

Graphs 24 – HV values compared with the magnetic quantities

The TEP and HV values were also compared but no correlation was found between the quantities.

3.4 Bainitic transformation – Box 3

In this paragraph six samples (from 3.1 to 3.6) of the BOX 3 are considered (produced in Italy with a good production quality) for the heat treatment.

Before making the heat treatments on the samples, preliminary TEP, AC measurement for the magnetic quantities and hardness Vickers tests are performed.

Also in this type of heat treatment, like the previous ones, one needs to use two furnaces at the same time, given the desire to obtain a bainitic structure.

The heat treatment used will be discussed below, then the process parameters will be defined; subsequently the test results will be graphed (before and after the heat treatments), the quantities discussed and compared.

At least general comparisons have been made between the quantities analysed like for the other paragraphs.

Bainitic transformation

Bainite is a particular structure of steel made up of ferrite and type of cementite; it is formed when the austenite is cooled to temperatures lower than those used to obtain a pearlitic structure.

Also in this case we consider the TTT isothermal transformation curves of an eutectoid steel showed previously; if the transformation of the austenite is examined when the temperature (kept constant) is lower than 550 ° C there is the formation of bainite and not more of perlite.

Initially the nucleation and growth of the ferrite, and subsequently that of an iron carbide called carbide-ε, (whose stoichiometry is different from that of the cementite occurs). Ferrite forms at the edge of austenitic grain in the form of a needle, while iron carbide is created by precipitation of carbon at the grain boundary of the ferrite, in an acicular form; the resulting structure is bainite.

When formed by continuous cooling, the cooling rate to form bainite is greater than that required for perlite, but less than that for martensite, in steels with the same composition; the lower hardness of bainite compared to martensite is precisely due to the lack of regularity in the distribution of carbon atoms in the crystal lattice of α iron.

From the TTT diagram the upper bainite is distinguished (it forms over 400 ° C) from the lower one (which forms below 400 ° C); the first has lower mechanical properties than the lower bainite which shows good ductility and toughness associated with hardness and resistance, thanks to the good dispersion of the cementite in the ferrite and to the numerous dislocations.

The upper bainite in fact consists of ferrite lamellae in which long particles of carbide ε are dispersed, while the lower bainite is composed of very thin ferrite needles in which carbide flakes are finely dispersed.

Bainite is generally harder and more ductile than perlite given that at the temperatures at which the bainitic transformation occurs the diffusional motions are very slow and the structures that are formed will be very fine, and will be so much so with the decreasing of the temperature. [12]

As regards the parameter of the heat treatment used, we used 2 ovens at the reported temperature and times:

1) Heating the first furnace at T = 800°C (austenitic zone) and put the samples inside for 6 min
2) Stepping quickly to the second oven that has a temperature of 490 °C; the residence time of each sample is different:
    a. Time sample 3.1→5 min
    b. Time sample 3.2→10 min
    c. Time sample 3.3→15 min
    d. Time sample 3.4→20 min
    e. Time sample 3.5→25 min
    f. Time sample 3.6→30 min
3) Cooling all the pieces in air, at room temperature

Results and comparisons

After the heat treatments the TEP, AC measurement and HV tests were repeated.

Given the process temperatures used, a microstructure with a upper bainite structure was obtained, but this will then be better shown in the chapter 4 concerning metallography.

The samples are oxidized and we must remove this oxidation with the abrasive paper; we noticed that the last remaining samples in the 2nd oven were more oxidized than the other samples.

We have also noticed that it is much easier to remove the oxidation, with the abrasive paper, in these samples than in the samples of BOX 2 that have pearlitic structure; the pieces of this box are more malleable, this is due to the fact that the initial hardness values of these samples were low even before the heat treatment.

The same approach of the BOX 2 is applied for the samples of the BOX 3, so the results obtained for the different quantities will be shown below in the graphs comparing with the samples considered, before and after the heat treatments.

In the graphs 25 and 26, showed in the next page, the TEP and the HV results, of the six samples have been evaluated, before and after the bainitic heat treatment:

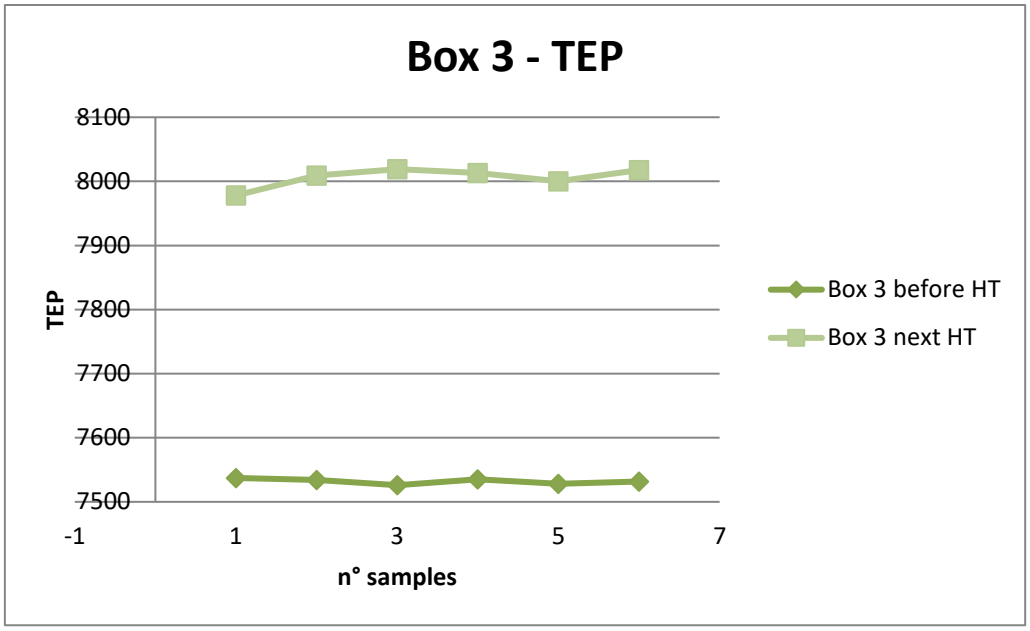

Graphs 25 – TEP values before and after banitic heat treatment

From the graph above a very huge increase of the TEP values is visible, more than the one of the pearlitic heat treatment mentioned before; this can be interesting for improving the material for some applications.

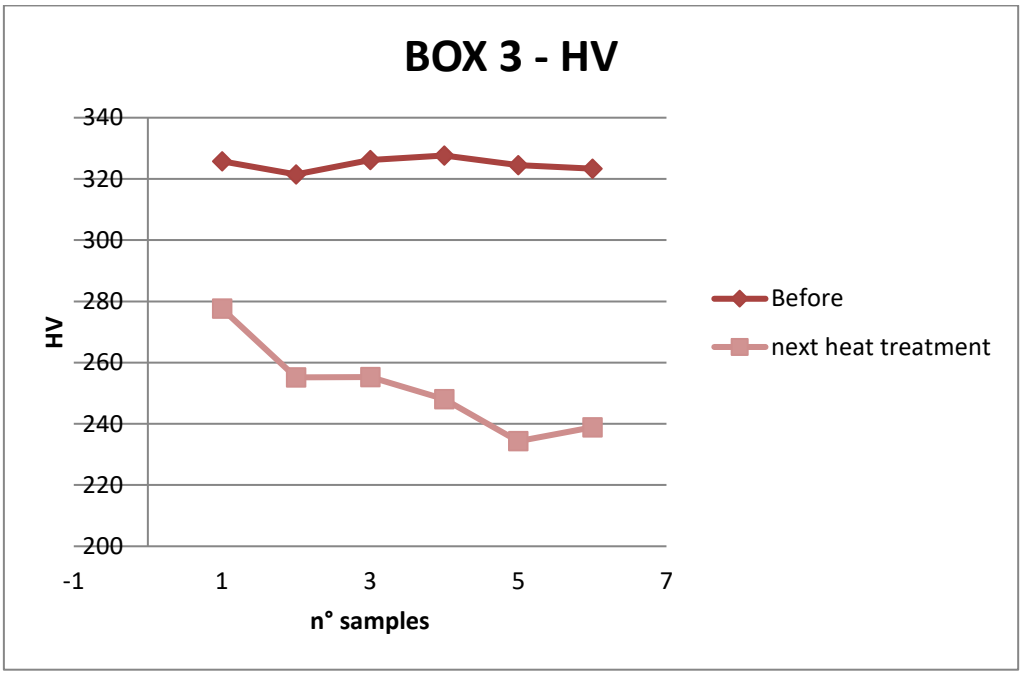

Graphs 26 – HV values before and after banitic heat treatment

About the hardness we notice that the hardness Vickers values decreases after the heat treatment, but they decrease less than the values after pearlitic transformation; these results reflect what was reported in the literature previously.

Regarding the magnetic quantities in the next graphs it is showed how the Br and the Hc values changes after the heat treatment:

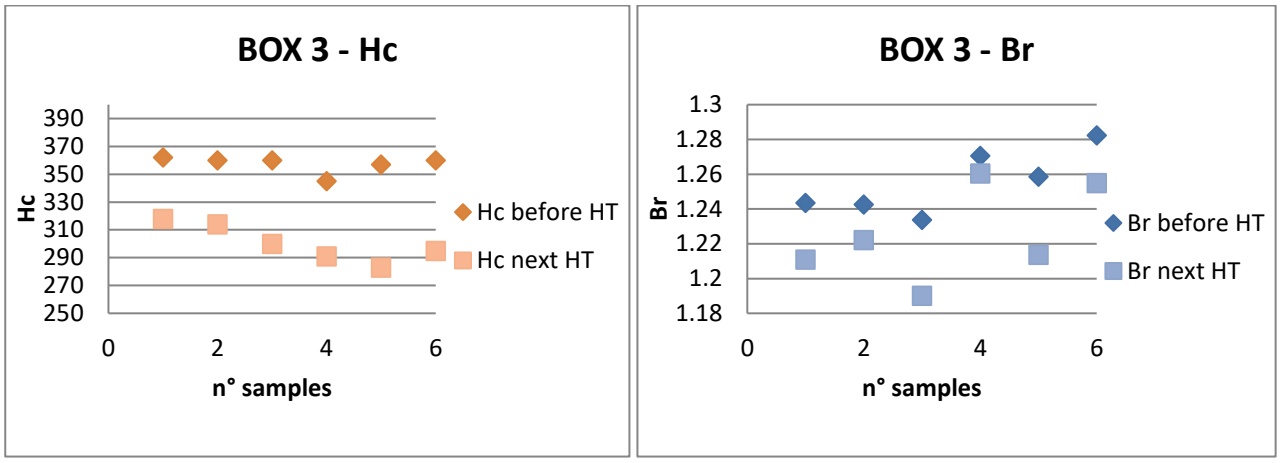

Graphs 27 – Br and Hc values before and after heat treatment

For both of the magnetic quantities shown above it is noticed that there is a small drop in the values after the heat treatment; the reasons are the same as those explained in the previous paragraph, namely that the Br value decreases due to the presence of residual austenite and the material becomes more paramagnetic while the Hc value decreases given the bond of this magnitude with the HV hardness values.

we then move on to the analysis of comparisons between the measured quantities, namely the TEP and the HV compared with the 3 magnetic quantities (Bmax, Br and Hc); different results are obtained:

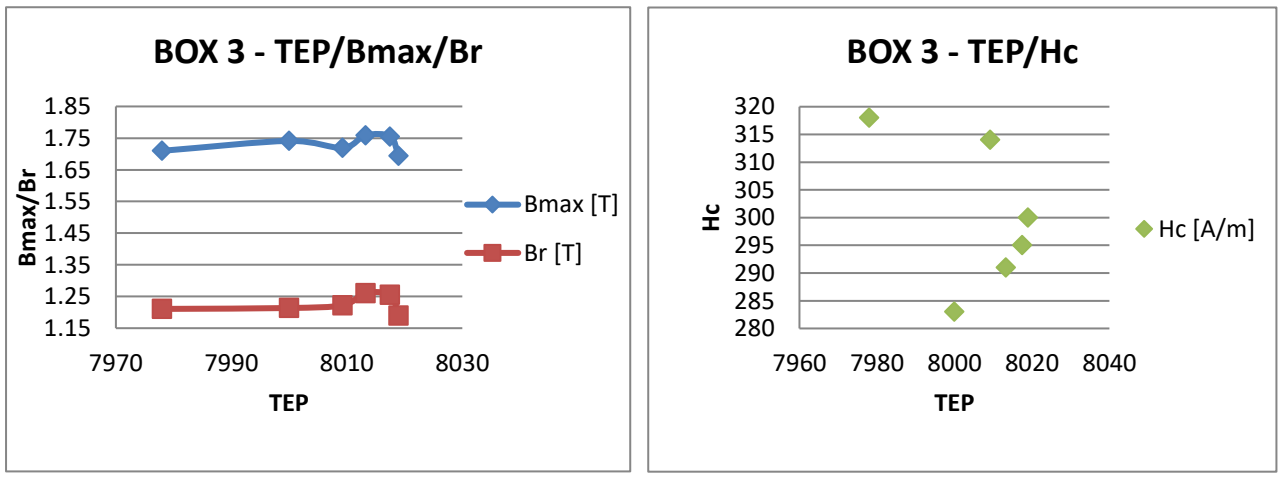

Graphs 28 – TEP values compared with magnetic quantities

Regarding the Bmax and the Br we can see a linear connection of these quantities with the TEP values while no correlation is noted between the coercivity, Hc, and the TEP values.

By analyzing and comparing the hardness values with the magnetic quantities Bmax and Br, it is visible to see again a linear connection between the quantities, with a certain approximation, as shown in graph 29:

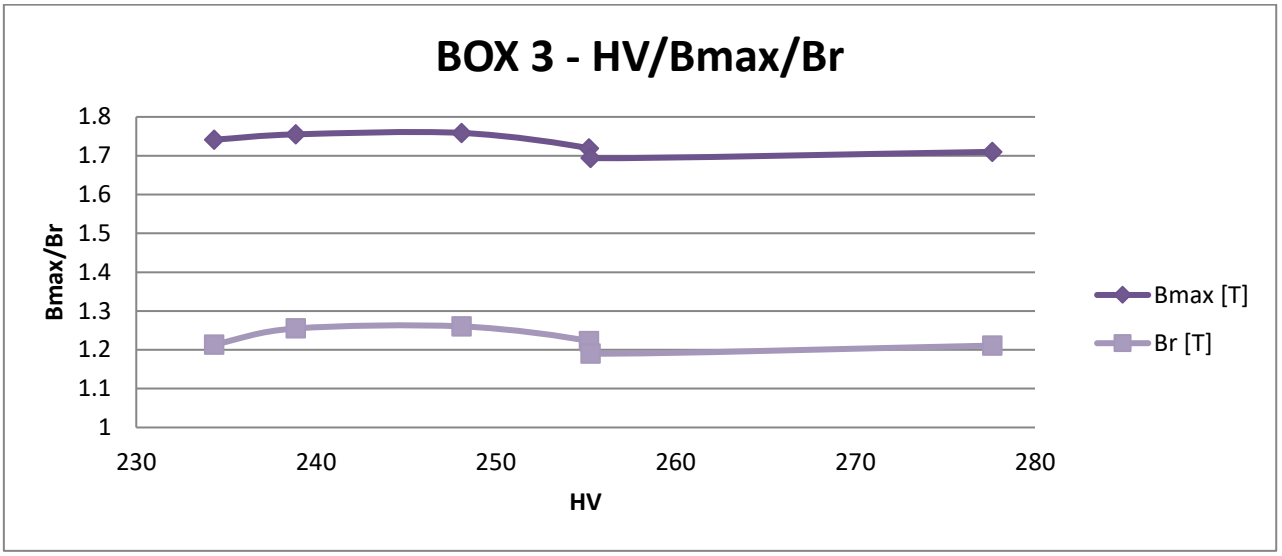

Graphs 29 – TEP values compared

It is interesting instead to see how in the case of Hc the link with hardness can be considered, taking into account that the values reported are all averages and therefore approximations, linear as shown by the line drawn in the average of the values in graph 30:

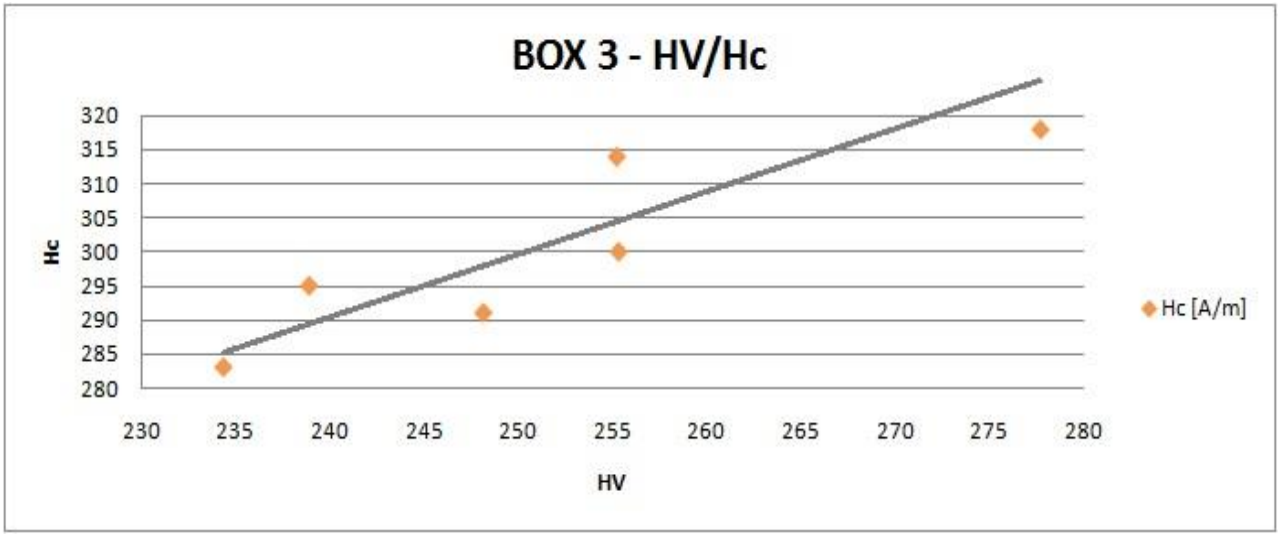

Graphs 30 – Correlation between HV and Hc

The linear connection between these two quantities is the result of an approximation of the data obtained; more samples would therefore be required under the same conditions and more measurements for both tests, to check whether the dependence is respected or not. If this result proves to be founded it could be used for new applications.

Finally, the TEP and HV hardness values were plotted but no correlation was found; therefore, to lighten the discussion, this graph will not be shown.

3.5 Comparisons between results

In this last paragraph of chapter 3 the data obtained before and after all the heat treatments performed and described in the previous paragraphs were compared, referring to all 4 boxes.

Specifically, the magnetic magnitudes of residual magnetic induction (Br) and coercivity (Hc) will be compared with the obtained TEP values and then the same will be compared with the HV hardness values.

The Bmax will therefore be excluded from the analysis since the changes noted do not depend on the microstructural changes brought about by the various heat treatments.

In the last graph then the values of TEP with those of Vickers hardness will be compared.

The first graph 31 analysed contains the TEP values compared with those of Br; it is noted that all the values after the heat treatments and also the preliminary values of TEP and of Br have been considered for BOX 2 and 3, while for the first two boxes the preliminary values of the magnetic quantities are not available:

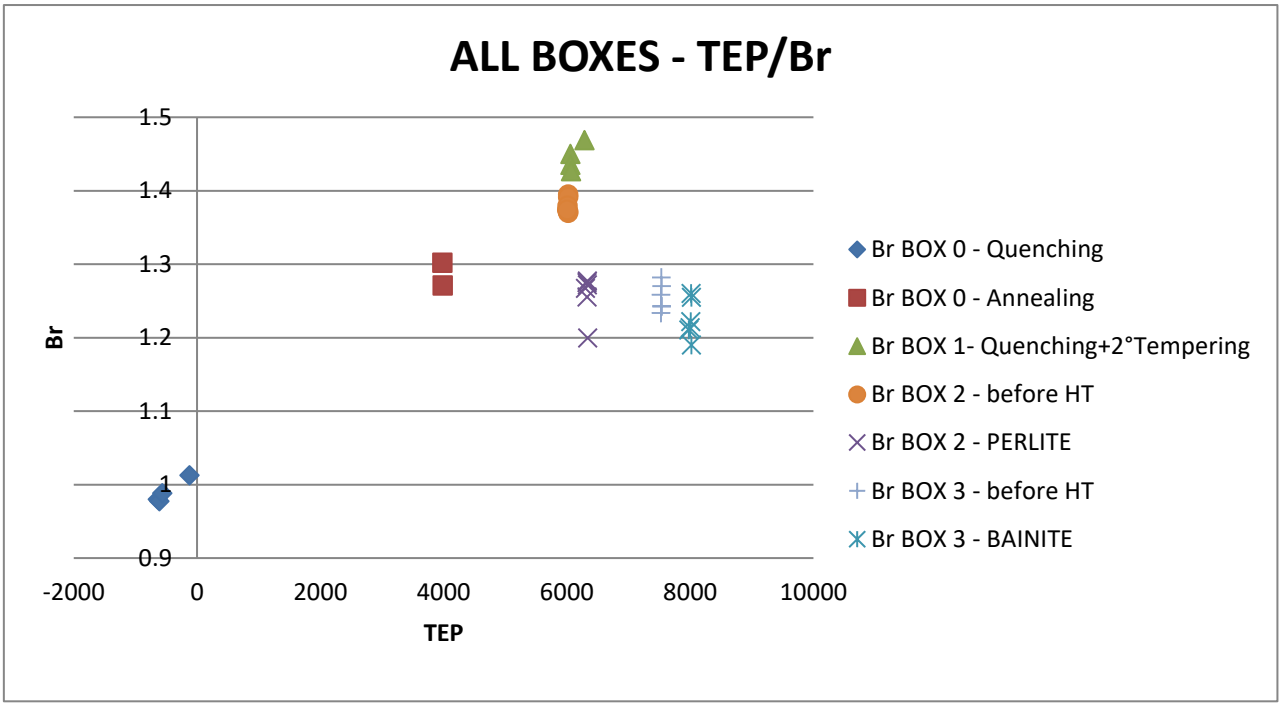

Graphs 31 – TEP and Br values compared for all boxes

As far as BOX 0 is concerned, it can be seen how the samples that were quenched have negative TEP values (and therefore there is the inversion of polarity) and there are very low Br values compared with the other heat treatments; this indicates that the material is more paramagnetic. The annealed samples have average values for both sizes.

The samples of BOX 1 that have been quenched and tempered (2 times) have the highest values of Br, therefore they are the most ferromagnetic materials.

In BOX 2 it is possible to notice how the Br values decrease after the thermal treatment which leads to the formation of perlite, making the material more paramagnetic, while the TEP values grow lightly after heat treatment.

On the contrary in BOX 3 it is noticed how the values of Br remain almost the same before and after the thermal treatment while the values of TEP grow.

It is generally noted that samples with a low TEP value have low Br values.

We then proceed to the coercivity analysis compared with the TEP values, shown in graph 32:

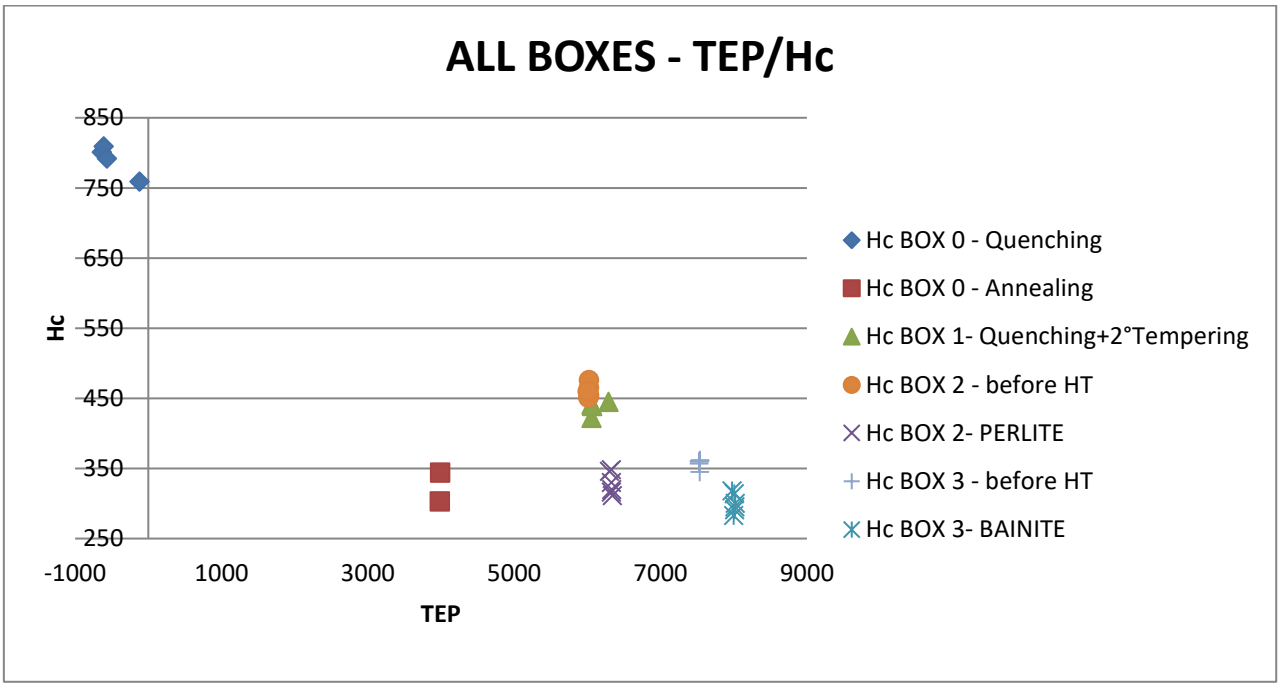

Graphs 32 – TEP and Hc values compared for all boxes

In the graph of coercivity we note how the trend is approximate as opposed to that of the residual induction Br.

In BOX 0 we notice how the quenched pieces have a high coercive value compared with the others while the annealed pieces have average values; from the quenched pieces it can be said that negative values of TEP bring high values of Hc.

The samples of BOX 1 quenched and tempered have higher values than the annealed ones and those of BOX 2 and 3.

With regard to BOX 2 we note that the samples before the heat treatment have higher Hc values while the TEP values grow slightly after pearlitic transformation.

In BOX 3 there is a slight decrease in the Hc values after heat treatment while the TEP values increase.

It is generally noted that samples with a high TEP value have low Hc values.

We will now proceed to the analysis of the correlations between the hardness values and the magnetic quantities Br and Hc, with the same approach that we had for the TEP before.

In graph 33 the correlations between Br and the HV hardness values are shown:

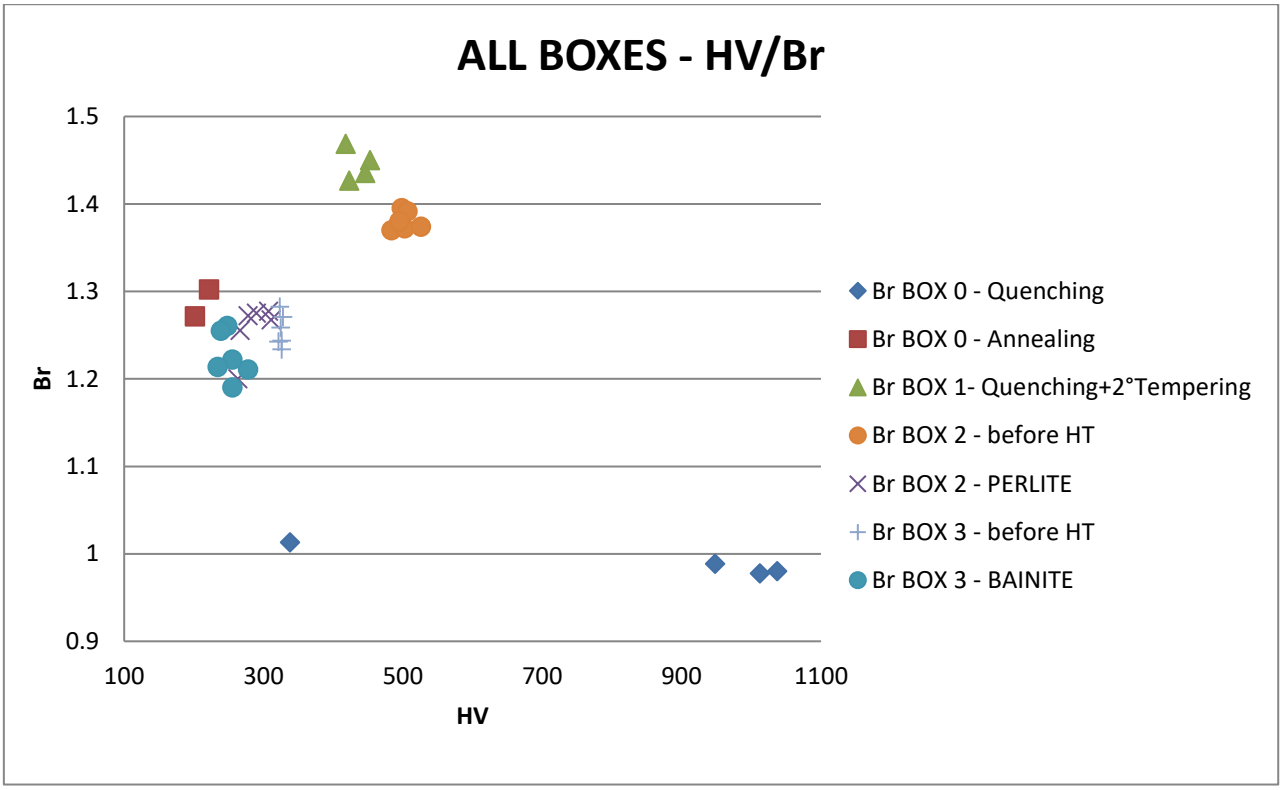

Graphs 33 – HV and Br values compared for all boxes

The graph shows that for the BOX there are high values of Br for the annealed samples with low hardness while there are low Br values for high hardness values obtained from the quenching; for the quenched samples it can be seen how it is possible to exclude the sample 0.2 (which has hardness values around 360 HV) from the analysis because it does not comply with the other results obtained. This exclusion had already been made in the preceding paragraphs in the analysis of other quantities.

For the samples of BOX 1 we have the highest values of Br, so the material is more ferromagnetic than the others.

In BOX 2 it is possible to notice how the samples before the heat treatment have higher Br values, and therefore there are more paramagnetic samples after the heat treatment, and furthermore we note how the HV hardness decreases after pearlitic transformation.

In BOX 3 we note instead that the values of Br remain almost constant while the values of hardness decrease.

We then proceed to the analysis of the link between the coercivity, Hc, and the hardness, HV, shown in graph 34 on the next page:

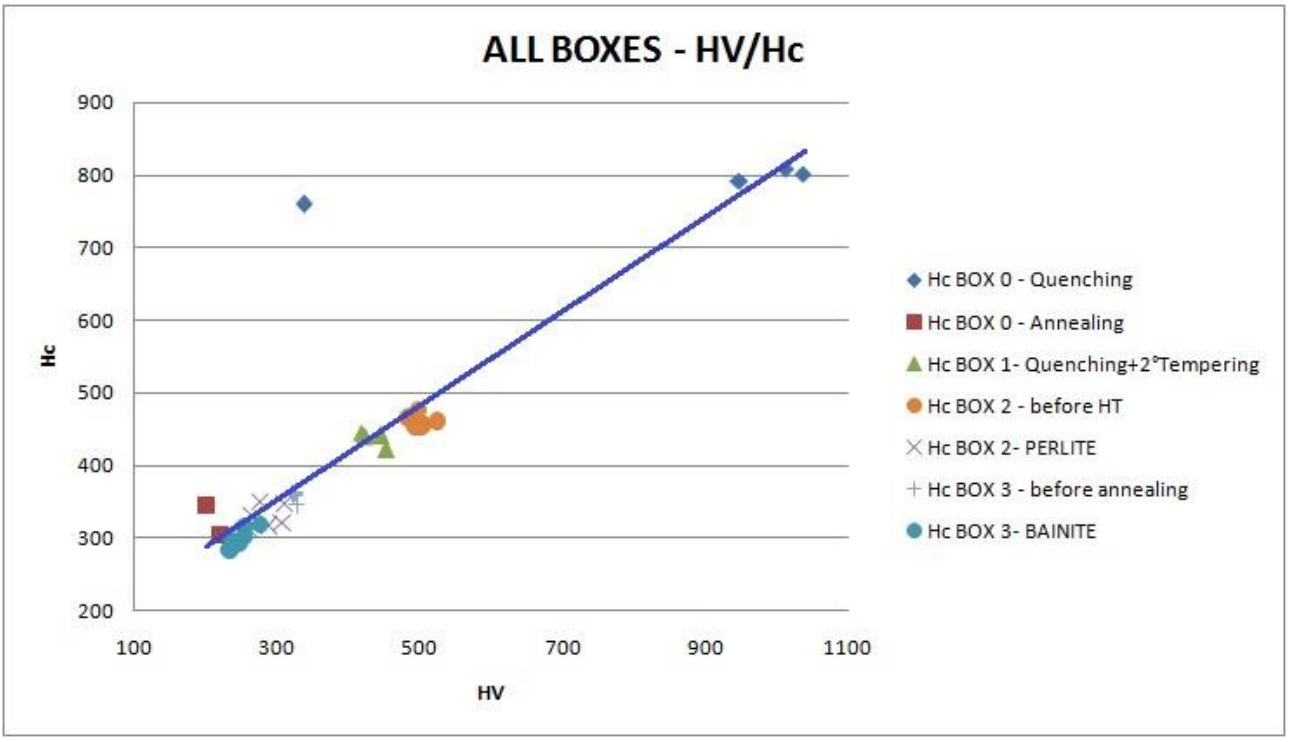

Graphs 34 – HV and Hc values compared for all boxes

From graph 34 we note an interesting link that can be considered, with the due approximations according to the data used that are averages and to possible measurement errors, of linear dependence between the HV and the Hc; this correlation is interesting for possible future applications with C75 steel.

As far as the analysis of the results of the individual BOXES is concerned, we have that for BOX 0 the annealed samples have low hardness and a low Hc value, while those quenched that have a high hardness have a high Hc; also in this case the sample 0.2 is excluded from the analysis due to the total inconsistency with the other results obtained.

The samples of BOX 1 (quenching + 2th tempering) have intermediate values of both HV and Hc, while BOX 2 regards as intermediate HV and Hc initial values before heat treatment, then there is a decrease of both sizes after pearlitic transformation.

Finally, for BOX 3 we note, as for the previous quantities, a slight decrease, after the bainitic transformation, of both hardness and coercivity.

In general, given the results obtained in the previous graphs, we note that Br has a behavior opposite to that of Hc.

The last comparison shown, on the next page, in graph 35 is that between the TEP and hardness values, HV; in this case the values are available both before and after the thermal treatments of all the boxes.

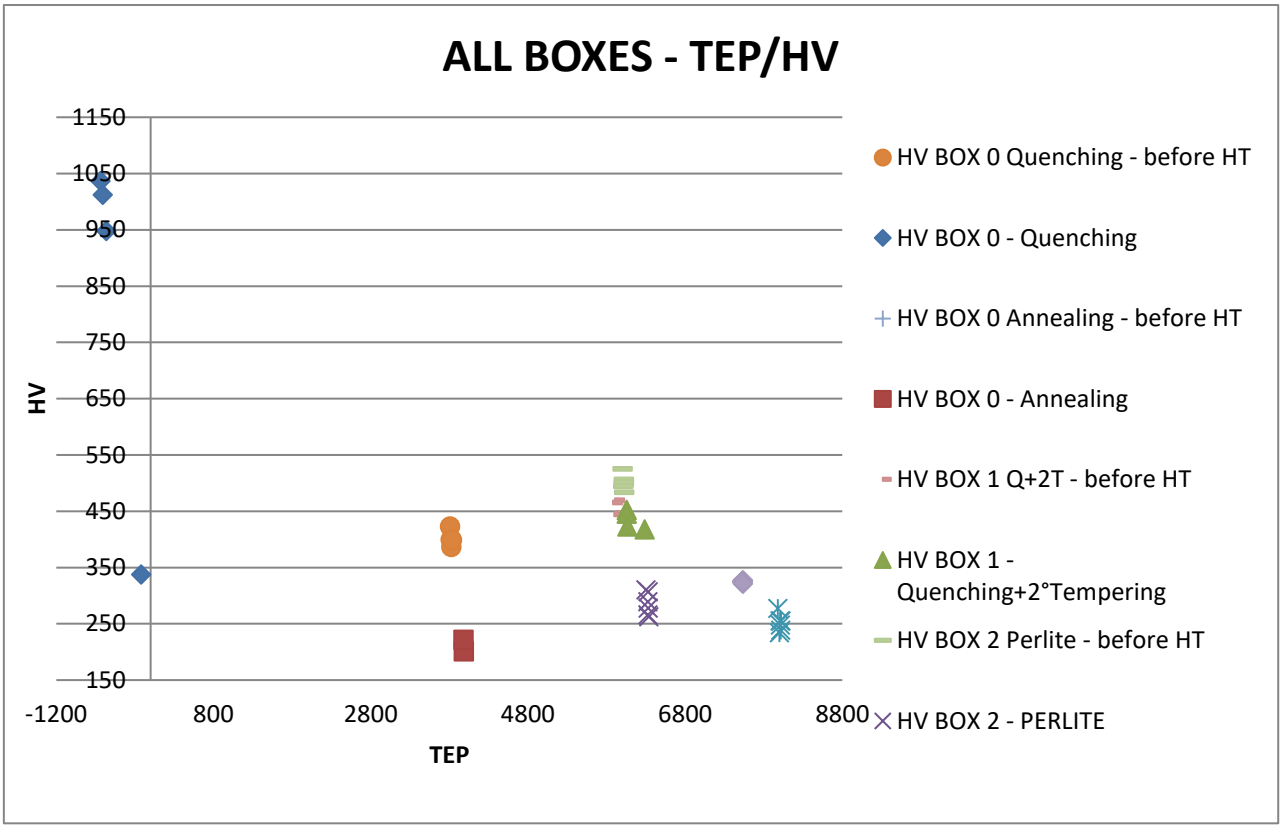

Graphs 35 – TEP and HV values compared for all boxes

From the graph we can see how the quenched pieces significantly increase their hardness values while drastically decreasing the TEP values up to invert the polarity.

The annealed samples, after heat treatment, decrease their hardness values while the TEP grows slightly.

Regarding BOX 1, it can be seen that the values of both TEP and hardness remain substantially the same before and after quenching.

Referring to BOX 2, the transformation of the microstructure into pearlitic instead leads to a lowering of the hardness values and an increase in the TEP values.

Finally, about the BOX 3, the bainitic transformation brings a slight decrease in hardness while bringing an increase in TEP values.

From the graph there are no macro links between the TEP values and the hardness, therefore the correlations are to be found only within the different samples and heat treatments performed.

CHAPTER 4

METALLOGRAPHY

4.1 Methodology

Optical metallography gives us the possibility to observe the internal structure of a metal material or a metal alloy; defects, microstructural aspects and any anomalous features can be highlighted.

The analyses, carried out by means of the metallographic optical microscope (OP), can have different objectives such as determining the conformity of the microstructures, identifying defects and understanding their genesis, verifying the correctness of heat treatments undergone, studying causes and the presence of any degradation phenomena (corrosion).

Fig 25. Optical miscroscope used for the metallography

Often the analyses carried out in optical metallography can be combined with microstructural analyses carried out using the scanning electron microscope but in this case only the optical microscope was used. [13]

The metallography was done on thermally treated samples C75 coming from the four different boxes subjected to the different heat treatments shown in chapter 3; It is important, in order to obtain a specimen that can be well analysed with OM, that several passages are completed with precision. These passages are the cutting of specimen, *mounting*, *grinding*, *polishing* and *etching*.

Starting from the cutting of a specimen, it is important to obtain a small sample of the piece that we want to analyse. There are several cutting methods but generally the piece is cut with abrasives or with a low speed diamonds saw or just mechanically; in this case the mechanical cut has been done.

Mounting is the second step of metallography samples preparation and it is usually done to handle the specimens more easily. The samples can be hot mounted (at around 200°C) but this step can alter the structure, therefore cold mounting, the one that was used in this case, is often preferred.
An original piece (before the heat treatment) and various pieces after the heat treatments were cut for each box. Specifically, we considered the plastic box 0 with the original and 2 pieces of the hardened box; the plastic box 1 with the original and 1 piece hardened and subsequently found twice; the plastic box 2 containing the original and 3 pieces with pearlitic transformation (with time of stay of 5min/15min/30min); and finally box 3 with the original inside and 3 pieces with bainitic transformation (with time of stay of 5min/15min/30min).
It is important to place the samples inside the plastic ring, with a little plastic support, that must be in the upper and superficial part, the one that will then be improved with the grinding and polishing, the longitudinal direction.
To create each box, a cylindrical plastic container was then taken where a silicone spray is first inserted and then epoxy resin mixtures (Durocryl plus) and an acrylic resin are made; subsequently solidification is expected, which is completed after approximately 45 min.
Next to this step the damaged layers in the surface can be removed by grinding.
Rotating disks of abrasive paper are used to grind and a liquid (generally water) flushes to remove heat and residues. The coarseness of the paper is indicated with a number that indicates the number of grains of SiC per square inch. Several papers are used with a decreasing coarseness (higher number) for each step; each grinding stage removes scratches caused by the previous stage so it is important to do the proocess step by step.
The sequence of grinding paper used in this third step is indicated in the Tab 3 below:

Number of particles	Size of particles [µm]
80	212-180
120	150-125
320	46
600	26
1200	15
2400	12
4000	8

Tab 3 - Number and size of particles used in grinding

The abrasive papers used in the grinding phase are shown in the figure 26 below:

Fig 26. Abrasive paper for grinding

During the process water is used for cooling. Once the scratches in surface belong only to the last grade (4000), the specimen's surface is washed with water first and then with alcohol.

Before going on to the polishing phase, the surface of the various samples is checked on the optical microscope; the surface must be the cleanest and with the lowest possible roughness.

Polishing is the fourth step, in which discs are covered with a cloth impregnated with a solution containing both lubricant and abrasive diamond particles. In metallography laboratory two particles grades are used. The first one used should remove scratches from finest grinding stage and these particles are characterized by a diameter of 3 μm; smaller particles characterized by a diameter of 1 μm are used in a second stage to produce a smoother surface.

Figure 27 are shows the polishing machine, 3 μm on the left and 1 μm on the right side of the picture:

Fig 27. Abrasive paper for grinding

After many minutes of work the surface is controlled under a microscope and the surface has continued to improve until it is mirrored; this surface is therefore ready for the etching phase.

The picture below was taken under the microscope and shows an example of a mirror surface obtained after the grinding and polishing phase; I used a 100x magnification setting on the microscope:

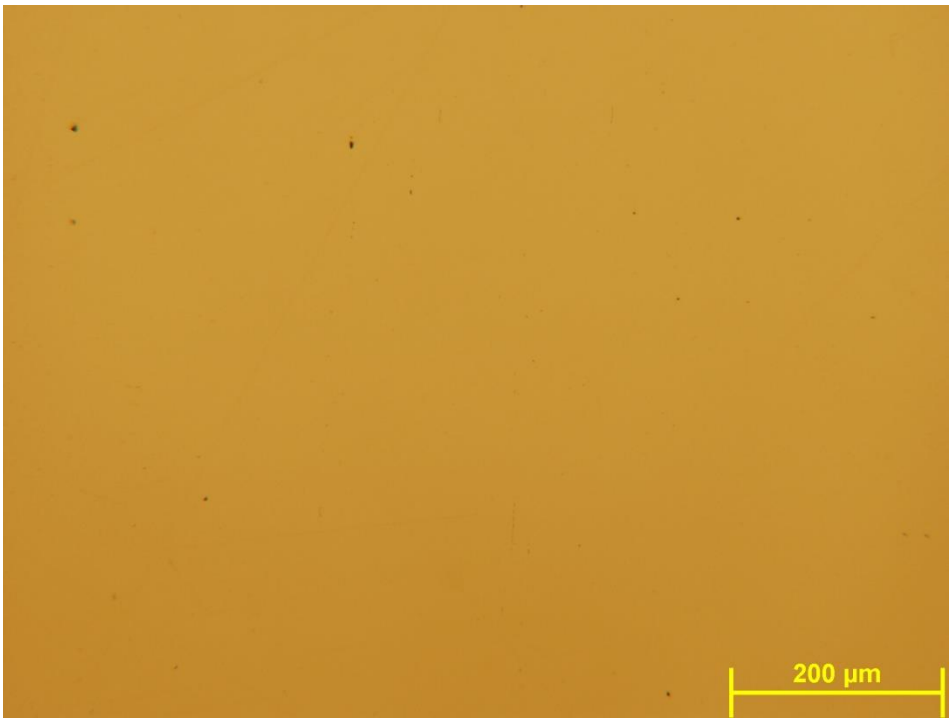

Fig 28. Mirror surface before etching process, magnification scale 100x setted

Grinding and polishing always leave a layer of disturbed materials on the surface of the specimen. Therefore, if specimens are very sensitive to this mechanical damage, electrochemical or chemical polishing can be done.

The samples are then shown below in figure 29 after the steps described above and before the etching phase:

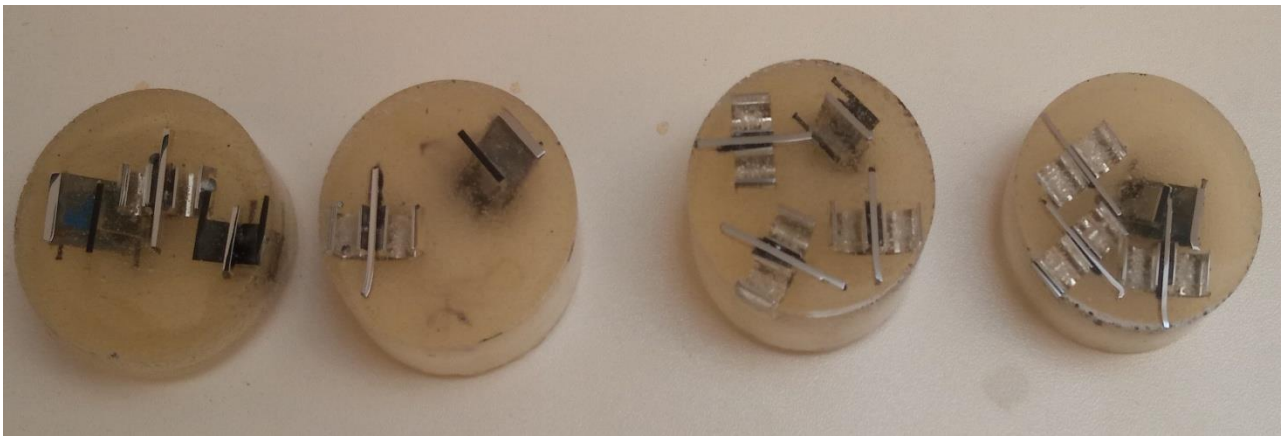

Fig 29. Plastic boxes with samples before etching

The last and probably most important step is etching, a necessary step in which chemical attack is used to reveal the microstructure of metal; If there is an alloy like steels, chemical attack is stronger in one phase than in the other one.

The result is a contrast between regions of the two phases through differences in reflectivity. The time of etching, that is the time in which the surface is exposed to the chemical solution, depends on the material and its surface properties. There are various reagents used during etching depending on the type of metal and on the phase that wants to be revealed.

In this case it was first used Nital (2%), as a reagent, with residence times ranging from 15 sec to 25, depending on the heat treatment; in fact, the samples from boxes 2 and 3 (pearlitic and bainitic transformation) require longer residence time in the acid to show results; next to this it is important to clean the surface of the samples with alcohol and water, and before going to the optical microscope the plastic boxes has to be dry with a hairdryer.

After a subsequent analysis with the optical microscope, excellent results are not noticed, therefore we pass to the use of another acid composed of HNO_3 and HCl in a proportion of 1:3 ; It is important to point out that before using this second acid it is necessary to clean the surface of the samples by repeating the polishing process (first with the 3 μm disc and then with the 1 μm disc).

Once the mirror surfaces are obtained, residence times of around 10 seconds are applied to each box due to the aggressiveness of the acid.

At this point, next to the use of alcohol, water and hairdryer to clean and dry the surface, it is possible to analyse the various surfaces obtained with an optical microscope and take photographs in the areas that best show the various microstructures; this will be done in the next paragraph of the thesis.

4.2 Microstructure and consideration

Once the process of preparing the various plastic boxes with the assembled samples is completed, we pass to the analysis of the various microstructures under an optical microscope.

The images captured by the optical microscope before and after the thermal treatments will then be compared; specifically, various photos were taken (in various positions of the piece, with the aim of finding the cleanest possible surface) for each sample, with a different magnification of the microscope (10x; 20x; 50x; 100x). It is important to report the fact that in the event that the images obtained were unclear the polishing process and then the etching process were carried out to further clean the surface and make the captured image of higher quality.

It was therefore chosen the sharpest image that most shows the microstructural characteristics for each heat treatment and it was also decided to use the images with a magnification of 100x to best show the results obtained; during the photo capture process it was important to find the right color and image focus to make it as sharp as possible.

As for the box 0 it was decided to analyse the hardened samples, omitting the annealed ones; the image of the quenched sample is shown in figure 30:

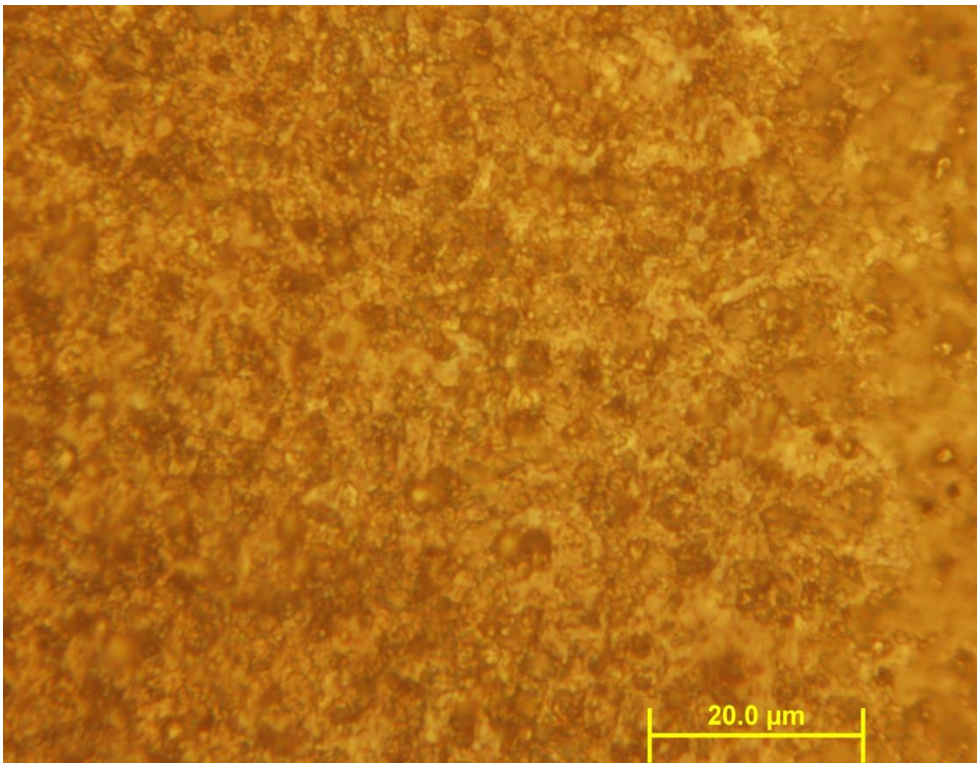

Fig 30. Metallography of the Quenched sample 0.3 (Box 0), magnification 100x

From the image we note that the tempered sample has a martensitic structure, as expected; the grain sizes are slightly larger than the original piece (without heat treatment).

The remarkable reticular deformations, which block the movement of the dislocations, are the first cause of the quenching. The martensitic structure is macroscopically fragile and highly tensioned.

It is also noted that the effects of the rolling process upstream on the piece are visible.

The images captured from box 1 are shown below in figure 31 and 32, comparing the sample before heat treatment and after the tempering and double tempering process:

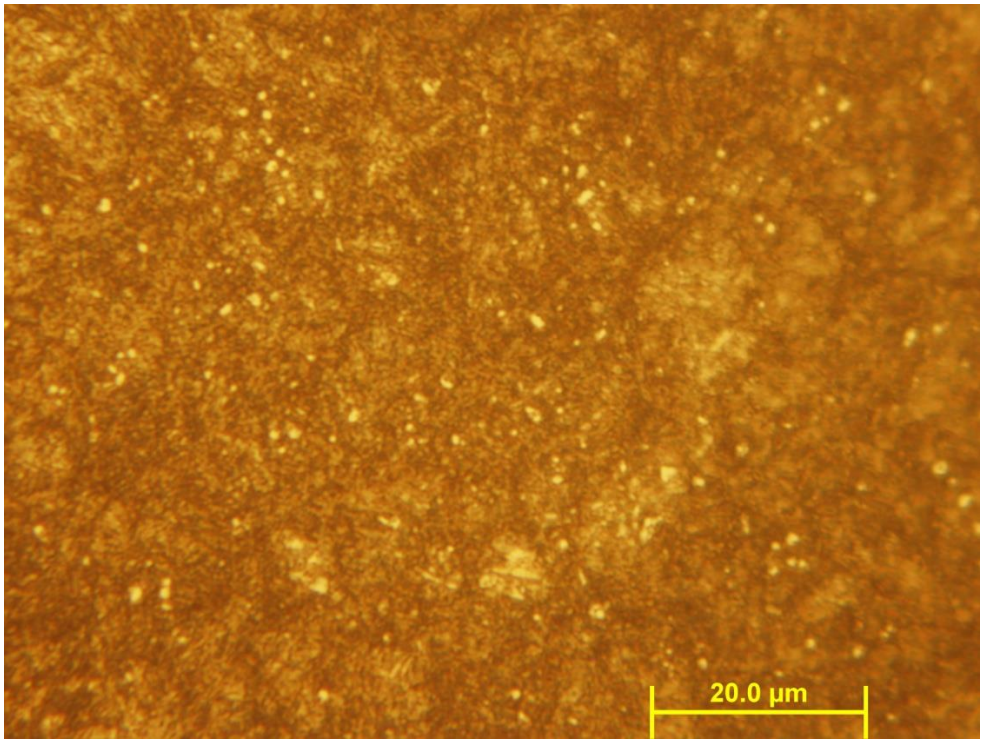

Fig 31. Metallography of the original sample (Box 1), magnification 100x

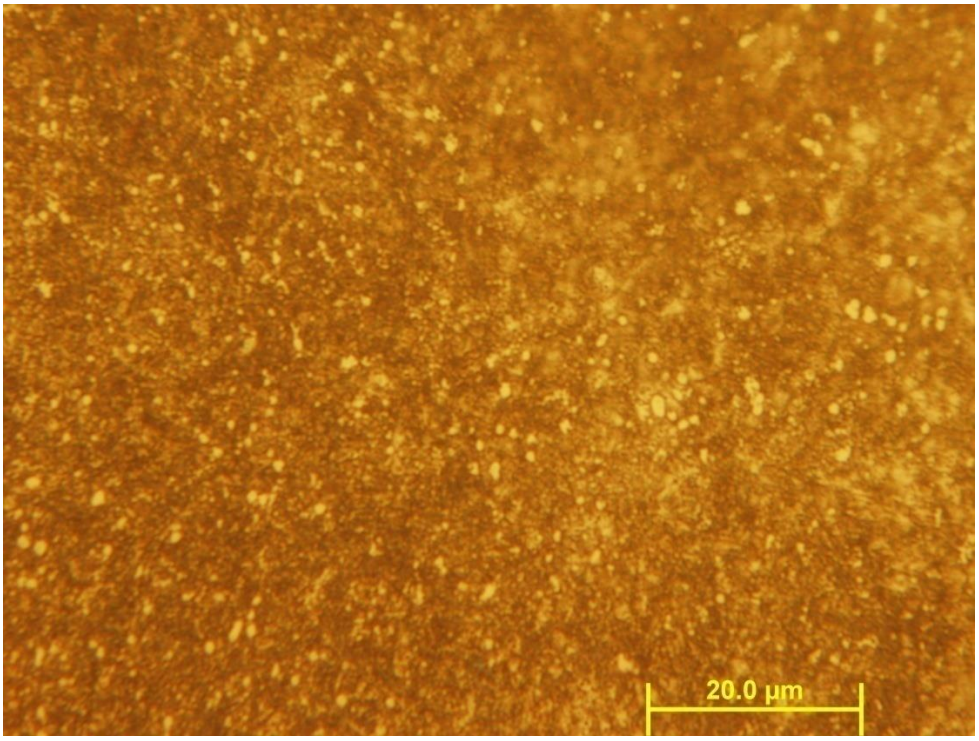

Fig 32. Metallography of the quenched+2°Tempering sample 1.1 (Box 1), magnification 100x

In this case we note how the two images obtained, before and after the heat treatment, are very similar with the difference that in the second image there is a martensitic structure due precisely to

the tempering process; in this case the double tempering carried out, as described in the literature, has the main task of reducing the internal tensional states. It is important to note that a coarse starting austenitic grain generates an equally coarse martensitic grain.

In box 2 the images were captured before and after the pearlitic transformation obtained with the heat treatment; below in figure 33 is the image of the original sample and in the following image 34 the clearest photo (of the 3 photos at 100x magnification) of the obtained pearlitic structure:

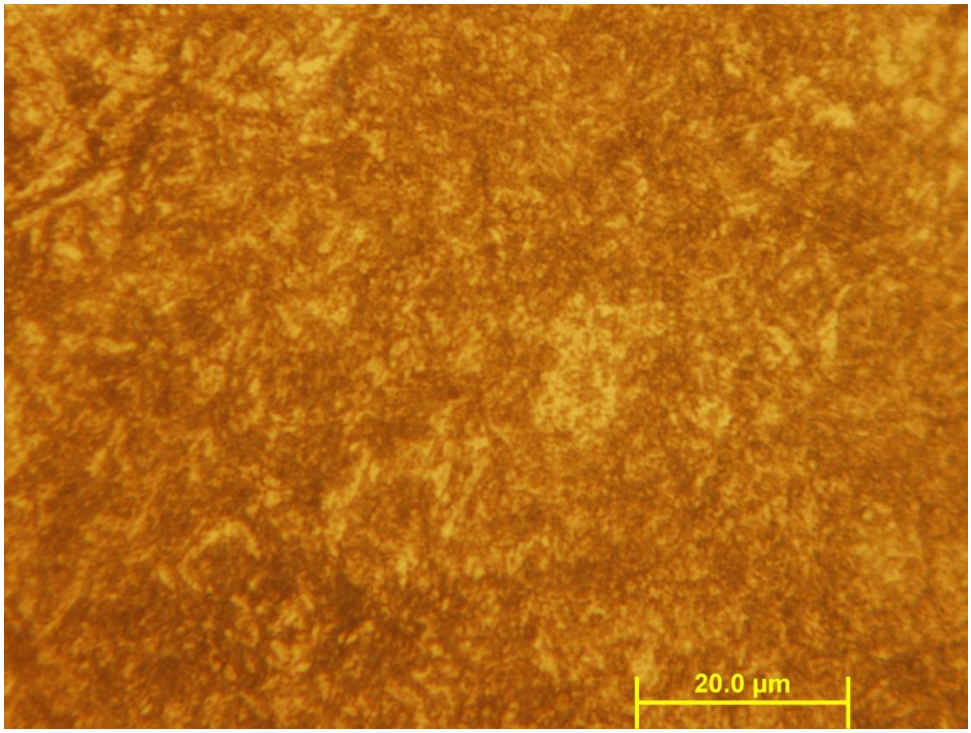

Fig 33. Metallography of the original sample (Box 2), magnification 100x

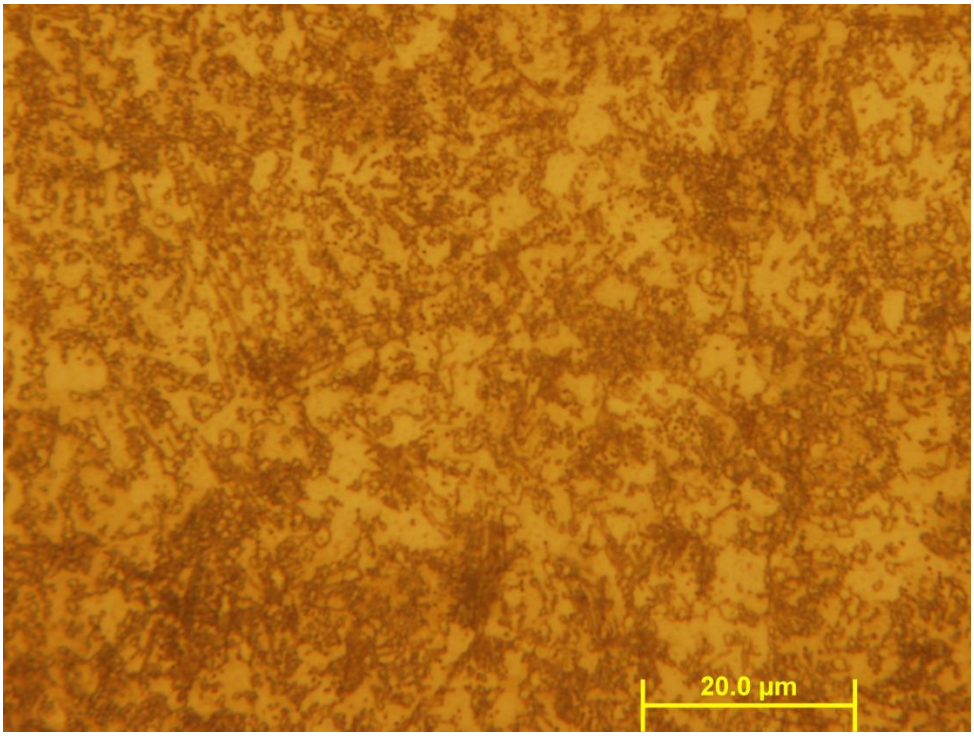

Fig 34. Metallography of the pearlitic structure 2.1 (Box 2), magnification 100x

From the images obtained it is possible to notice the change of structure brought by the heat treatment. Figure 34 shows how many dark parts are present in black, in an uneven way, and they exactly represent the pearlitic structure that is a coarse lamellar structure; the lighter parts however, much less present, represent the ferritic structure; The microstructure of perlite, as said in the theory before, is characterized by the regular alternation of lamellas, specifically ferrite and cementite alternate. The signs of the rolling process remain visible.

Finally from the last plastic box, the number 3, the last two images are shown,figures 35 and 36, which represent the original piece (before the heat treatment) and then the sample with superior bainitic structure:

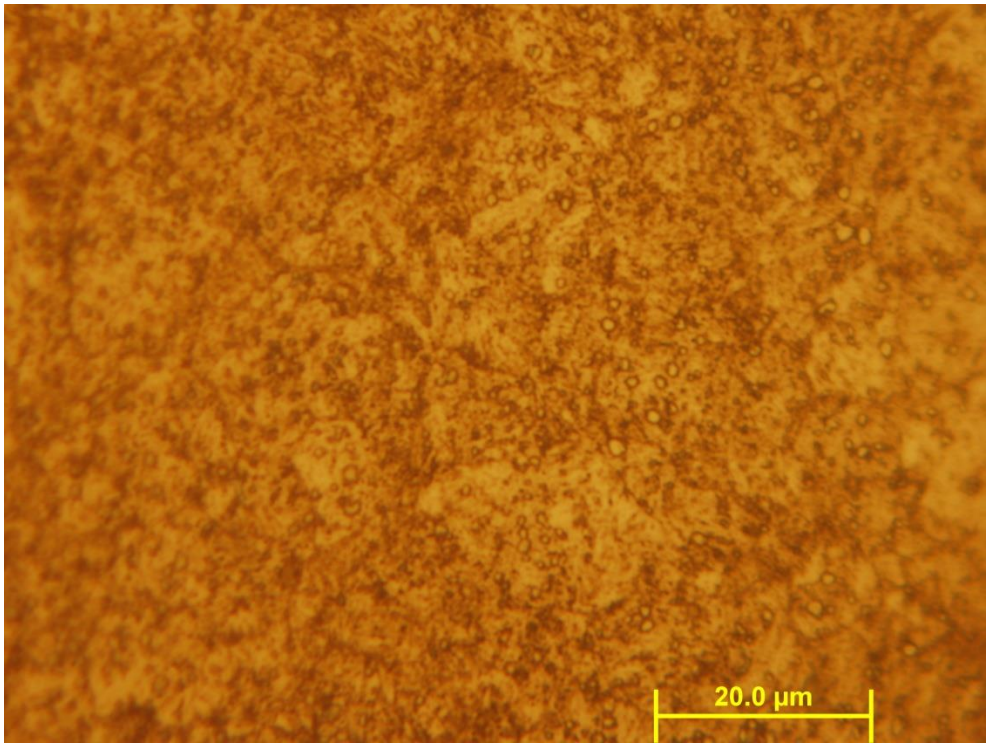

Fig 35. Metallography of the original sample (Box 3), magnification 100x

The bainitic structure assumes, from the metallographic point of view, acicular morphologies. In particular they are subdivided, based on their structures and properties, into higher bainites, in which the cementite has the form of small elongated sticks and the ferrite is arranged parallel to the first, and lower bainites, in which the ferrite and the cementite assume the form of very minute needles forming angles of about 60º.

In our case is it visible that there is an upper bainitic structure because of the temperature used during the heat treatment.

From the crystallographic point of view, bainite is composed of ferrite and cementite (carbides) and differs from martensite which is likewise ferrite supersaturated, due to the fact that in the first the carbon atoms are arranged at random, while in the second they are arranged more regularly.

Also in this case we can see how the signs of the rolling process remain visible.

In the figure 36 below it is shown the lamellar acicular structure of the upper bainite obtained:

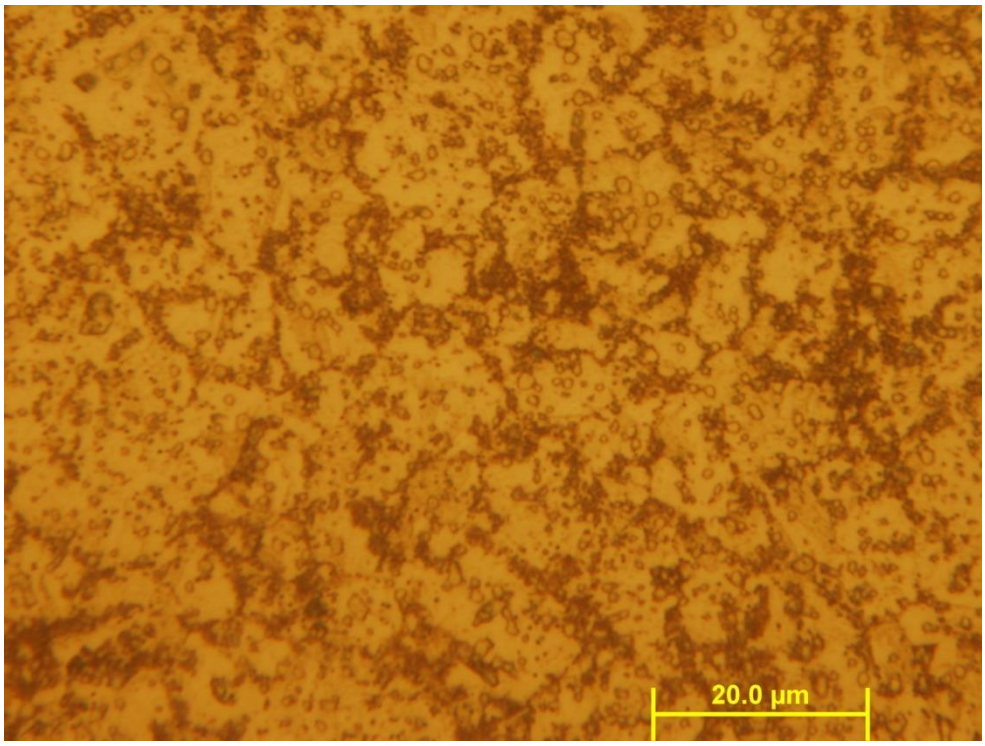

Fig 36. Metallography of upper bainitic structure 3.1 (Box 3), magnification 100x

CONCLUSIONS

In regards to the first objective of the thesis, namely the effects of nitrogen present in the samples, as an interstitial element present in C75 steel formed during the process, on the various properties taken into consideration. In part of this work several magnetic properties, thermoelectric power (TEP) and Vickers hardness was investigated.

We observed a practically linear connection between nitrogen content and the quantities B_{max} B_r, μ_{max} and μ_i. On the other hand the nitrogen content does not have significant effect on other properties studied like TEP, Hc and HV in contrast to what was expected.

In the comparisons between the different quantities we also noticed a linear connection between the values of μ_{max} and μ_i with respect to the TEP values obtained while there is no other correlation between the other quantities.

It is however important to mention the fact that these conclusions are valid only for the studied steel grade range, obtained by the average of the test (from 0.0083% to 0.0129% of N). Therefore it is not absolutely excluded that the percentages of nitrogen higher or higher the results obtainable with the same methods and types of tests could be completely different.

Focusing on the second part of the thesis concerning the thermal treatments, made on the 4 different boxes, some interesting results were obtained that had not been expected.

Among the most salient we can mention the strong decrease (up to polarity inversion) of the TEP values, of the samples, after tempering (BOX 0) and the subsequent slow growth of these values after 40h as well as the direct proportionality links between the TEP values and the HV hardness.

In the samples of BOX 1 an interesting result obtained to the values of TEP that are similar to the originals (before the heat treatment), after quenching + tempering, to indicate how the recovery has restored these values; It is also interesting to note the inversely proportional trend, with a hyperbola trend, of the TEP and HV hardness values.

As for BOX 2 (pearlitic transformation) and 3 (bainitic transformation) it was expected to find different results for the various quantities due to the various residence times applied in the second furnace (5 '; 10'; 15 '; 20'; 25'; 30') and instead the results are independent from this; in box 3 it was interesting to see a direct proportionality link between coercivity, Hc, and hardness, HV.

In the last section of the third chapter, it was also interesting to compare the results of the 4 boxes, where interesting considerations emerge between the heat treatments and the values of the quantities, above all a linear dependence between the values of the 4 boxes of Hc and HV.

However, it should be emphasized that each of the 4 boxes came from different coils, so the macro comparisons made in the 3.6 paragraph should be considered as non-indicative and only as hypothetical, given the different production process of each BOX and the consequent differences and influences on the characteristics of the starting samples.

As far as metallography is concerned, the results were quite good because the structures and characteristics reported in the literature were found after the different heat treatments, although the sharpness of the images is not perfect to show all the details about microstructures.

ACKNOWLEDGEMENTS

To my family who has always supported me in these years during all the difficulties.
To all the people who, for better or for worse, have been present during this growth process and in particular to my closest friends.
I also thank the University of Padua for the teaching offered in these years and for giving me the opportunity to carry out the thesis in Budapest through the Erasmus program and in particular Prof. Calliari for the supervision of the thesis; it was a professionally educational experience but above all it enriched me from a human point of view. I therefore thank Prof. Meszaros for the guide and the supervision during all my period in Budapest and all the other teachers and technicians of the BME University involved in the research.

Ad maiora semper

References

[1] M. BONIARDI, A. CASARIOLI, *Steel metallurgy*, Gruppo lucefin, 2017

[2] E. PERELOMA, D. EDMONDS, *Phase Transformations in Steels: Fundamentals and Diffusion-Controlled Transformations*, 2012

[3] V. G. GAVRILJUK, *CARBON, NITROGEN and HYDROGEN in STEEL: SIMILARITIES and DIFFERENCES in THEIR EFFECT on STRUCTURE and PROPERTIES,* 2010

[4] H. MIURA, *Handbook of Metal Injection Molding*, 2012

[5] *Thermoelectric Effects in Metals: Thermocouples* (© Safa O. Kasap 1997 - 2001)

[6] McGraw-Hill textbook *Principles of Electronic Materials and Devices, Second Edition*

[7] CULLITY, GRHAM, *Introduction to Magnetic Materials*, Second Edition, John Wiley & Sons Publication, (2009)

[8] FIORILLO, *Measurement and characterization of magnetic materials*, Elsevier Academic Press (2004)

[9] VERTESY, MESZAROS, TOMAS, *Nondestructive magnetic characterization of TRIP steels*, NDT&E International 54 (2013) 107-114

[10] W.D. CALLISTER, *Material science and engineering*, 7th edition, (2006)

[11] M. CAZERES, G.M. LOZANO, D.E. GUERRERO-MATA, M.P. COLAS, and G. TOTTEN E.,"High-Speed Quenching of High Carbon Steel", *Materials Performance and Characterization*

[12] G.M. PAOLUCCI, *Lezioni di metallurgia,* edizioni libreria progetto Padova

[13] M. COLONNA, *Corso di didattica di tecnologia dei materiali "analisi metallografica",* Università degli studi dell'Aquila